Studies on Oriented Polysaccharide Materials Prepared from Evaporative Air-LC Interface

GARGI JOSHI

Japan Advanced Institute of Science and Technology

Doctoral Dissertation

Studies on Oriented Polysaccharide Materials Prepared from Evaporative Air-LC Interface

Gargi Joshi

Supervisor: Prof. Tatsuo Kaneko

Graduate School of Advanced Science and Technology
Japan Advanced Institute of Science and Technology
[Materials Science]
June 2019

“Life is not easy for any of us. But what of that ……?
We must have perseverance and above all confidence in ourselves.
We must believe that we are gifted for something,
and that this thing must be attained”

- *Marie Curie*

Abstract

Studies on Oriented Polysaccharide Materials Prepared from Evaporative Air-LC Interface

Gargi Joshi

s1620033

Kaneko Laboratory, Graduate School of Advanced Science and Technology, Japan Advanced School of Science and Technology

Introduction

Nature has bestowed organisms with different structural designs to adapt them to survive, even under some of the extreme living environments. The human mind and creative intelligence have led us to synthetically mimic these structural designs and improve the living standards. Liquid crystal (LC) state of polymers is the most preferred for such applications due to their intrinsic combination of mobility and ordering. However, the use of naturally available polymers has rarely been the focus of research and thus we are still unaware of many of the key processes of survival strategies. In this work, I have studied the self-assembly of LC polysaccharide (sacran and xanthan gum) aqueous solutions under a drying environment. The self-assembled deposited structures were found to be highly oriented and upon crosslinking, anisotropically swelling hydrogels were prepared.

Results & Discussion

Sacran solution dried in a limited space, deposited as a thin membrane by bridging the narrow gap between the substrates, by splitting the evaporative air-LC interface. This partitioning phenomenon was analyzed theoretically using the standard equation of a meniscus. The derived equation proved that the splitting of the original meniscus into two menisci actually doubled the available area for evaporation in the limited space. In order to control the deposition of LC domains, xanthan gum was used due to its intrinsic property of thermotropic isotropization with increase in temperature. Stepwise deposition of a transverse lid-like membrane preceding the growth of a vertically deposited membrane bridging the two substrates was recorded. A temperature-concentration-morphology phase diagram could be formulated for the variety of deposited structures and anisotropically swelling hydrogel was prepared upon crosslinking the membranous structure. The size of the LC domains in the drying solution was also found to be major factor governing bridging of the gap between the substrates. Self-assembled platelet-sized domains in the sacran solution could deposit, bridging an eight times wider gap.

Conclusion

The theoretical and experimental results presented here provide an understanding of the behavior of polysaccharides under natural environment. The condensation and deposition approach explored in this work promises a versatile methodology of directional control to design novel biomimetic materials with highly-ordered structures.

Keywords: Self-assembly, liquid crystals, polysaccharides, drying interface, orientation

Preface

The present dissertation is submitted for the Degree of Doctor of Philosophy at Japan Advanced Institute of Science and Technology, Japan. The dissertation presents the results of the research works on the "Studies on Oriented Polysaccharide Materials Prepared from Evaporative Air-LC Interface" under the guidance of Prof. Tatsuo Kaneko at the Graduate School of Advanced Science and Technology, Japan Advanced Institute of Science and Technology during July 2016 – June 2019.

High orientation is desired in almost every application related to materials science today, so as to have an advantage of directional control. In spite of mimicking the techniques of hierarchical structural design found in the natural environment, there has been a dearth in original research utilizing the naturally available resources. In this thesis, the main target has been to uncover the aspects of structural organization of polysaccharides under a drying atmosphere. Manipulating the process of self-assembly and conditions, to then achieve highly oriented materials was the ultimate goal.

The work presented in this thesis was done to grasp experimental as well as theoretical understanding of controlled evaporation of polysaccharide solutions from evaporation front and their self-assembling along the drying air-LC interface. The relevant information from the existing literatures has been indicated at appropriate places in the text. To the best of the author's knowledge, the work consists of original ideas, results, presentation approach and that no part of the thesis has been plagiarized.

Graduate School of Advanced Science and Technology Gargi Joshi

Japan Advanced Institute of Science and Technology

June 2019

Acknowledgements

Firstly, I wish to express my sincere gratitude to my supervisor *Prof. Tatsuo Kaneko,* Graduate School of Advanced Science and Technology, Japan Advanced Institute of Science and Technology, for providing me with the opportunity to be his student. His kind guidance, valuable suggestions and constructive criticism contributed the necessary impetus in the completion of this work. His utmost faith in me was the prime source of motivation for me to stay focussed during the entire time of research and preparation of this thesis.

I would also like to thank the members of the review committee *Prof. Tetsu Mitsumata* (Niigata University, Niigata), *Prof. Noriyoshi Matsumi* (JAIST), *Prof. Yoshifumi Oshima* (JAIST), *Assoc. Prof. Hidekazu Tsutsui* (JAIST), who have spent their valuable time to read the thesis and agreed to be a part of the review committee.

I owe a deep sense of gratitude for *Sr. Lectr. Kosuke Okeyoshi* (JAIST) for his constant motivation and belief. He always inspired me to push myself and explore my potential to the fullest. The challenging journey of Ph.D. has been equally satisfying due to countless stimulating discussions with him. Furthermore, I would like to express special thanks to *Dr. Maiko K. Okajima* for her valuable suggestions throughout my time at a professional as well as personal level.

Research work requires high level of technical skills and scientific discussions. I wish to thank Mr. Osamu Notoya and Mr. Nobuaki Ito of the Center for Nano Materials and Technology (JAIST) for teaching me and helping with the SEM analysis; Prof. Heikki Tenhu, Head of Department of Chemistry and Prof. Francoise M. Winnik (University of Helsinki), for accepting me as a visiting student; Prof. Miklos Zrinyi (Semmelweis University, Budapest) for his cheerful attitude and advices about research life. I am also grateful to all the Kaneko lab members, for their timely inputs, cooperation and discussions, for all the time we were working together before deadlines, and for all the fun we had. I consider myself very lucky to have met so many people along the way and gathered memories to be cherished forever.

The financial support, travel grants and research facilities are unquestionably crucial for the completion of any project. I am humbled by the fellowship granted by the Japan Society

for the Promotion of Science (JSPS) along with the Grant-in-Aid for Young Fellows JSPS KAKEHNI (#18J11881) for this proposal. It is a matter of deep respect and pride to have received this prestigious fellowship. I would also like to extend my thanks to JAIST for monetary support during off-campus research in Helsinki and international conference in the USA.

Lastly, I express my heartfelt gratitude to my parents and brothers, for their positivity, relentless support and encouragement in difficult times. I would like to dedicate this work to my parents, who have always believed in me and my dreams. Their faith makes me stronger every time and fuels my passion to dream big.

Graduate School of Advanced Science and Technology Gargi Joshi
Japan Advanced Institute of Science and Technology
June 2019

Table of Contents

Page No.

Chapter 1

General Introduction

1.1 The sense of direction

Life on Earth exists as it is said because of 'order and harmony'. Orientation and alignment is a major factor that drives organisms towards evolution.[1–3] The essence of directionality manifests itself in several ways throughout materials science and is also an integral part (**Fig. 1.1**). Propagating information in one preferred direction over many others is a characteristic property, referred to as 'anisotropy' of materials. The most basic example is that of any of electronic devices wherein their performance relies on charge carrier ability which must be unidirectional, most popular being organic semiconducting materials as well as solar cells.[4–6] Same can be convincingly stated for substrates for tissue engineering applications[7,8] where the alignment of cell is primary and is crucial for biomimetic applications.[9–11]

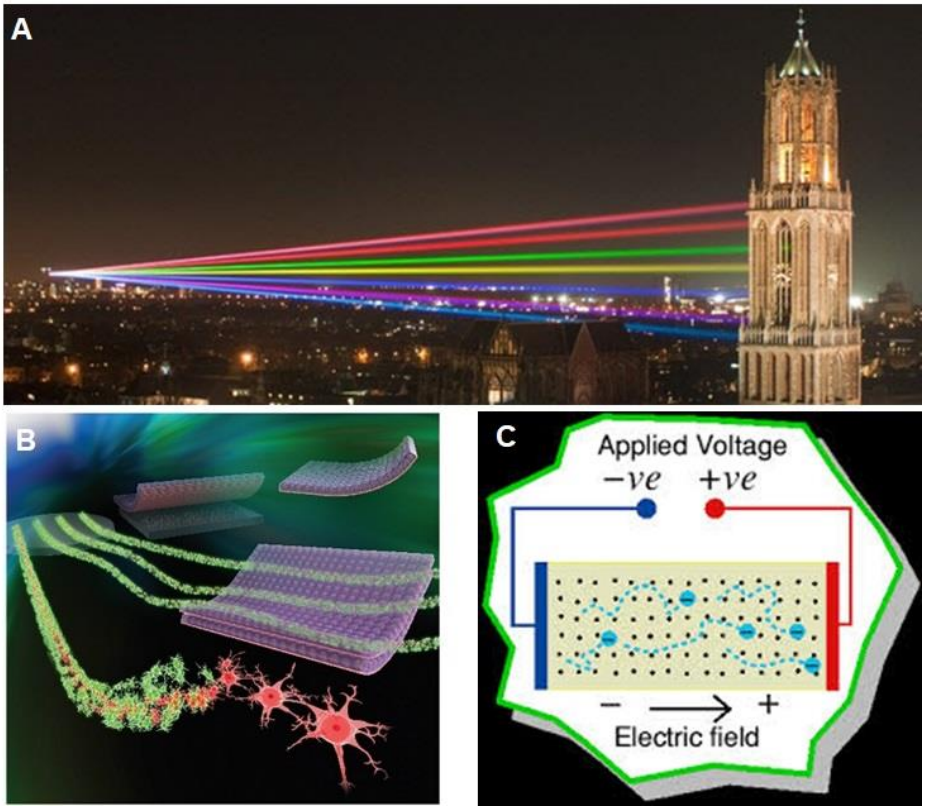

Figure 1.1 The importance of directionality in everyday life. **A.** Light travels along a straight path. **B.** Scaffolds for tissue engineering are prepared with preferably anisotropic structures. **C.** Electrical and magnetic applications are based on unidirectional flow of electrons.

The alignment helps in strengthening the material and imparting certain particular features. Depending on that properties imparted, sought-after applications include fabrication of catalytic[12], sensing[13,14], tunable optics[15], and cleansing materials.[16–18]All these applications rely on fine tuning of particle arrangement within the actual framework for modification of corresponding properties.

Liquid crystalline phases of materials are often preferred for bottom-up approach of synthesis/organization as they possess inherent ordering nature.[19–21]These are one of the states of matter having order of a solid but with also the freedom of motion of liquids, thus representative of the name, liquid crystals (LC). The units/domains of LC, known as mesogens, have individual orientational vectors till the time a change is initiated. As a response to some stimulus, temperature, solvent etc., the mesogens start self-assembling along a common director orientation. They have been in use since a long time now but still the complete potential is under exploration towards new dynamic applications.[22]

1.2 Learning Self-assembly from Nature (Bio-inspiration & Biomimetics)

Starting from the smallest possible example of ordering, that is of the homologous pairing of DNA chromatids[23], the nature gives us direct reasons to explore materials with alignment in structural design. The protein filaments, actin and myosin, in the striated and smooth muscles have nematic and smectic LC structural organization respectively. The complex structure of fibrillar type I collagen presents different morphologies for different functions. In bones it provides rigid and shock-resistant tissues, while it possess low rigidity and high deformation to rupture in tendon behaving like an elastomer and optical properties of transparency in cornea.[24,25]

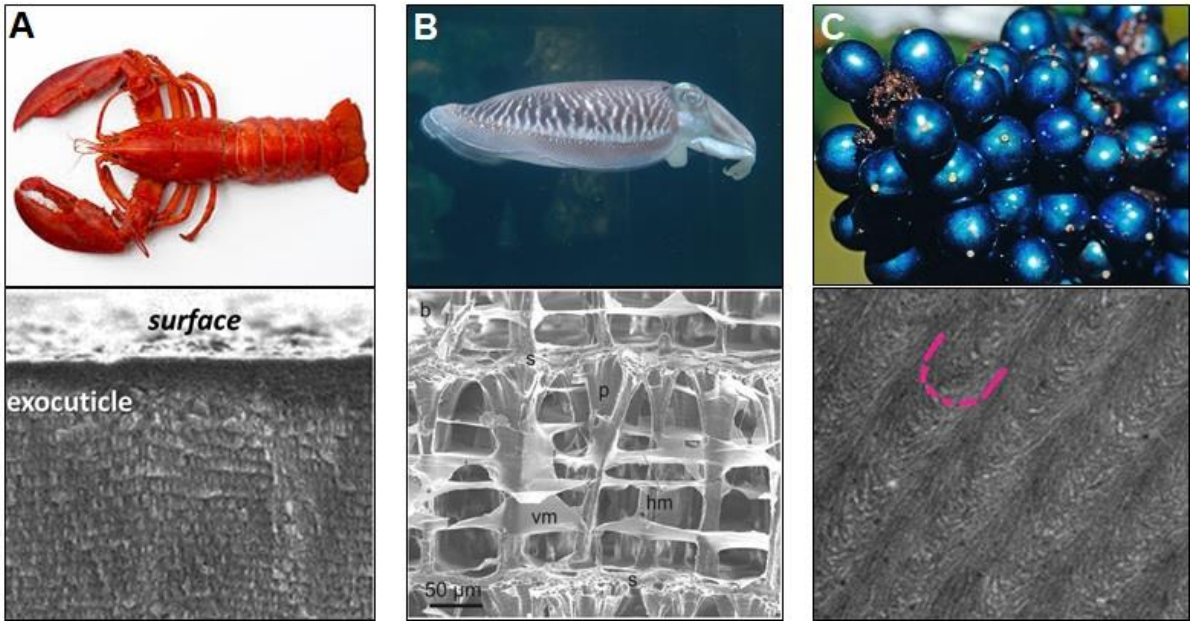

Figure 1.2 Variations in natural structural designs. A. The tightly-packed layered structure of arthropod shell impart them with fracture resistance and protection. **B.** The hollow lightweight cuttle bone of the cuttle fish provides buoyancy. **C.** The structural color, and not the pigmental color in some fruits, give them an intense appearance.[26]

The self-assembled structures are not only an organization of cells/tissues but function as the basic survival strategies all across the living world.[27] **Fig. 1.2** shows three examples of the

naturally oriented architectures. **A)** The exoskeleton of crabs is composed of polysaccharide chitin in liquid crystalline state with an increased level of calcium content. Such a design is present throughout the phylum Arthropoda and qualifies as a superior protection against crack propagation. **B)** The cuttlebone of the cuttlefish is a highly sophisticated buoyancy tool composed of multiple chambers along with a complex array of calcified pillars as well as polysaccharide membranes. The membranes have a layered structures arguably for a stable performance under the hydrostatic pressure. **C)** The epicarp or the outer skin layer of the *P. condensata* fruit is liquid crystalline cellulose structure showing arc patterns in TEM observations. The brilliant appearance gives fresh appearance to an otherwise 40-50 years old fruit. This attracts the seed dispersers and saves the energy expense of producing fresh pulp for the pollinating agent.

The mention of polysaccharides crops up in every literature review done for natural self-assembled organization. Thus, there is a clear indication of involvement of polysaccharides in the design of almost every structural hierarchy found on Earth. The next question arises, are they responsible/part of orientation control mechanism as well?

1.3 Role of polysaccharides in orientation

Polysaccharides are a class of biopolymers with long chain composed of monosaccharide units linked together by glycosidic bonds. They are extracted from plants (cellulose, guar, starch, pectin), animals (hyaluronic acid, chitin), fungi (pullulan, scleroglucan) and bacteria (xanthan, gellan, dextran).Their solution properties are determined by the nature of their repeating units, making them amorphous and sometimes insoluble in water. Polysaccharides play a number of roles like storage, starch and glycogen; structural, cellulose and chitin; or for survival, xanthan gum and sacran. Bacterial exopolysaccharides are considered the first choice from application point of view, due to their availability in abundance and economical value.[28,29]

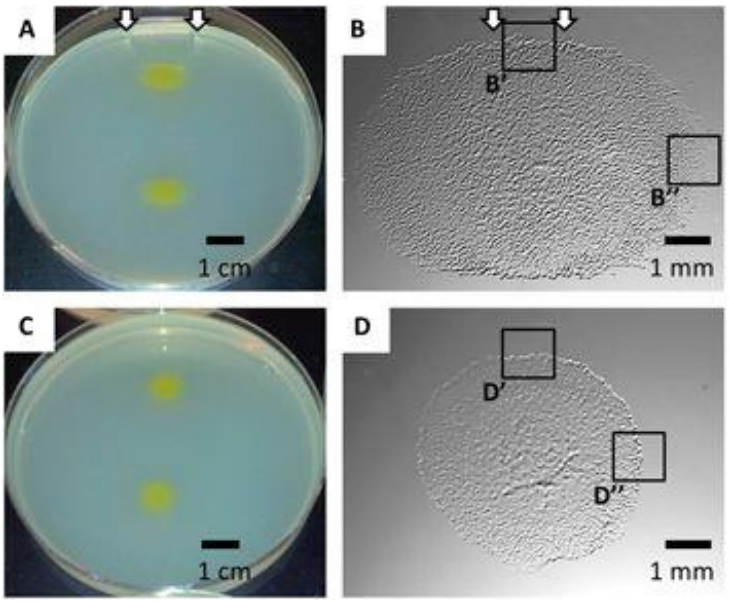

Figure 1.3 *M. xanthus* flares and colonies on compressed and uncompressed agar. Whole colony morphologies on compressed (**A**,**B**) and uncompressed agar (**C**,**D**) are shown.[30]

Majority of the bacteria live in colonies by secreting surface-associated biofilms which primarily comprise of polysaccharides.[31] The behavior of the bacteria and their subsequent

growth is affected by the changes in the surrounding polysaccharide film. Directional compression of the polysaccharide substrate has been investigated to lead to physical movement and realignment of bacterial cells (**Fig. 1.3**).[30] Such a directed collective movement is a form of active biological process as a response to specific physical stimuli. The deformation guides the orientation of bacterial cells due to the induced alignment of polysaccharide fibers.

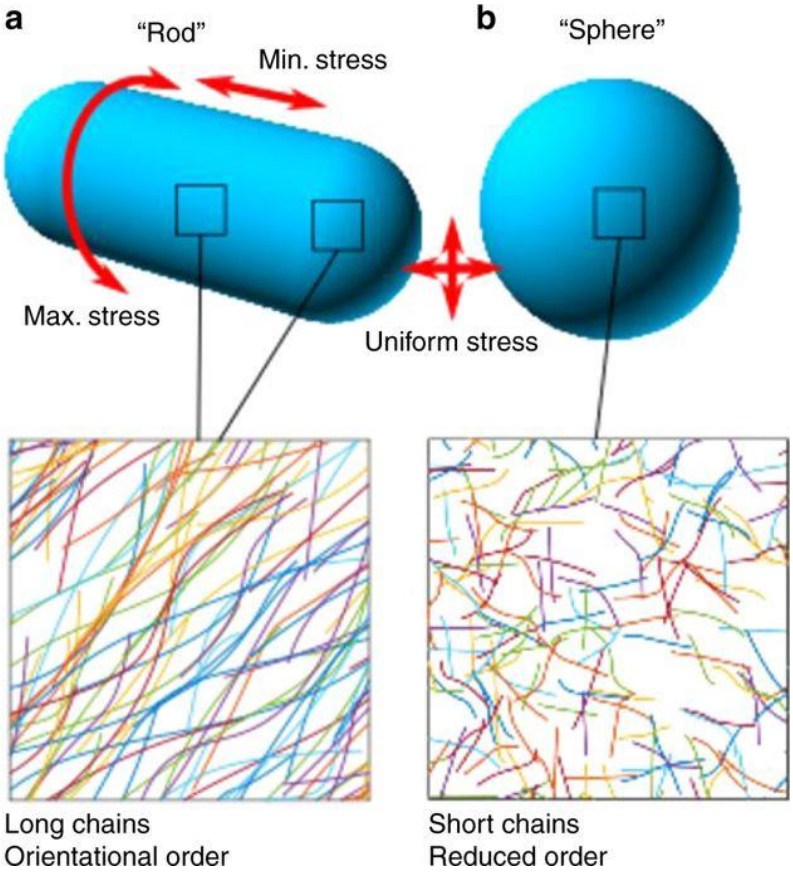

Figure 1.4 Conceptual diagrams of Peptidoglycan from rod-shaped *E. coli* has quantifiable orientational order and Peptidoglycan from spherical *E. coli* is much less ordered and has shorter glycan chains.[32]

Foster *et al.* have provided the first direct visualization and comparison between the arrangement of glycan within rod-shaped and spherical-shaped *E. coli* bacteria.[32] The rod-shaped strain was characterized by longer glycan chains which were much more ordered as compared to the spheroid shaped bacteria comprising of shorter chains with significantly less order (**Fig. 1.4**). This is principally balanced by the cell membrane curvature and multi-protein filaments and their relation gives insight into the molecular mechanism by which varying degrees of oriented glycan can be synthesized.[33]

The formation of parallel orientation or entanglement causing mesh formation of cellulose fibres is a common process during cellulose microfibril deposition in cell wall. The mesh formed is related to the number of inter-fibrillar links (hydrogen bonding or van der Waals interactions) and provides the necessary rigidity. The deposited pattern and degree of orientation in different plant cell walls is specifically dependent on the polysaccharide present.[34] It has been also reported that this deposition is a part of the intrinsic signalling network, acting as the target site of polar growth and differentiation during cell division.[35] In the wood cells, their assembly, including orientation of microfibril and degree of lignification is governed by non-cellulosic saccharides like pectin, xylan, galactan, mannan *etc*.[36]

1.4 Functions of Extracellular polysaccharides

The secondary metabolites secreted by microorganisms, known as the extra-cellular matrix (ECM), comprises of different types of biopolymers out of which polysaccharides are unquestionably predominant. In-depth analysis has reported that adherence to substrates is associated with a higher production of polysaccharides in the biofilm matrix.[37] They act as scaffold for the biofilm as an architecture in three-dimensions and help the adhesion and cohesion functions.[38] Referred to as, “the dark matter of biofilms” ECM polysaccharides have

been found to be difficult to completely analyze and can be easily influenced due to the shear forces, concentration and temperature conditions.[39] It has been experimentally proven that ECM is responsible for compartmentalization within the microbe colony for efficient management and sustainability. Lawrence *et al.* reported that the ECM of microbes is predominantly composed of polysaccharides and provided detailed experimental proof of their role in creation and management of micro-spaces as physically segregated units within the colony.[40] Considering the very famous HeLa cells, one of the striking facts about them involves the crucial role played by their ECM during cytokinesis. The ECM pattern of the mother cell is deposited prior to mitosis as a substrate for daughter cells which in turn leads to them acquiring mother's footprints.[41]

In this thesis, I have used sacran and xanthan gum as the extracellular polysaccharides. Both of these polysaccharides are characterized as high molecular weight biomaterials with extremely rigid structures at liquid crystalline concentrations.

1.4.1 Sacran

Sacran is a cyanobacterial exopolysaccharide with a molecular weight of more than 2×10^7 g/mol.[42] It is extracted from the extracellular matrix of a cyanobacteria as a river plant named *Aphanothece sacrum* which grows in the Kyushu and Kumamoto region of South of Japan. The saccharide chain contains carboxylate groups (17 mol %) and sulphate groups (12 mol %) relative to the sugar residues, that shows, sacran is a heteroanionic polyelectrolyte. According to a detailed characterization, it forms double helixes at concentrations $c > 0.09$ wt%, a weak gel at $c > 0.25$ wt %, and finally huge LC domains with centimeter scale lengths at $c > 0.5$ wt %. This is quite a low concentration when compared to conventional LC polysaccharides. An aggregate of oriented helices was seen as a LC macroscopic domain at a concentration of more than 0.2 wt%. Such large LC domains point to an extremely long persistence length (rigid

part of the helix) as compared to other polysaccharides.[43] Furthermore, this polymer was reported to be a functional biomaterial with anti-inflammatory high moisturizing ability, lyotropic liquid crystallinity, and anisotropic hydrogel swelling properties.[44] In a recent study, the probable mesogenic unit of sacran LC state was shown to be huge rod with a diameter of 1 μm and more than 20 μm in length.[45] They have been shown to be thermally stable even up to a temperature of 60 °C.

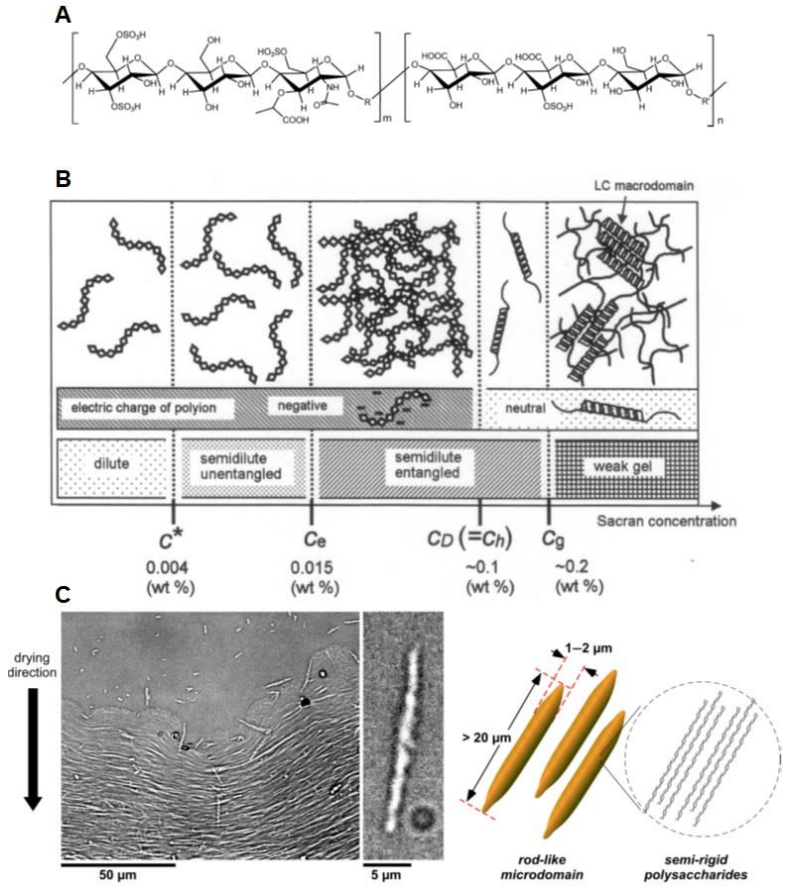

Figure 1.5 Structure of sacran. **A.** Partial chemical structure where R and R' refers to sugar residues such as hexoses, 6-deoxyhexoses, pentoses and so on.[46] **B.** Schematic illustrations representing the chain conformation of sacran in salt-free solutions [($c*$) overlap concentration, (c_e) entanglement concentration, (c_D) critical polyelectrolyte solution, (c_h) helix transition concentration, (c_g) gelation concentration].[43] C. Optical microscopic images of sacran after drying the aqueous solution and schematic illustration of rod-like microdomain of sacran.[45]

Sacran hydrogels were successfully prepared by physical/chemical crosslinking with high anisotropy in swelling.[46,47] The swelling variations due to the temperature of annealing is due to the efficient increase in the amount of crosslinking junctions with increasing temperature (**Fig. 1.6**). A higher amount crosslink density in turn resist too much swelling. However, it is interesting that a film crosslinked at 140 °C follows the same trend and swells anisotropically along the *z*-axis.

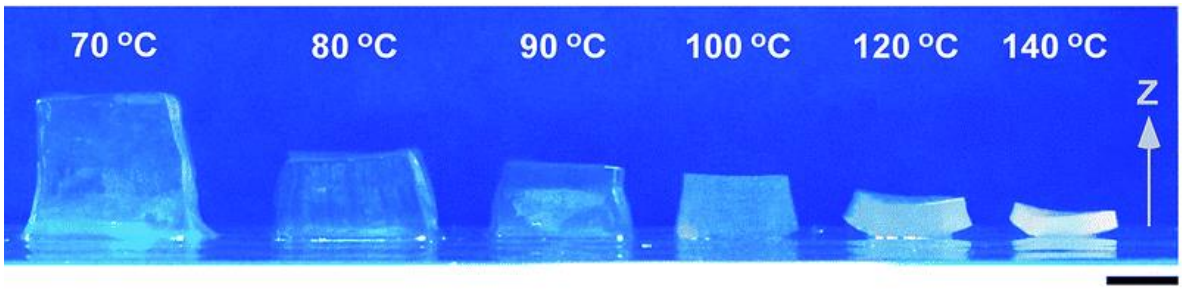

Figure 1.6 Digital images of sacran hydrogels annealed at the respective temperature. Scale bar: 5 mm[46]

1.4.2 Xanthan gum

Xanthan is a double-helical exopolysaccharide extracted from *Xanthomonas* bacteria and is commercially used to control viscosity in foods and cosmetics. The sugars present are D-glucose, D-mannose, and D-glucuronic acid. The glucose units are linked to form a β-1,4-D-glucan cellulosic backbone, and alternate glucoses have a short branch. This side chain consists of β-D-mannose-(1,4)-β-D-glucuronic acid-(1,2)-β-D-mannose (**Fig. 1.7A**). The terminal mannose moiety may carry pyruvate residues linked to the 4- and 6-positions.The internal mannose unit is acetylated at C-6. The acetyl and pyruvic acid content vary with the fermentation conditions. Usually, the degree of substitution for pyruvate varies between 30 and

40%, whereas for acetate the degree of substitution is as high as 60-70%. Some of the repeating units may be devoid of the trisaccharide side chain.

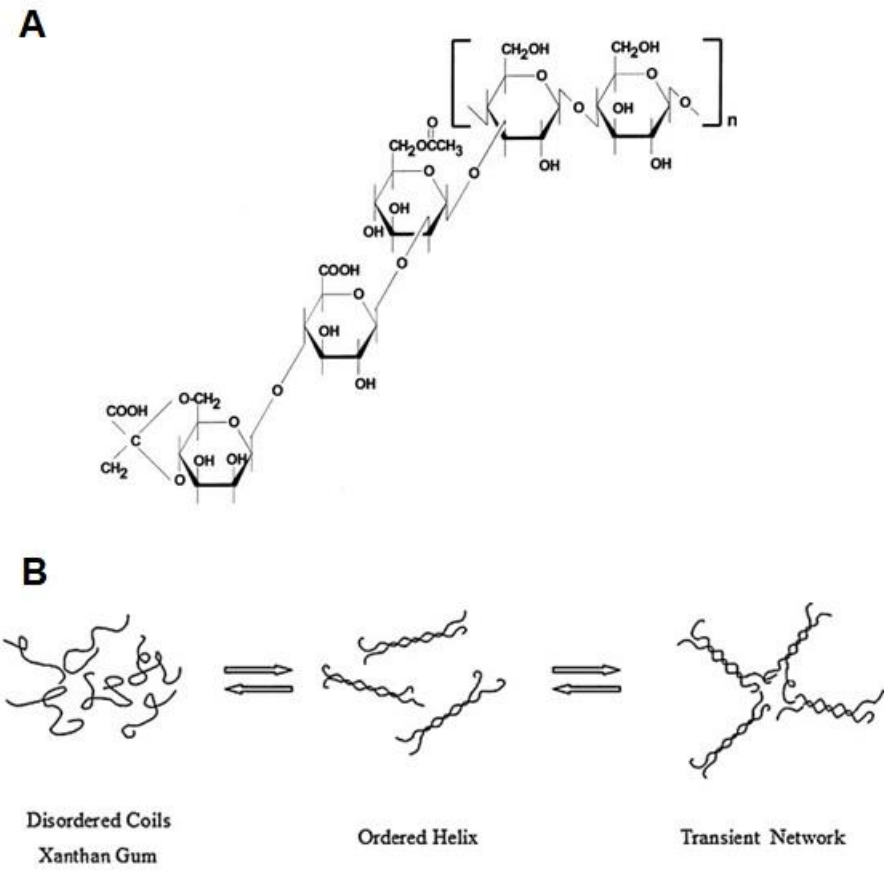

Figure 1.7 A. Structure with the repeating unit of xanthan gum.[48] **B.** Schematics of the network formation in xanthan chains with increase in concentration.

It has a high molecular weight between 2 – 50 × 10^6 g/mol depending on the extraction conditions and strain of bacteria. It is quite rigid due to the double helical structure and has a persistence length of 100–120 nm.[49] Due to this, it is able to enhance the viscosity of aqueous solutions. Xanthan's double helices are known to unwind in aqueous solutions with low ionic strengths at high temperature (denaturation) and also rewind in solutions with high ionic

strengths at low temperature (renaturation). As represented in **Fig. 1.7B** molecular aggregation is difficult due to electrostatic repulsion considering the charged sidechains of xanthan gum. Instead a transient network is formed with increased concentration which easily disassociates due to shear or temperature changes. This biopolymer has been shown to be biocompatible, biodegradable and exhibits gel-like properties, being widely used in food, cosmetic and pharmaceutical industries because of the positive reports on non-toxicity.[50]

In a recent study it was shown that xanthan gum LC domains were much smaller compared to sacran (**Fig. 1.8**) and it was further suggested that the size of such microdomains affect the orientation direction in the self-assembled macrodomains. The small size of the microdomains can be a result of smaller molecular weight or possibly due to conformation fluctuations with temperature.

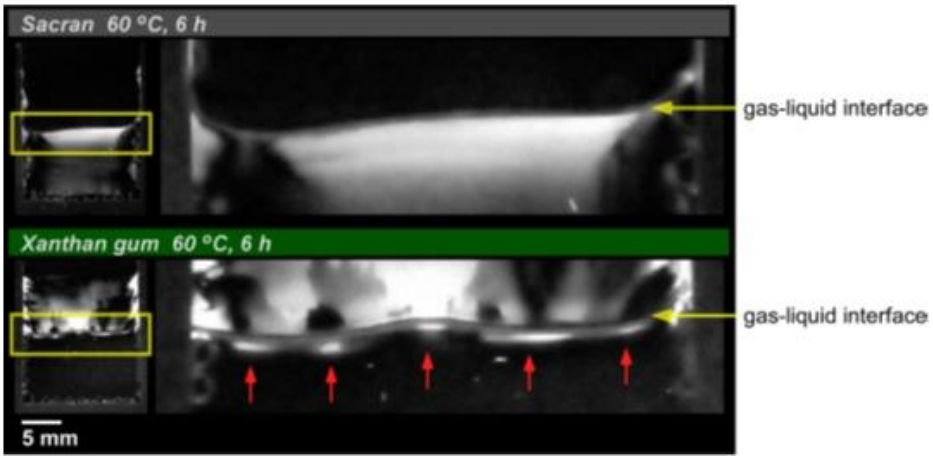

Figure 1.8 Polarized images of the interface of the solutions of sacran (top) and xanthan gum (bottom) during drying in a container.[45]

1.5 Techniques for Self-assembly

Formation of an organized structure from an originally disorganized system due to specific, local non-covalent interactions result in what is known as self-assembly. It is ubiquitous in nature for formation of lipid bilayers, phase-segreagated polymers, liquid cystalline states, and even folding of polypeptides. Because of the range of functionalities afforded, techniques available for fabricating self-assembled strutcures are many and have diverged over the years. Han *et al.* have reviewed the basic strategies employed as methods of self-assembly as shown in **Fig. 1.8**. The routes vary depending upon the properties of the material and the desired architecture of the coating.

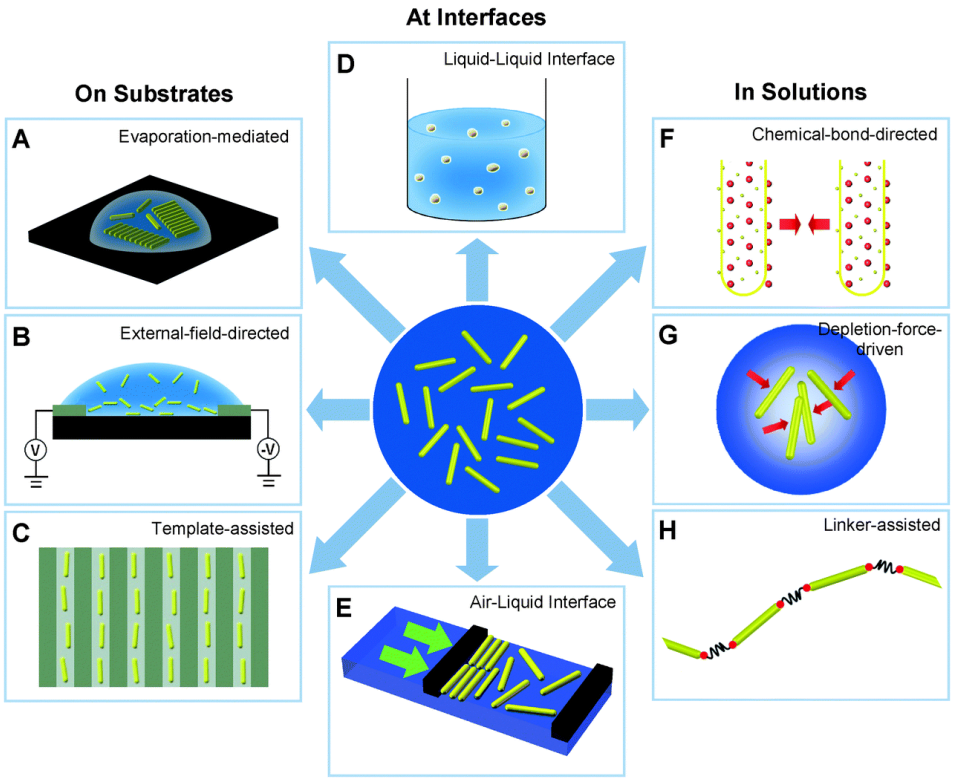

Figure 1.8 Randomly arranged colloidal 1D nanocrystals (shown in the center) can be self-assembled to form ordered structures on substrates (A–C), at interfaces (D and E) and in solutions (F–H) through a variety of self-assembly techniques.[51]

Specifically, patterning of surfaces with a nano- or micro-level design offers potential in the development of small-scale devices such as lab-on-chip applications.

Originally, developed by Denkov *et al.* for controlled deposition of particle coatings, evaporation based convective self-assembly techniques have gained prominence in the recent years. The controlled rate of solvent removal is one of the crucial factors for the uniformity of the structures. The methods have evolved keeping in mind the purpose of application, and they can be, surfactant-mediated, solvent mixtures, to a range of grooved/patterned substrates *etc.*

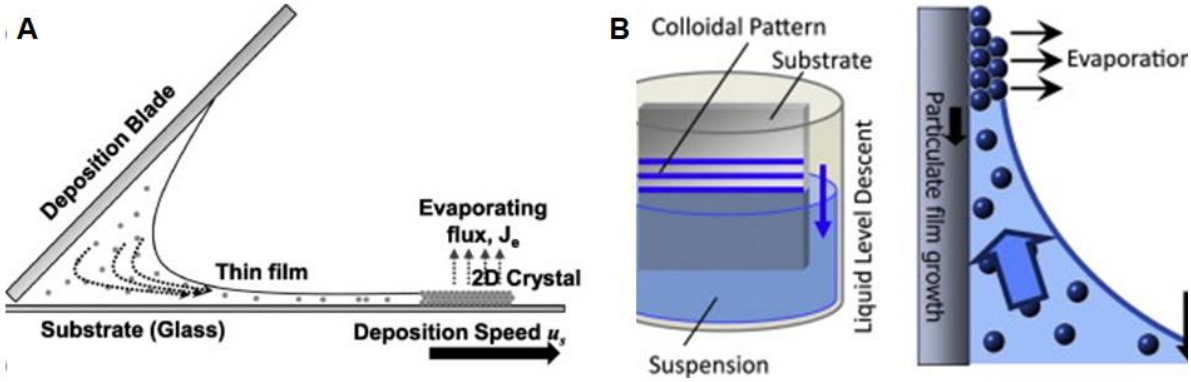

Figure 1.9 Primary techniques used for evaporative self-assembly. **A.** Moving a plate at a controlled rate and angle to deposit particles on a substrate. **B.** Withdrawal of a substrate at a controlled rate from a colloidal suspension.[52]

However, certain challenges are blocking the applicability, the major one being non-uniformity of organization due to the inherent lattice defects. From an ecological perspective, use of synthetic particles like polystyrene, PMMA and also gold nanoparticles is rampant and thus the routine use of biopolymers needs to be addressed.

1.6 Planar v/s Linear Evaporation front

Liquid crystalline polymers like cellulose, chitin, DNA and collagen self-assemble in living organisms to provide a variety of functions. Deriving inspiration and biomimicking their structural hierarchy has led researchers to explore a number of fields especially evaporation based self-assembly of particles. One of these is the use of air-liquid crystalline (LC) interface for organization of polymer LC domains into highly ordered films. Understanding this regulation is crucial to further applications in advanced biomedical materials, such as selective semipermeable membranes, drug delivery systems, and bioactuators. In previous studies, our group reported the orientational and deposition control from a planar and a linear evaporative front. **Fig. 1.10A** shows the method to control the evaporation front for deposition of the polymer, by varying the width of the container.[53] It was shown that drying 0.5 wt% sacran solution through a planar evaporation front led to hierarchical assembly from nano and submicron range ultimately resulting in a dried layered structure (**Fig. 1.10B**) demonstrating uniaxial swelling.[54] Additionally, it has been observed that drying the solution in a container with thickness less than capillary length leads to nucleation and deposition of micro-rods in a form of a vertical membrane which swells along its length.[55]

This study of geometrical control in the evaporation-induced self-assembly behavior of a polysaccharide solution through planar as well as linear evaporative fronts challenges curiosity. The planar front leads to deposition of layered, in-plane oriented film. Whereas, a linear front lead to nucleation followed by a vertically deposited membrane formed by the splitting of the interface. It is envisioned that optimizing drying conditions and concentration, other polymeric solutions can also split meniscus and deposit similarly in some definite patterns.

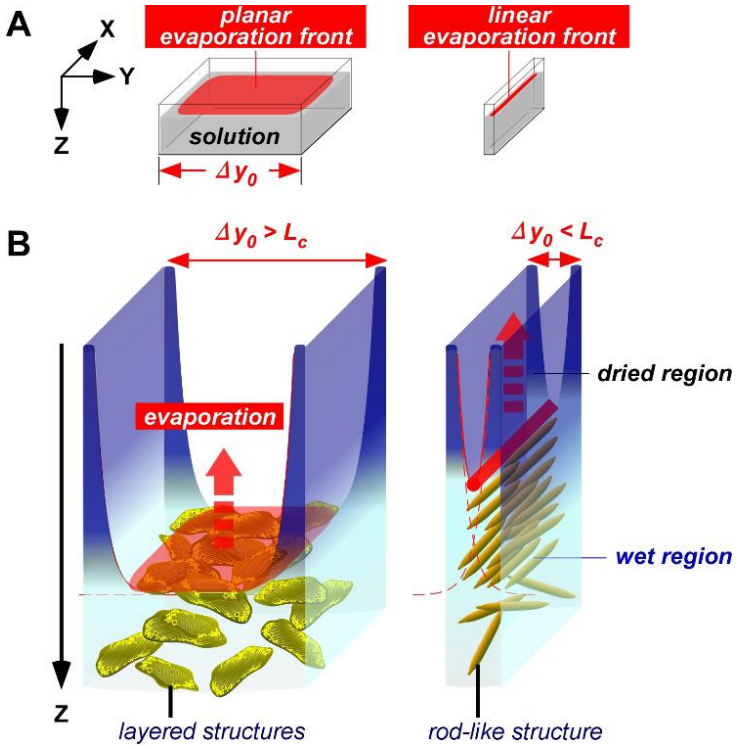

Figure 1.10 A. Geometrical control for planar or linear evaporation front by regulating the dimensions of container. **B.** Hypothesis of layered structure formation on a planar evaporation front and of rod-like structure formation on a linear evaporation front. The Δy_0 indicates the shorter length of the cuboid container. L_c indicates the critical capillary length, ~2 mm.[56]

1.7 Space-Partitioning phenomenon

Geometric control of the soft matter structure has been achieved at many scales through the interfacial and mechanical processes or instabilities.[57,58] The most well-known of these are the fingering patterns generated from viscous liquids[59–61] as well as the buckling patterns formed during the swelling/deswelling cycle of gels.[62–64] In a recent research by our group, sacran solution was dried from a limited space resulting in a non-equilibrium state between sacran deposition and hydration.[55] Sacran microdomains oriented parallel to the drying air-LC interface resulting in fusion and formation of a milliscale macrodomain. This 'skin layer'[65] macrodomain prevents the water evaporation causing a situation of thermodynamic dissipation, and a structure vertically bridging the gap between the two substrates, is deposited (**Fig. 1.11**).

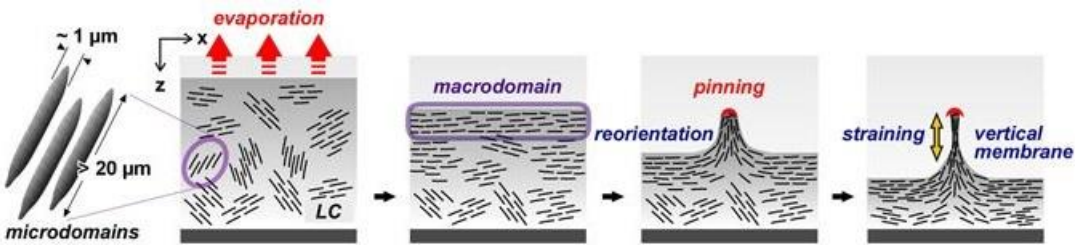

Figure 1.11 Schematic illustration for formation of vertical membranes by drying of a LC polymer solution in limited space with a narrow gap. Rod-like microdomains orient from the air-LC interface parallel to the contact line in the drying process. By drying in limited space, the non-equilibrium state between deposition and hydration near the interface causes pinning and vertical membrane formation between the narrow gap. The *Z*-direction is parallel to the direction of gravity. The gap between glass slides is Δy_0 = 1 mm. Initial concentration of sacran: 0.5 wt%. Drying atmosphere: 60 °C under air pressure.[55]

It was observed that the side walls had oriented adsorption which induced the initial pinning. The liquid phase showed orientation along the *Z*-direction whereas the top section was oriented along the *X*-axis. After this pinning, the polymer deposition was positioned along the *YZ*-plane and a thin membrane was formed bridging the glass substrates. The authors have shown a clear schematic illustration of the whole ongoing process along with the specific forces involved

(**Fig. 1.12**). According, the strained state with capillary force in the upward, *Z*(-)-direction and the gravity in the *Z*(+)-direction led to pinning and deposition of the nucleus. After this the effect of the capillary force was pacified and the microdomains reoriented along the *Y*-axis with ease.

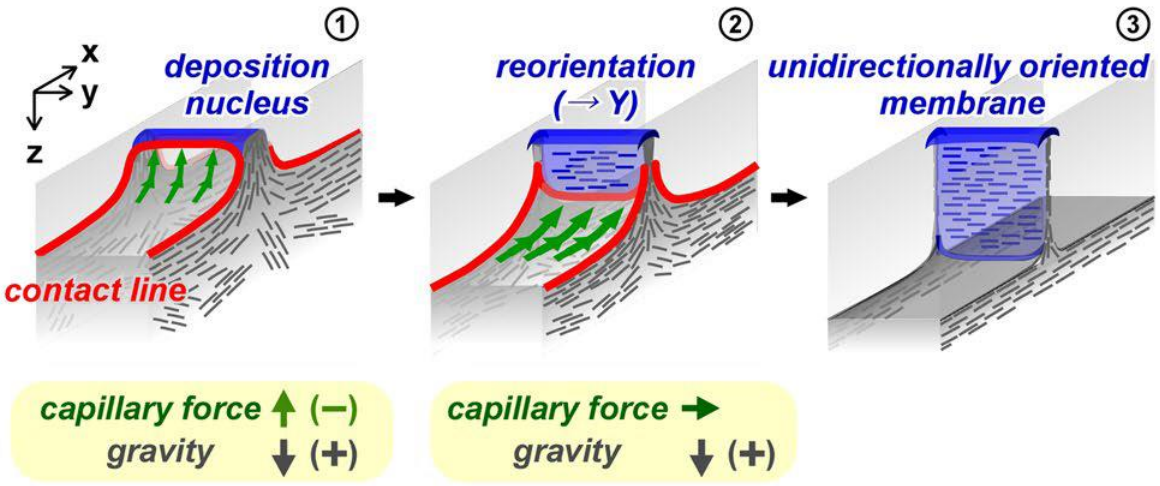

Figure 1.12 Schematic illustration of a unidirectionally oriented membrane formation utilizing the air-liquid-solid phase contact line during the drying process in limited space. 1) Just after generation of nucleus, which links the glass slides, the capillary force on the nucleus is in the direction opposite that of gravity. 2) After formation of the nuclei-cap, the effect of the capillary force in the *Z*-direction is relieved. 3) The microdomain integrates with the contact line to form a unidirectionally oriented membrane.[55]

This partitioning phenomenon is explained as a balance between the rate of polymer deposition and evaporation rate. When the X-width was increased keeping other factors constant, the side wall polymer deposition could not keep up with the evaporation rate resulting in additional deposits at specific positions on the substrate. Thus, the partition created with this additional polymer deposition helped prevent further growing of the macrodomain at the air-LC interface.

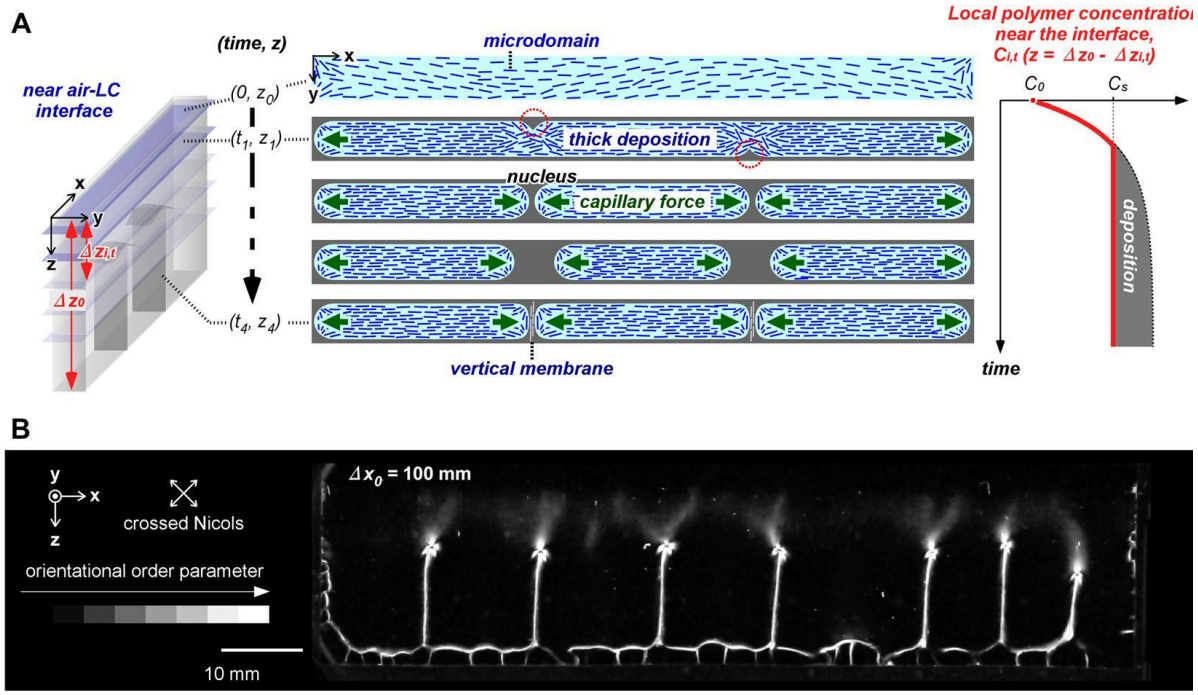

Figure 1.13 Macro-space partitioning via membrane walls in top-side-open cell. (**A**) Schematic illustrations of cross-sectional views in the *XY*-plane near the air-LC interface, and the change in polymer concentration in time course. When the concentration is saturated at the interface, the polymer is deposited at several specific points as thick nuclei on the walls. These points grow into a link between the slides, and the capillary force enhances the formation of vertical membranes. C_0: initial concentration; C_S: saturated concentration; C_i,t: local polymer concentration near the interface in a partitioned space *i* at time *t*. (**B**) Macro-space partitioning by multiple vertical membranes dried in limited space with *X*-width, Δx_0 = 100 mm. The *Y*-thickness is Δy_0 = 1 mm. Initial concentration of sacran: 0.5 wt%. Drying atmosphere: 60 °C under air pressure.[55]

1.8 Objectives of this Research

The liquid crystal forms of biological origin have not received due importance in the research community despite they being an integral part of every life form. The major challenge is the study of organization of biopolymers with the polydispersity in the fibrils of these macromolecules posing as a bottleneck in measurements. However, shifting the focus on techniques that can take advantage of these anisotropic aggregates can be fruitful (**Fig. 1.14**). The inherent hierarchical self-assembly of sacran during the drying process was a high motivation for further research.

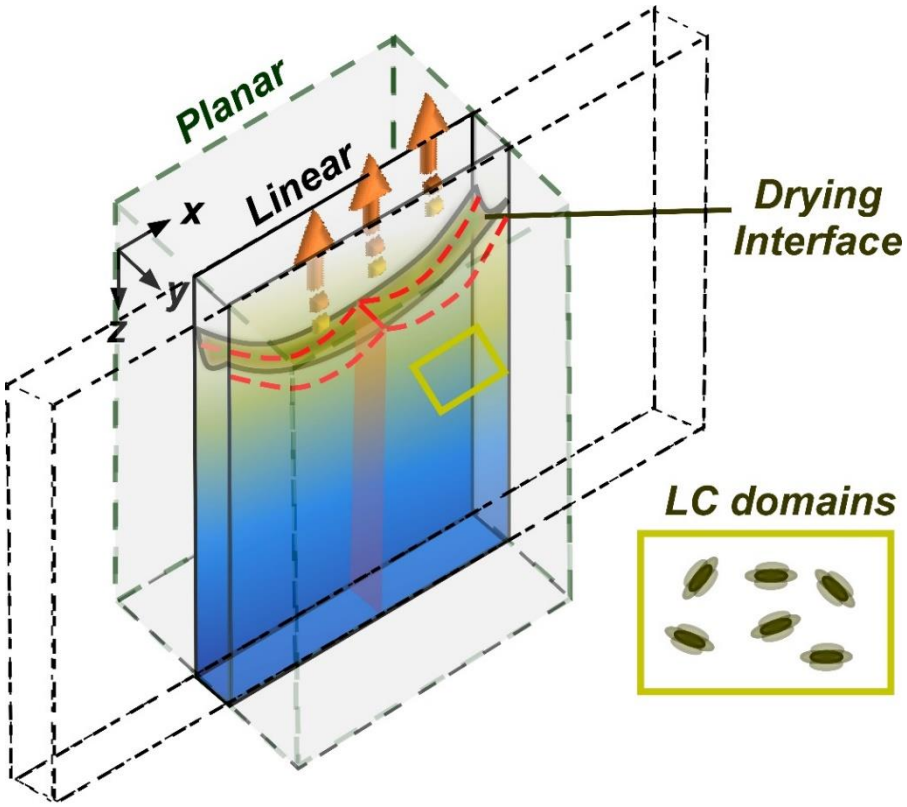

Figure 1.14 Schematic illustration for the different factors (like geometry of the container, drying temperature, size and mobility of LC domains *etc*.) affecting the drying of a LC solution.

The work in this thesis was initiated so as to shed light on the following,

- Understanding the theoretical aspects of interfacial curves during drying of polysaccharide solution in a linear evaporation front.
- Proposing and executing a strategy to control the assembling and orientation of LC domains of polysaccharides at the micron-level .
- Determining the key factors affecting the deposition and bridging during drying process .

The space-partitioning phenomenon has opened a novel, unique and highly convenient route to prepare oriented films of micrometre thickness. The technique is simple to apply as shown for sacran solutions and involves just drying under appropriate conditions. However, there are still many unresolved issues to deal with. Is this process applicable to other polysaccharide solutions ? Is only vertical bridging possible ? What is the theory behind such kind of a space-dependent partitioning ? What will be the effect of varying experimental factors ?

References

1. Springer, N. M., Lisch, D. & Li, Q. Creating Order from Chaos: Epigenome Dynamics in Plants with Complex Genomes. *Plant Cell* **28**, 314–325 (2016).
2. Skarda, C. A. & Freeman, W. J. How brains make chaos in order to make sense of the world. *Behav. Brain Sci.* **10**, 161–173 (1987).
3. Rogers, A. R. Order emerging from chaos in human evolutionary genetics. *Proc. Natl. Acad. Sci. U. S. A.* **98**, 779–780 (2001).
4. Fechtenko, A. Self-Organized Discotic Liquid Crystals for High-Efficiency Organic Photovoltaics. *Science* **1119**, 1119–1123 (2008).
5. O'Neill, M. & Kelly, S. M. Ordered materials for organic electronics and photonics. *Adv. Mater.* **23**, 566–584 (2011).
6. Liu, Y. *et al.* Self-organized cholesteric liquid crystal polymer films with tunable photonic band gap as transparent and flexible back-reflectors for dye-sensitized solar cells. *Nano Energy* **26**, 648–656 (2016).
7. Sornkamnerd, S., Okajima, M. K., Matsumura, K. & Kaneko, T. Micropatterned Cell Orientation of Cyanobacterial Liquid-Crystalline Hydrogels. *ACS Appl. Mater. Interfaces* **10**, 44834–44843 (2018).
8. Agarwal, A. *et al.* Micropatterning alginate substrates for in vitro cardiovascular muscle on a chip. *Adv. Funct. Mater.* **23**, 3738–3746 (2013).
9. Osada, Y., Okuzaki, H. & Hori, H. A polymer gel with electrically driven motility. *Nature* **355**, 242 (1992).
10. Kim, Y. S. *et al.* Thermoresponsive actuation enabled by permittivity switching in an electrostatically anisotropic hydrogel. *Nat. Mater.* **14**, 1002–1007 (2015).
11. Meena, R. S. Possession and transfer of copyrights of a cinematograph film. *J. Intellect. Prop. Rights* **21**, 283–287 (2016).

12. Xia, Y., Gates, B., Yin, Y. & Lu, Y. Monodispersed Colloidal Spheres: Old Materials with New Applications. *Adv. Mater.* **12**, 693–713 (2000).

13. Nelson, E. E. & Guyer, A. E. NIH Public Access. **1**, 233–245 (2012).

14. Rickert, J., Weiss, T. & Göpel, W. Self-assembled monolayers for chemical sensors: molecular recognition by immobilized supramolecular structure. *Sensors Actuators B Chem.* **31**, 45–50 (1996).

15. Mitov, M. Cholesteric liquid crystals with a broad light reflection band. *Adv. Mater.* **24**, 6260–6276 (2012).

16. Wasan, D. T. & Nikolov, A. D. Spreading of nanofluids on solids. *Nature* **423**, 156 (2003).

17. Bhushan, B., Jung, Y. C., Niemietz, A. & Koch, K. Lotus-like biomimetic hierarchical structures developed by the self-assembly of tubular plant waxes. *Langmuir* **25**, 1659–1666 (2009).

18. Kim, D. S., Suh, A., Yang, S. & Yoon, D. K. Grooving of nanoparticles using sublimable liquid crystal for transparent omniphobic surface. *J. Colloid Interface Sci.* **513**, 585–591 (2018).

19. Bisoyi, H. K. & Kumar, S. Liquid-crystal nanoscience: An emerging avenue of soft self-assembly. *Chem. Soc. Rev.* **40**, 306–319 (2011).

20. Lagerwall, J. P. F. & Scalia, G. A new era for liquid crystal research: Applications of liquid crystals in soft matter nano-, bio- and microtechnology. *Curr. Appl. Phys.* **12**, 1387–1412 (2012).

21. Maeda, H. & Maeda, Y. Liquid Crystal Formation in Suspensions of Hard Rodlike Colloidal Particles: Direct Observation of Particle Arrangement and Self-Ordering Behavior. *Phys. Rev. Lett.* **90**, 18303 (2003).

22. Kato, T., Mizoshita, N. & Kishimoto, K. Functional liquid-crystalline assemblies: Self-

organized soft materials. *Angew. Chemie - Int. Ed.* **45**, 38–68 (2005).

23. Tsai, J.-H. & McKee, B. D. Homologous pairing and the role of pairing centers in meiosis. *J. Cell Sci.* **124**, 1955–1963 (2011).
24. Giraud-Guille, M. M. Twisted plywood architecture of collagen fibrils in human compact bone osteons. *Calcif. Tissue Int.* **42**, 167–180 (1988).
25. Cen, L., Liu, W., Cui, L., Zhang, W. & Cao, Y. Collagen tissue engineering: Development of novel biomaterials and applications. *Pediatr. Res.* **63**, 492–496 (2008).
26. Mitov, M. Cholesteric liquid crystals in living matter. *Soft Matter* **13**, 4176–4209 (2017).
27. Hamley, I. W. Liquid crystal phase formation by biopolymers. *Soft Matter* **6**, 1863–1871 (2010).
28. Nwodo, U. U., Green, E. & Okoh, A. I. Bacterial exopolysaccharides: Functionality and prospects. *Int. J. Mol. Sci.* **13**, 14002–14015 (2012).
29. Diversity, S. & Versatility, F. *P O L YS A C C H A R I D E S.*
30. Lemon, D. J., Yang, X., Srivastava, P., Luk, Y. Y. & Garza, A. G. Polymertropism of rod-shaped bacteria: movement along aligned polysaccharide fibers. *Sci. Rep.* **7**, 1–13 (2017).
31. Wang, H., Wilksch, J. J., Strugnell, R. A. & Gee, M. L. Role of Capsular Polysaccharides in Biofilm Formation: An AFM Nanomechanics Study. *ACS Appl. Mater. Interfaces* **7**, 13007–13013 (2015).
32. Turner, R. D., Mesnage, S., Hobbs, J. K. & Foster, S. J. Molecular imaging of glycan chains couples cell-wall polysaccharide architecture to bacterial cell morphology. *Nat. Commun.* **9**, (2018).
33. Hussain, S. *et al.* MreB filaments align along greatest principal membrane curvature to

orient cell wall synthesis. *Elife* **7**, 1–45 (2018).

34. Xylinum, A. XYLINUM * VIII . On the Formation and Orientation of Bacterial Cellulose Fibrils in the Presence of Acidic Polysaccharides. 191–207 (1962).
35. Shaw, S. L. & Quatrano, R. S. The role of targeted secretion in the establishment of cell polarity and the orientation of the division plane in Fucus zygotes. *Development* **122**, 2623–2630 (1996).
36. Donaldson, L. A. & Knox, J. P. Localization of Cell Wall Polysaccharides in Normal and Compression Wood of Radiata Pine: Relationships with Lignification and Microfibril Orientation. *Plant Physiol.* **158**, 642–653 (2012).
37. Zolghadr, B. *et al.* Appendage-mediated surface adherence of Sulfolobus solfataricus. *J. Bacteriol.* **192**, 104–110 (2010).
38. Flemming, H.-C. & Wingender, J. The biofilm matrix. *Nat. Rev. Microbiol.* **8**, 623 (2010).
39. Shim, S. E., Yashin, V. V. & Isayev, A. I. Ultraschall-devulkanisation von siliconkautschukvulkanisat mit gefällter Kieselsäure. *Gummi, Fasern, Kunststoffe* **55**, 304–311 (2002).
40. Lawrence, J. R., Swerhone, G. D. W., Kuhlicke, U. & Neu, T. R. In situ evidence for microdomains in the polymer matrix of bacterial microcolonies. *Can. J. Microbiol.* **53**, 450–458 (2007).
41. Marshall, W. F. Origins of cellular geometry. *BMC Biol.* **9**, (2011).
42. Okajima-Kaneko, M., Ono, M., Kabata, K. & Kaneko, T. Extraction of novel sulfated polysaccharides from Aphanothece sacrum (Sur.) Okada, and its spectroscopic characterization. *Pure Appl. Chem.* **79**, 2039–2046 (2007).
43. Mitsumata, T. *et al.* Ionic state and chain conformation for aqueous solutions of supergiant cyanobacterial polysaccharide. *Phys. Rev. E* **87**, 42607 (2013).

44. Okajima, M. K., Sornkamnerd, S. & Kaneko, T. Development of Functional Bionanocomposites Using Cyanobacterial Polysaccharides. *Chem. Rec.* **18**, 1167–1177 (2018).

45. Okeyoshi, K., Okajima, M. K. & Kaneko, T. Milliscale Self-Integration of Megamolecule Biopolymers on a Drying Gas–Aqueous Liquid Crystalline Interface. *Biomacromolecules* **17**, 2096–2103 (2016).

46. Okajima, M. K. *et al.* Anisotropic swelling in hydrogels formed by cooperatively aligned megamolecules. *RSC Adv.* **5**, 86723–86729 (2015).

47. Amornwachirabodee, K., Okajima, M. K. & Kaneko, T. Uniaxial Swelling in LC Hydrogels Formed by Two-Step Cross-Linking. *Macromolecules* **48**, 8615–8621 (2015).

48. Rees, D. A. Shapely polysaccharides. The eighth Colworth medal lecture. *Biochem. J.* **126**, 257–73 (1972).

49. Milas, M. & Rinaudo, M. Properties of xanthan gum in aqueous solutions: Role of the conformational transition. *Carbohydr. Res.* **158**, 191–204 (1986).

50. Palaniraj, A. & Jayaraman, V. Production, recovery and applications of xanthan gum by Xanthomonas campestris. *J. Food Eng.* **106**, 1–12 (2011).

51. Zhang, S. Y., Regulacio, M. D. & Han, M. Y. Self-assembly of colloidal one-dimensional nanocrystals. *Chem. Soc. Rev.* **43**, 2301–2323 (2014).

52. Kaplan, C. N., Wu, N., Mandre, S., Aizenberg, J. & Mahadevan, L. Dynamics of evaporative colloidal patterning. *Phys. Fluids* **27**, 92105 (2015).

53. Okeyoshi, K. *et al.* Drying-Induced Self-Similar Assembly of Megamolecular Polysaccharides through Nano and Submicron Layering. *Langmuir* **33**, 4954–4959 (2017).

54. Joshi, G., Okeyoshi, K., Okajima, M. K. & Kaneko, T. Directional control of diffusion

and swelling in megamolecular polysaccharide hydrogels. *Soft Matter* **12**, 5515–5518 (2016).

55. Okeyoshi, K., Okajima, M. K. & Kaneko, T. Emergence of polysaccharide membrane walls through macro-space partitioning via interfacial instability. *Sci. Rep.* **7**, 5615 (2017).

56. Okeyoshi, K. *et al.* Drying-Induced Self-Similar Assembly of Megamolecular Polysaccharides through Nano and Submicron Layering. *Langmuir* **33**, 4954–4959 (2017).

57. Glansdorff, P. & Prigogine, I. Thermodynamic Theory of Structure, Stability and Fluctuations. *Am. J. Phys.* **41**, 147–148 (1973).

58. Cross, M. C. & Hohenberg, P. C. Pattern formation outside of equilibrium. *Rev. Mod. Phys.* **65**, 851–1112 (1993).

59. Cazabat, A. M., Heslot, F., Troian, S. M. & Carles, P. Fingering instability of thin spreading films driven by temperature gradients. *Nature* **346**, 824 (1990).

60. Rondelez, J. B. B. and F. B.-W. and F. Exponential Growth of Fingering Instabilities of Spreading Films Under Horizontal Thermal Gradients. *EPL (Europhysics Lett.* **19**, 97 (1992).

61. Lajeunesse, E., Martin, J., Rakotomalala, N. & Salin, D. 3D Instability of Miscible Displacements in a Hele-Shaw Cell. 1–4 (1997).

62. Drummond, W. R., Knight, M. L., Brannon, M. L. & Peppas, N. A. Surface instabilities during swelling of pH-sensitive hydrogels. *J. Control. Release* **7**, 181–183 (1988).

63. Tanaka, T. *et al.* Mechanical instability of gels at the phase transition. *Nature* **325**, 796 (1987).

64. Tallinen, T., Biggins, J. S. & Mahadevan, L. Surface sulci in squeezed soft solids.

Phys. Rev. Lett. **110**, 1–5 (2013).

65. Suzuki, A., Yoshikawa, S. & Bai, G. Shrinking pattern and phase transition velocity of poly(N-isopropylacrylamide) gel. *J. Chem. Phys.* **111**, 360–367 (1999).

Chapter 2

Drying from Planar Evaporation Front

2.1 Introduction

Drying in a container resembles the case of planar front as water evaporation takes place only from the 2D interface. The ordering of particles of the solute can be brought about while drying with the rising concentration of the solution through that time duration. Anisotropy in the material is introduced through a variety of techniques like directional freezing,[1] elongating,[2–4] directional diffusion[5] and also solvent-casting.[6,7] The most commonly used and perhaps easiest of all is the solvent casting method for preparing films. A stress induced in the system due to the solvent removal results in the in-plane molecular orientation. When crosslinking points are introduced in these oriented films by chemical or physical treatments, the films swell in solvent to form oriented gel matrix. Hydrogels are said to be physically crosslinked in case of chain aggregation, association, complexation, crystallization or hydrogen bonding.[8] This is famously referred to as in-situ hydrogelation. The dried film can be stored for a long period of time as a precursor without any decaying in the meanwhile. It can thus be rehydrated just prior to the use. It has been reported that thinner films are effective in driving the orientation of the polymer chains as compared to thicker films. However, too thin films are not self-supporting and in practise cannot be used as precursors for further preparation of hydrogels. Again, self-supporting films can behave as precursors, but they fail to achieve high degree of in-plane molecular orientation precisely. This, it is difficult to prepare such films with the overall desirable properties using solvent-casting technique.

This problem has been resolved by using sacran solution to prepare the dried sacran film and then after crosslinking, re-swelling the films to obtain hydrogels.[9,10] Sacran adopts a nematic liquid crystalline state even at a very low concentration of 0.2 wt%.[11] The formation of state at an extremely low critical concentration is indicative of the fact that sacran chains have high rigidity.[12] The orientation degree was evaluated by WAXS imaging, which gave values comparable to the value of nematic solutions.[9] Considering these potentials, functional

biomaterials such as smart drug targeting systems could be designed, if water diffusion via uniaxial swelling could be controlled. However, directional relation between the water diffusion and the swelling behavior of anisotropic hydrogels still remains unclear.

There has been significant development in the area of smart hydrogels. However, commercial hydrogels suffer from limited utility owing to their size dependence and thus it is difficult to manipulate their swelling/shrinking kinetics.[13] In this regard, the swelling and shrinking kinetics of every gel has been described to e under the influence of diffusion limited polymer network transport. Moreover, the proportionality relation stands as the inverse of the rate to the square of the gel dimension.[14,15]

In this chapter, I demonstrate the directional control of diffusion and swelling in sacran hydrogels for water absorption by focusing on the anisotropic structures. Investigating the swelling ratio and swelling kinetics along the three-dimensions, the effects of the anisotropic structure on diffusion are discussed. In addition, clarification of the structural features responsible for the uniaxial swelling is necessary for the design of anisotropic soft materials. The macroscopic directional control of water diffusion is critical for the practical application of these hydrogels.[16–18] The ability to manipulate the size, diffusion or rate of release and swelling properties of a hydrogel is indispensable for its further application in biomaterials, medical applications and tissue engineering.

2.2 Materials and Methods

2.2.1 Materials: Sacran was extracted from *Aphanothece sacrum* as per the procedure described in a previous study.[19]

2.2.2 Preparation of gels: 0.5% sacran solution was prepared by dissolving sacran fibers in pure water (< 80˚C) on a magnetic stirrer for ~12 hours. The resulting solution (~50 mL) was then poured into a 5 cm × 5 cm polypropylene case and kept in a temperature regulated oven at 60 ˚C for 24 hours with continuous air purging to prepare a dried thin film. The films were then annealed at 80 °C, 100 ˚C and 120 ˚C for 2 hours to obtain the required crosslinked gel films, which were left at ~25 ˚C to be used for swelling and kinetics experiments.

2.2.3 Measurements of swelling kinetics: The swelling kinetics of the hydrogel was measured from a dried state to a wet state in a pH 7 buffer solution for a duration of 24 hours, and their swelling rate was evaluated. The parameters, relaxation time (τ) and diffusion coefficient (D) were then calculated using the following equations.[20,21]

$$\ln\left[\frac{L_\infty - L(t)}{L_\infty - L_0}\right] \approx -\frac{1}{t}t + \ln\left[\frac{6}{p^2}\right] \quad (1)$$

$$D = \frac{L_{z\infty}^2}{\pi^2 \tau} \quad (2)$$

2.2.4 Measurements of swelling ratio: Samples were cut and kept in pH 8 buffer solution for 16 hours after measuring their initial thickness at ~25 ˚C. The change in length and thickness of the sample was analyzed using a cross-nicol polarimeter (**Fig. 2.1**). Next, the sample was transferred to buffer solutions of decreasing pH for over 45 minutes. The same procedure was repeated until swelling measurements were made in pH 2.2 buffer solution. The buffer

solutions (pH 2.2—8.0) were controlled by mixtures of citric acid and Na_2HPO_4. The swelling ratio was calculated by normalizing the dimensions at a given pH with the initial dimensions, L_0. This swelling ratio was eventually plotted against pH to obtain the equilibrium swelling graph.

2.2.5 SEM observation: The dried polymer films cut in 5 mm x 5 mm square, were observed by scanning electron microscopy (Hitachi, S-4500) without any metal modification.

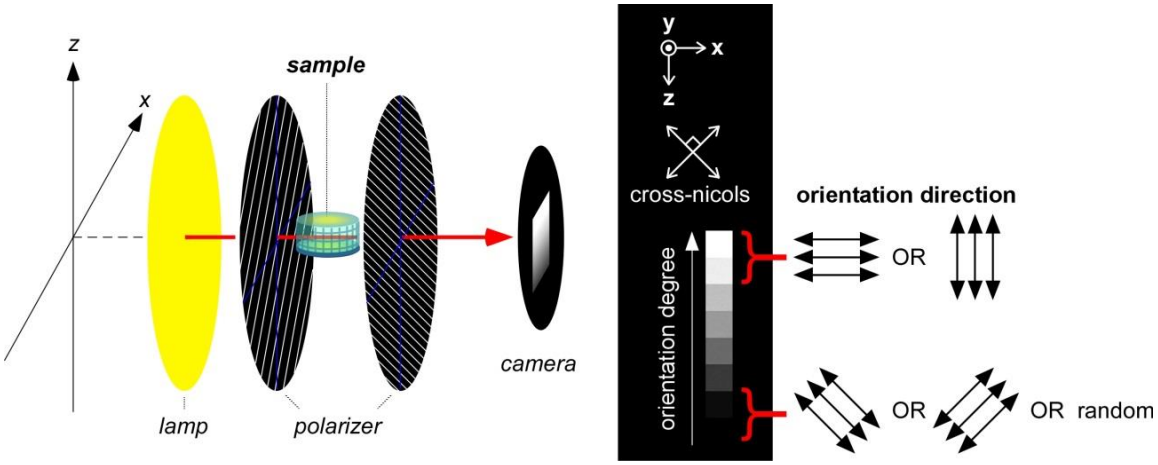

Figure 2.1 Schematic illustration of the experimental setup used for observations under cross-polarized light. The polarizers were normally adjusted to 45° and 135°. The transmitted light intensity was analysed by ImageJ to evaluate the degree of orientation.

2.3 Estimation of diffusion and swelling directions

The hydrogels were prepared in two steps (**Fig. 2.2**):

i) 0.5 wt% aqueous solution was dried at 60˚C in a container, and

ii) the dried polymer films were annealed at a given temperature to introduce crosslinking points according to previous studies.[9]

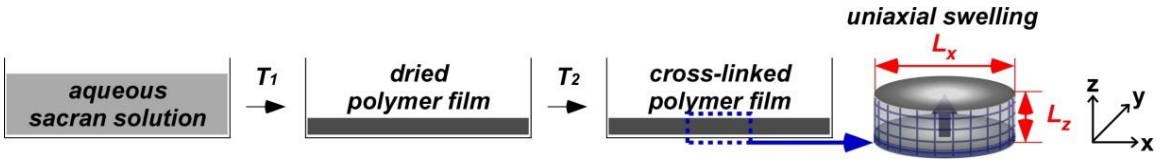

Figure 2.2 Schematic illustration of preparation of polymer film and introduction of crosslinks. An aqueous sacran solution is dried at T_1 as the first step, and the dried polymer film is annealed to introduce crosslinking points as the second step ($T_2 > T_1$).

To investigate the swelling kinetics and the subsequent orientation change, the swelling of a disk-shaped film with a diameter of 4 mm was monitored through the cross-nicols. As shown in **Fig. 2.3**, the change in the L_z showed a continuous increase with an oriented structure over time. This indicates that the oriented structure is maintained during the swelling process, even if the inclusion of water directly increases the distance between the crosslinked submicron-layers in the sacran film.

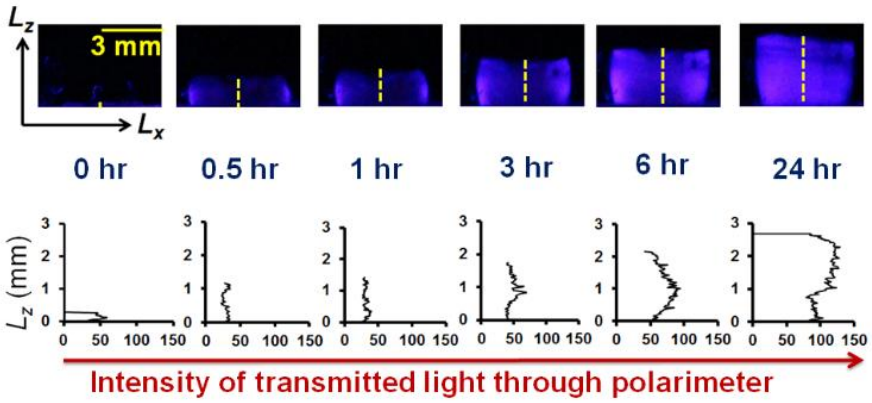

Figure 2.3 Thickness (L_z) showing a time dependent increase with an oriented structure.

To get an idea of the equilibrium time required for maximal swelling a gel sample was left in pH 7 buffer solution and checked at regular intervals. (**Fig. 2.4A**) It was found that the hydrogel swelled to its maximum capacity in 24 hours and thus all further kinetics experiments were performed for this much time duration. From the calculated value of the relaxation time τ for a number of gel films, the average value of the diffusion coefficient D, was found to be in the range of $10^{-7} – 10^{-8}$ cm^2 sec^{-1} (**Fig. 2.4B**).

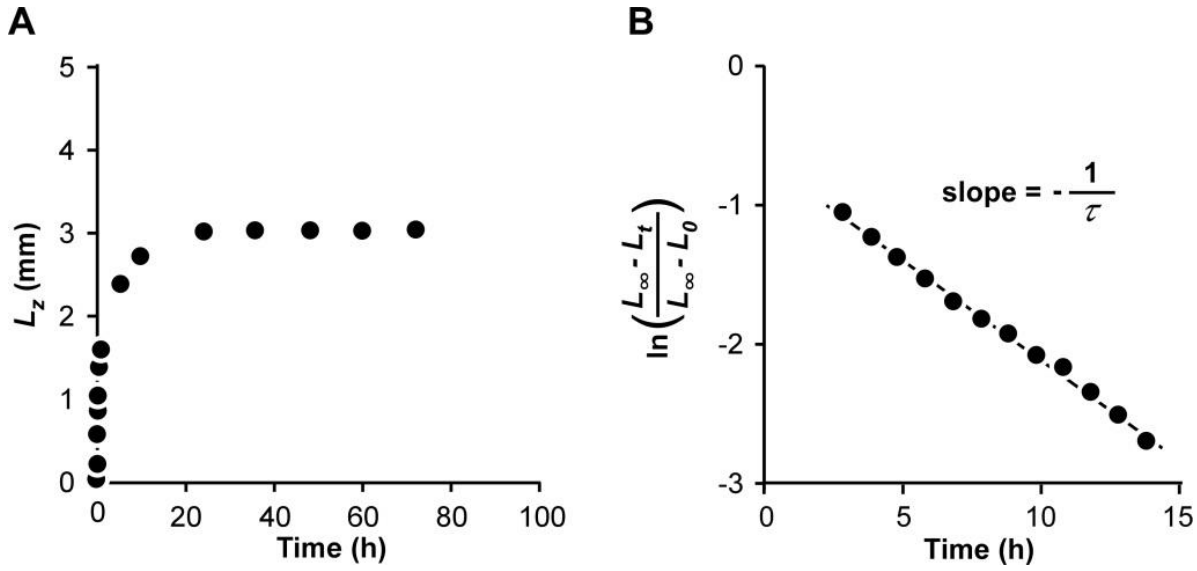

Figure 2.4 A. Swelling kinetics in the Z-direction of sacran gels from dried state to wet state at pH7 over 3 days. **B.** The linear plot obtained after solving equation (1).

Although this value is similar to that of typical hydrogels, it is estimated to be the combination of the diffusion coefficients in the direction of the XY-plane and in the direction of the Z-axis (**Fig. 2.5A**). To evaluate the direction of water diffusion into the hydrogels, two film samples with equal dimensions were used to analyze swelling kinetics. Silicon grease was used to inhibit water absorption through the top and bottom surfaces of one sample, and swelling kinetics were compared to another non-greased sample (**Fig. 2.5B**). Interestingly, in spite of the fact that the non-greased film had ~60 times more initial area available for water absorption, (non-greased film: $2\pi rL_{z0} + 2\pi r^2$ = 25.5 mm^2, greased film: $2\pi rL_{z0}$ = 0.414 mm^2), there was little difference in the swelling speed. Using the dried films with an initial thickness of 33 μm, the non-greased film swelled to 970 μm and the greased film swelled to 890 μm in the initial 30 minutes. Eventually both films swelled to the same extent: 1200 μm after 10 hours.

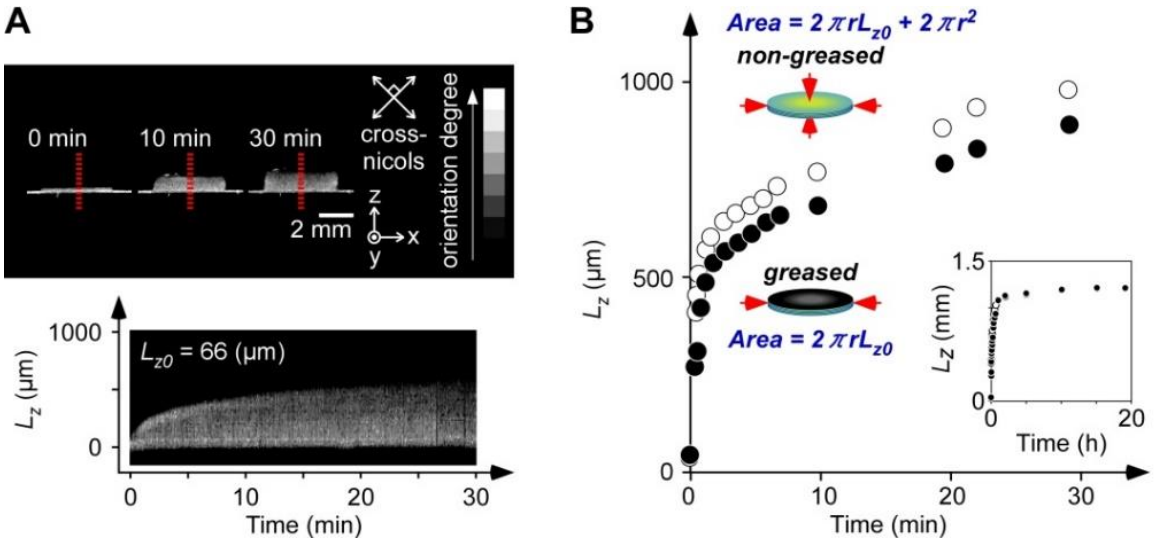

Figure 2.5 Kinetics of the uniaxially-swelling gels and control of the diffusion direction. **A.** Side views of the hydrogel film from a dry state to a wet state under cross-polarized light, and swelling kinetics constructed from a sequential line up of the dotted lines. **B.** Comparison of the swelling kinetics between a non-greased sample (white circle) and a sample that was greased on the top and bottom (black circle). Initial thickness: 33 μm.

These results are clearly suggestive of the fact that diffusion occurred mostly along the XY-plane leading to swelling in the Z-direction along the thickness (**Fig. 2.6**).

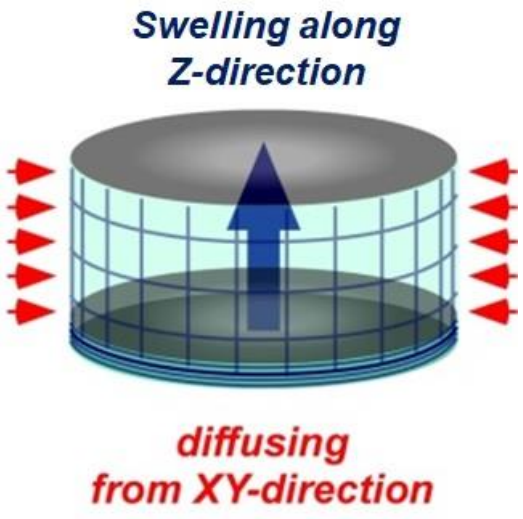

Figure 2.6 Schematic illustration of the directions of diffusion and swelling of the sacran hydrogel.

2.4 Estimation of equilibrium swelling ratio

To evaluate the swelling behaviors in pH ranges of physiological conditions, the dried films were cut for measurement of the equilibrium swelling ratio (**Fig. 2.7**).

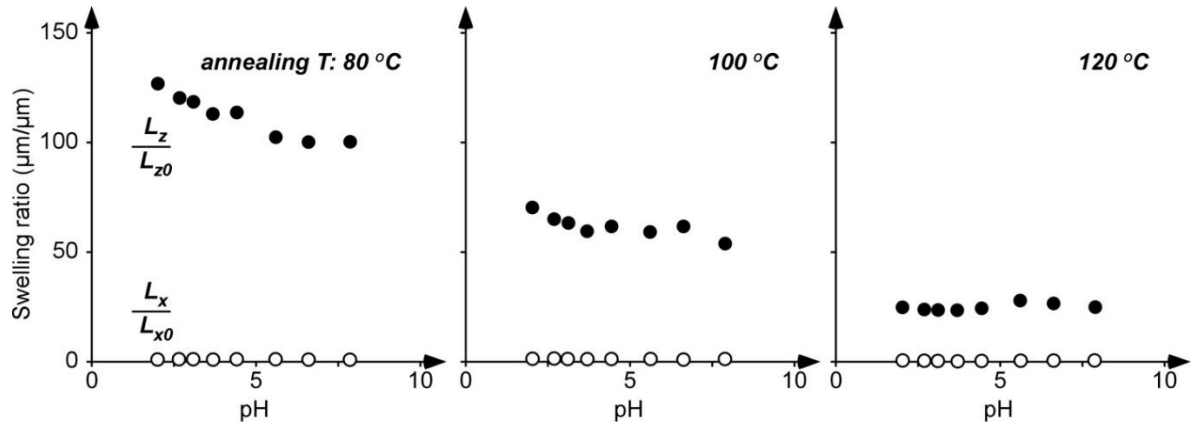

Figure 2.7 pH-dependence of the swelling ratio in the planar direction and the perpendicular direction for sacran hydrogels annealed at a given temperature. Drying temperature: 60 ˚C. L_{x0} = length of the dried gel film in the X-axis direction, L_{z0} = length of the dried gel film in the *Z*-axis direction. L/L_0: normalized lengths of the gel film. L_{z0} = 21 μm (annealing temperature for physical crosslinking: 80 ˚C), 21 μm (100 ˚C), and 25 μm (120 ˚C).

At any annealed temperature, the swelling ratios of the L_z/L_{z0} (≈ 30—130) were much larger than those of L_x/L_{x0} (≈ 1.0—1.5), indicating the uniaxial swelling in the *Z*-direction at all pH conditions. With an increase in the annealing temperature, this ratio decreased due to the increased amount of the introduced crosslinking points. In case of samples annealed at 80 ˚C or 100 ˚C, the pH-dependence of L_z/L_{z0} was detected in the acidic pH range of pH 2 – 6, which is thought to be due to the inter-layer hydrogen bonding between the amino and oxygen of the carboxyl group, broken at lower pH due to protonation of the amino group.

To estimate the effect of the annealing temperature, and by extension the induced crosslinking, on the inter-layer structure, the dependence of the initial thickness (L_{z0}) on the swelling ratio L_z/L_{z0} of the gel film was measured at pH 7 (**Fig. 2.8A**). In the range of L_{z0} > ~25

μm L_z/L_{z0} showed a gradual increase; but in the range of L_{z0} < ~25 μm, L_z/L_{z0} showed a remarkable increase with decreasing L_{z0}. The thinner films swelled to a larger extent than their thicker counterparts. This is probably because of the availability of more crosslinking junctions in thicker films as the micro-domains might be oriented in a random fashion instead of the in-plane aligned domains in the thinner films.

To clarify the effect of the initial thickness on the swelling behaviors, the cross-section of the dried polymer film was observed by scanning electron microscope (SEM) (**Fig. 2.8B**). As can be seen, thinner films (L_{z0} = 25 μm) had layered structures whereas thicker films (L_{z0} = 60 μm) had similarly layered structures only in the upper half but not in the lower half. In the middle, tilted layered structures and non-layered structures could be observed. From these images, it can be seen that the number of inter-layer crosslinking junctions in thicker films with non-uniformity of layering is higher than and thus there is a lesser swelling in thicker films (**Fig. 2.8C**). In addition, to check the thickness of each layer, the SEM images were analyzed by ImageJ (see red line, **Fig. 2.8B**). The submicron-layer thickness was estimated to be 0.1—0.2 μm on average, and the number of layers in a film with 25-μm-thickness was calculated to be more than 100 layers. This estimation supports the existence of inter-layer crosslinking junctions and thereby their role in the effective swelling of the hydrogel. Therefore, the thickness, which is a critical attribute of the film is related to the effective thickness of the oriented structure at the gas-liquid interface while drying during preparation procedures. Controlling the gas-liquid interface during drying is much more effective for enhancing the orientation parallel to the interface than controlling the solid-liquid interface. In fact, a polymer film with a highly oriented structure was easily prepared by controlling the height of the aqueous solution during the drying process.

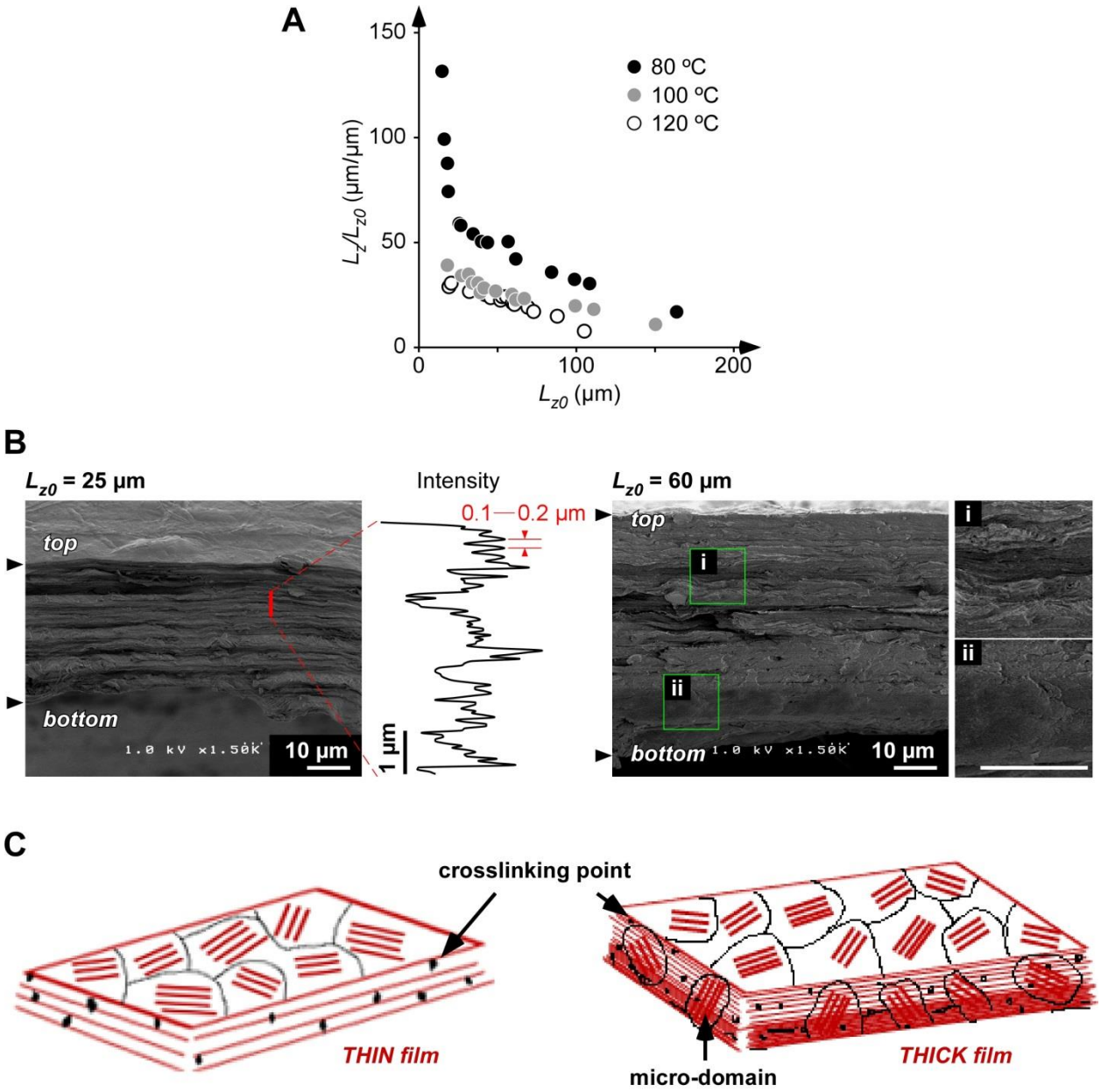

Figure 2.8 Anisotropic structures of sacran hydrogels and the effect of the thickness on swelling properties. **A.** Swelling ratio in the *Z*-direction as a function of the thickness of the dried films. L_{z0} = length of the dried gel film in the *Z*-axis direction. L/L_0: normalized lengths of the gel film. pH = 7.0. **B.** Cross-sectional views of the dried films at a given thickness observed by SEM. **C.** Schematic illustration of the layered structure affected by the directions of the micro-domains for thin and thick films.

2.5 Conclusions

The uniaxial swelling of sacran hydrogels was clarified by focusing on the relation of the swelling direction and the anisotropic structures. From the SEM observation, the dried polymer film was found to have a layered structure, 0.1 μm thick in planar orientation. These characteristics substantially contribute to uniaxial swelling. Due to the presence of this layered structure in the hydrogel, the directional control for diffusion parallel to the planar direction and swelling in the lateral direction was possible. It is believed that these hydrogels with uniaxial swelling will be useful for dynamic control in biomedical applications such as engineering replacement tissues, reconstructive surgeries, and the design of sustained drug delivery device.

References

1. Momoda, J., Monobe, K., Shimamura, K., Achife, E. C. & Yokoyama, F. Morphology of optically anisotropic agarose hydrogel prepared by directional freezing. *Colloid Polym. Sci.* **268**, 552–558 (2005).

2. Haque, M. A., Kamita, G., Kurokawa, T., Tsujii, K. & Gong, J. P. Unidirectional alignment of lamellar bilayer in hydrogel: One-dimensional swelling, anisotropic modulus, and stress/strain tunable structural color. *Adv. Mater.* **22**, 5110–5114 (2010).

3. Kaneko, T., Ogomi, D., Mitsugi, R., Serizawa, T. & Akashi, M. Mechanically drawn hydrogels uniaxially orient hydroxyapatite crystals and cell extension. *Chem. Mater.* **16**, 5596–5601 (2004).

4. Yang, W., Furukawa, H. & Gong, J. P. Highly Extensible Double-Network Gels with Self-Assembling Anisotropic Structure. *Adv. Mater.* **20**, 4499–4503 (2008).

5. Masumoto, J. *et al.* Studies on the Formation Mechanism and the Structure of the Anisotropic Collagen Gel Prepared by Dialysis-Induced Anisotropic Gelation. *Biomacromolecules* **13**, 29–39 (2011).

6. Shimada, H., Nobukawa, S. & Yamaguchi, M. Development of microporous structure and its application to optical film for cellulose triacetate containing diisodecyl adipate. *Carbohydr. Polym.* **120**, 22–28 (2015).

7. Machell, J. S., Greener, J. & Contestable, B. A. Optical Properties of Solvent-Cast Polymer Films. *Macromolecules* **23**, 186–194 (1990).

8. Siepmann, J., Siegel, R. A. & Rathbone, M. J. *Fundamentals and applications of controlled release drug delivery*. *Fundamentals and Applications of Controlled Release Drug Delivery* (2012).

9. Okajima, M. K. *et al.* Anisotropic swelling in hydrogels formed by cooperatively aligned megamolecules. *RSC Adv.* **5**, 86723–86729 (2015).

10. Amornwachirabodee, K., Okajima, M. K. & Kaneko, T. Uniaxial Swelling in LC Hydrogels Formed by Two-Step Cross-Linking. *Macromolecules* **48**, 8615–8621 (2015).

11. Mitsumata, T. *et al.* Ionic state and chain conformation for aqueous solutions of supergiant cyanobacterial polysaccharide. *Phys. Rev. E* **87**, 42607 (2013).

12. Okajima, M. K., Kaneko, D., Mitsumata, T., Kaneko, T. & Watanabe, J. Cyanobacteria That Produce Megamolecules with Efficient Self-Orientations. *Macromolecules* **42**, 3057–3062 (2009).

13. Aoyagi, T. *et al.* Smart biomaterials. *Springer* (2014).

14. Feksa, L. R. *et al.* Hydrogels for biomedical applications. *Nanostructures Eng. Cells, Tissues Organs From Des. to Appl.* **64**, 403–438 (2018).

15. Caló, E. & Khutoryanskiy, V. V. Biomedical applications of hydrogels: A review of patents and commercial products. *Eur. Polym. J.* **65**, 252–267 (2015).

16. Barba, A. A. *et al.* On the Behavior of HPMC/Theophylline Matrices for Controlled Drug Delivery. *J. Pharm. Sci.* **98**, 4100–4110 (2009).

17. He, H. *et al.* Hydrogel with Aligned and Tunable Pore Via 'Hot Ice' Template Applies as Bioscaffold. *Adv. Healthc. Mater.* **5**, 648–652 (2016).

18. Chang, C., He, M., Zhou, J. & Zhang, L. Swelling behaviors of pH- and salt-responsive cellulose-based hydrogels. *Macromolecules* **44**, 1642–1648 (2011).

19. Okajima-Kaneko, M., Ono, M., Kabata, K. & Kaneko, T. Extraction of novel sulfated polysaccharides from Aphanothece sacrum (Sur.) Okada, and its spectroscopic

characterization. *Pure Appl. Chem.* **79**, 2039–2046 (2007).

20. Ritger, P. L. & Peppas, N. A. A simple equation for description of solute release. *J. Control. Release.* **5**, 23–36 (1987).

21. Tanaka, T. *et al.* Mechanical instability of gels at the phase transition. *Nature* **325**, 796 (1987).

22. Joshi, G., Okeyoshi, K., Okajima, M. K. & Kaneko, T. Directional control of diffusion and swelling in megamolecular polysaccharide hydrogels. *Soft Matter* **12**, 5515–5518 (2016).

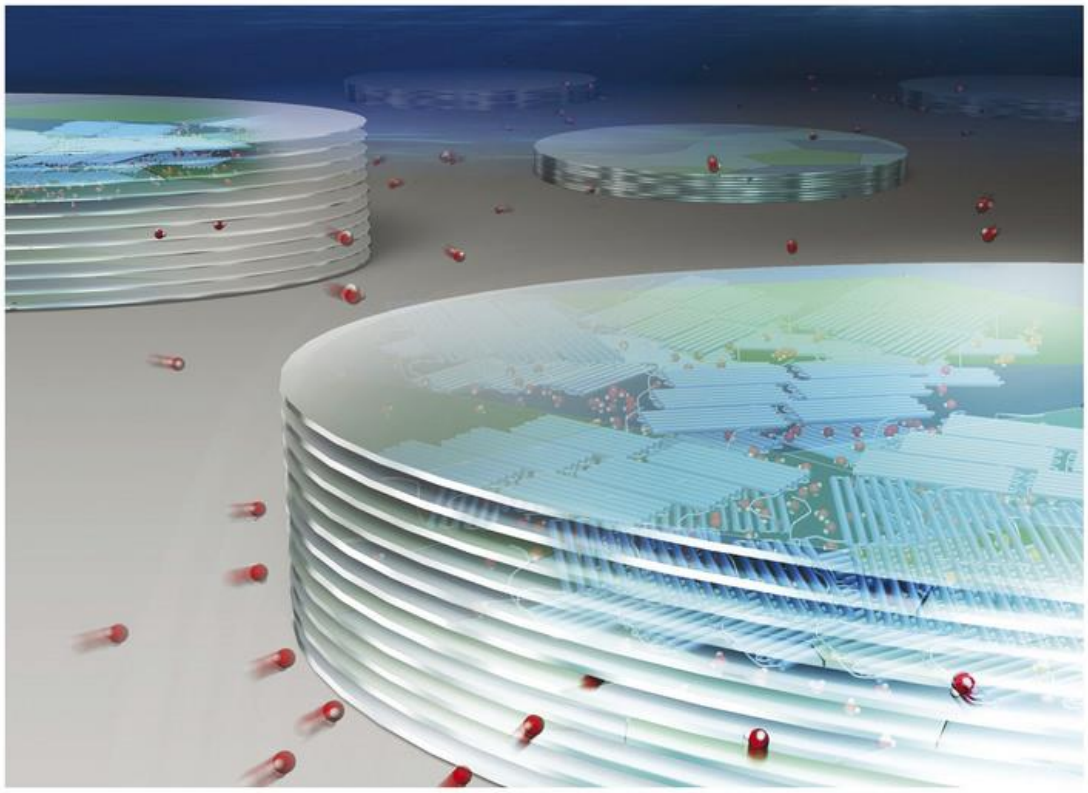

Showcasing work by G. Joshi, K. Okeyoshi, M. K. Okajima and T. Kaneko at Japan Advanced Institute of Science and Technology, Japan

Directional control of diffusion and swelling in megamolecular polysaccharide hydrogels

The presence of a layered structure in a megamolecular polysaccharide hydrogel enables directional control for diffusion of water and the swelling.

As featured in:

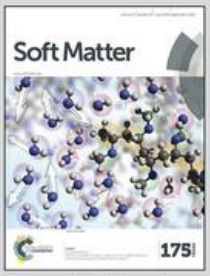

See K. Okeyoshi, T. Kaneko *et al.*, *Soft Matter*, 2016, **12**, 5515.

ROYAL SOCIETY OF CHEMISTRY

www.softmatter.org

Registered charity number: 207890


May 23, 2017 Volume 33, Number 20
pubs.acs.org/Langmuir
LANGMUIR
The ACS journal of fundamental interface science
Drying-Induced Self-Similar Assembly of Megamolecular Polysaccharides through Nano and Submicron Layering
ACS Publications
Most Trusted. Most Cited. Most Read.
www.acs.org

Chapter 3

Estimations for Splitting Curves of Air-LC Interface in the Space-Partitioning Phenomena

3.1 Introduction

Geometrical boundaries, interfacial variations, curvature *etc.* of cells and their surroundings play an important role in growth cum survival mechanisms of organisms.[1–5] In material research and design techniques also, due importance is given to geometrical specifications and changes in boundary conditions.[6–8] Convective self-assembly is the routine process for controlling this deposition of particles for a variety of applications ranging from biosensing, data storage, optical to ordered porous materials and templates.[9–11] It involves self-assembly assisted by controlled solvent evaporation of a solution with non-volatile particles to achieve patterned ordered structures at all scales.[12,13] By manipulating factors like contact angle, drying time and speed, substrate, surfactants or solvent, it stands out as a versatile method to achieve patterned surfaces with high level of accuracy.[14,15] The researches till now have been severely restricted to synthetic spherical particles,[16–18] with a dearth of literature on anisotropic particles[19,20] of biological origin.[21,22]

The reported phenomenon of macrospace partitioning by polysaccharide membranes upon drying its aqueous solution opens a simple and new avenue for preparing oriented materials.[23] It was shown that the viscous polysaccharide solution is in a nonequilibrium process between the polymer deposition and hydration during drying. Because of the extremely-high viscosity (dynamic moduli of the 0.5 wt% solution at 1 Hz frequency: storage moduli, $G' \approx 4$ Pa; loss moduli, $G'' \approx 2$ Pa),[24,25] the polymer around the air–liquid interface deposits through a drastic increase of the polymer concentration. This partitioning is a result of vertical membrane formation in a top-side-open cell accompanied by parallel orientation of the micrometer scale, rod-like domains with the three-phase contact line. During the drying of polymer solution in the cell, the air–liquid interface is in a similar state as the skin layers of a deswelling gel with buckling patterns.[26–28] The deposited polymer on the air–liquid interface behaves like a lid and the evaporation is restricted. By drying in limited space with a narrow gap, the nonequilibrium state between deposition and

hydration near the interface causes accumulation of small depositions at several specific points (pinning).

The work clarified the mechanism of deposition of a vertical structure with justification of the roles of capillary forces and triple-phase contact line. In this chapter, I mathematically approximated the role of interfacial curves and necessary conditions for the membrane formation. The theoretical estimations could strongly support this splitting of the meniscus to deposit a vertical membrane as a measure to provide more area for evaporation. This state could continuously achieve both deposition and the evaporation. As a result, the deposited polymer bridges the two parallel substrates as the vertical membrane grows.

3.2 Estimation of the balanced *Y* position showing the slope, $\Delta Z/\Delta Y = 1$

When a liquid/solution is in a container, the surface is mostly horizontal due to gravity (g) effects, except very near to the vertical walls. At this position, Young's relation comes into play causing such a distortion of the surface with a contact angle $\theta_E < \pi/2$ in case of a wetting liquid. The capillary forces result in the curvature of the interface whereas the gravity forces act in an opposite direction to it.[8]

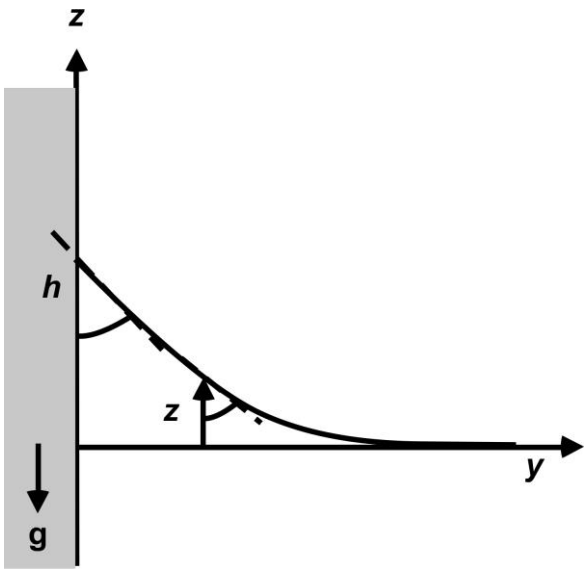

Figure 3.1 Meniscus for a solution that is attracted to the vertical wall and makes $\theta_E < \pi/2$.[8]

Considering an interfacial meniscus, where the edge rises to an equilibrium height *z*, in order to set the prescribed wetting angle, θ depending on the substrate, as illustrated in **Fig. 3.1** along the horizontal projection.

$$\gamma sin\theta + \frac{1}{2}\rho g z^2 = \gamma \qquad \ldots\ldots (3.1)$$

Where, γ = surface tension

ρ = density of solution

g = acceleration due to gravity

It can be rewritten as,

$$\rho g z^2 = 2\gamma(1 - sin\theta)$$

$$z = \sqrt{\frac{2\gamma(1 - sin\theta)}{\rho g}}$$

The above equation helps to calculate the maximum height (h) up to which the meniscus rises.

∴ At Young's condition, $z = h$ and $\theta = \theta_E$

$$h = \sqrt{2}\kappa^{-1}(1 - sin\theta_E)^{1/2} \qquad \text{……} \quad (3.2)$$

where $\kappa^{-1} = \sqrt{\frac{\gamma}{\rho g}}$ is known as the capillary length, within which gravity effects becomes insignificant.

Now, maximum height is reached at $\theta_E = 0°$, according to Young's condition.

$$h = \sqrt{2}\kappa^{-1}$$

$h = 2.828$ mm ;taking $\kappa^{-1} = 2$ mm as is the general case.

This height of the meniscus gives direct inference on the value of the capillary length.

The equation valid for meniscus curve very near to the wall is given as

$$Y - y_0 = \kappa^{-1} cosh^{-1}\left(\frac{2\kappa^{-1}}{z}\right) - 2\kappa^{-1}\left[1 - \frac{z^2}{4\kappa^{-2}}\right] \qquad \text{……..} \quad (3.3)$$

Here, y_0 is the distance at which equation (3.3) gives $Z = h$

Where h = max height up to which meniscus rises, and

$Y = 0$.

Hence, putting the respective values in this equation and solving for y_0,

$$0 - y_0 = 2\,cosh^{-1}[\frac{2(2)}{2.828}] - 2(2)[1 - \frac{2.828^2}{4(2^2)}]$$

$$y_0 = 0.539 \text{ mm}$$

Now, near the wall after the meniscus angle curve, $\theta < 45°$, the surface is almost flat. This point can be considered as the balanced Y position with slope $\Delta Z/\Delta Y = 1$, as schematically shown in **Fig. 3.2**.

$$Z = \sqrt{2}\kappa^{-1}(1 - sin\theta)^{1/2}$$

$$= \sqrt{2}(2)(1 - sin\ 45°)^{1/2}$$

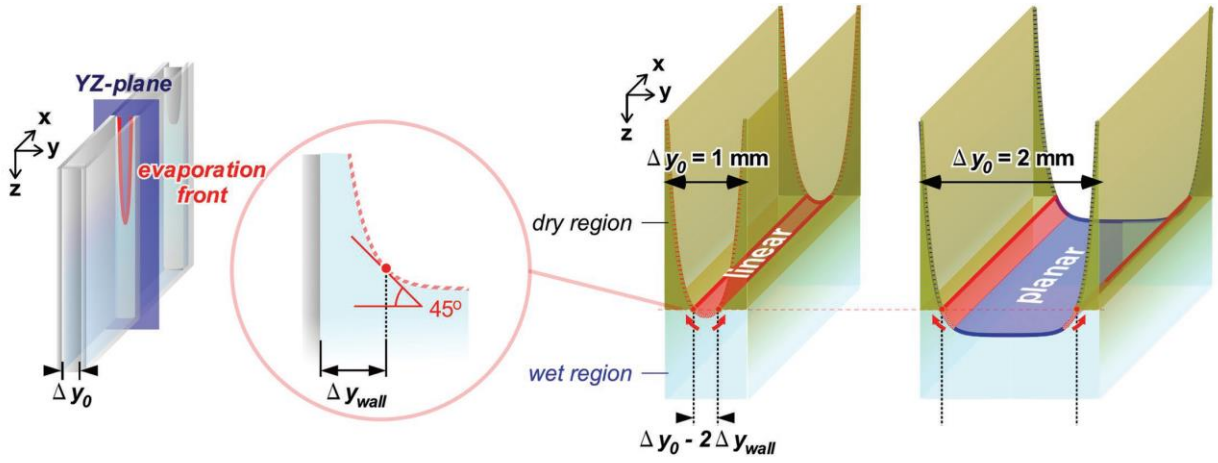

Figure 3.2 Schematic illustration of the cross-sectional view of the partitioning in a top-side-open cell with gap Δy_0 along the interface in the YZ-plane.[29]

This position, as the distance from the substrate, Δy_{wall} can be calculated as follows,

The value of z when $\theta = 45°$

$$z = 1.53 \text{ mm}$$

Therefore, at the value of Z = 1.53 mm, Y will be the value at which meniscus curve is 45°.

Substituting these values in equation (3.3),

$$Y - y_0 = \kappa^{-1} cosh^{-1}\left(\frac{2\kappa^{-1}}{z}\right) - 2\kappa^{-1}\left[1 - \frac{z^2}{4\kappa^{-2}}\right]$$

[Taking Z = 1.53 mm, y_0 = 0.539 mm and κ^{-1} = 2 mm]

Y = 0.222 mm

According to this estimation, the y range between the two substrates, showing the slope $\Delta Z/\Delta Y < 1$, i.e., $\Delta y_0 - 2\Delta y_{wall}$ is 0.56 mm in case of Δy_0 = 1 mm, and 1.56 mm in case of Δ_{y0} = 2 mm. These values clearly mean that the evaporation front under the condition of Δy_0 = 1 mm is a mostly curved interface in comparison with the case under the condition of Δy_0 = 2 mm.

Thus, by estimating the interfacial curve in the YZ-plane (**Fig. 3.2**), the evaporation front is mostly curved surface meniscus when the Δy_0 = 1 mm, while it is mostly flat surface when the Δy_0 = 2 mm. Considering that the typical capillary length (κ^{-1}) is ≈ 2 mm, the interfacial curve under the condition of Y-thickness, Δy_0 < 1 mm has been calculated as a hyperbolic curve from Equation (3.3).

Also,

$$\kappa^{-1} = \sqrt{\frac{\gamma}{\rho g}}$$

Where κ^{-1} = capillary length

γ = surface tension

ρ = density of the solution

More or less, the value of κ^{-1} is dependent upon properties of the polymer solution that is density and surface tension; and in turn depending on the value of κ^{-1}, the value of meniscus curve is fixed. Due to this, it should not depend upon the value of y_0 taken. Increasing y_0 = 1 mm, 2 mm, 3 mm, and so on, is not going to change the size of the curved edges but will definitely provide more surface area for evaporation. But as we go on decreasing the width, the area available for evaporation is highly limited and thus the polymer solution develops such a vertical film so as to maximize evaporation.

3.3 Mathematical estimation for effectiveness of meniscus splitting

Considering the case of a wetting solution bounded by vertical walls, the height *z* will be small far enough from the wall, when $\kappa.x > 1$.

Equation for the curvature as shown in **Fig. 3.3**[8]

$$\frac{\partial^2 z}{\partial^2 x} = \kappa^2 z$$

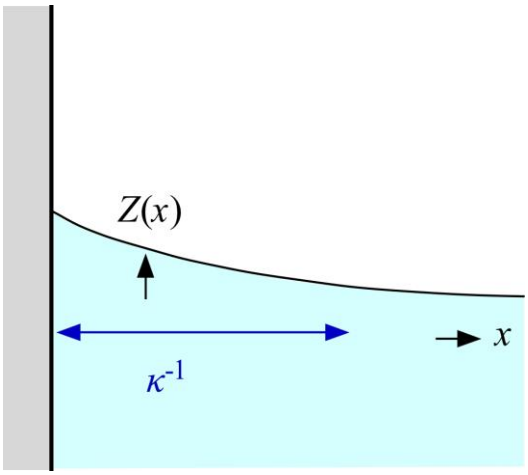

Figure 3.3. A wall perturbs the surface of the liquid over a distance κ^{-1} called the "capillary length".[8]

Solution for this equation is of the form

$$z = z_0 . e^{(\pm \kappa x)}$$

In order to explain the occurrence of partitioning phenomena, I extended this standard equation of meniscus. Considering both exponentially decaying and ascending curvature, as illustrated in **Fig. 3.4**.

$$Z(X) = \frac{Z_0}{2}[e^{\kappa\left(X-\frac{\Delta X_0}{2}\right)} + e^{-\kappa\left(X+\frac{\Delta X_0}{2}\right)}]$$

$$Z(X) = A[e^{\left(X-\frac{\Delta x_0}{2}\right)} + e^{\left(-\left(X+\frac{\Delta x_0}{2}\right)\right)}] \qquad \ldots\ldots (3.4)$$

Here A has a constant value, specific for a polymer solution and also dependent on the drying conditions.

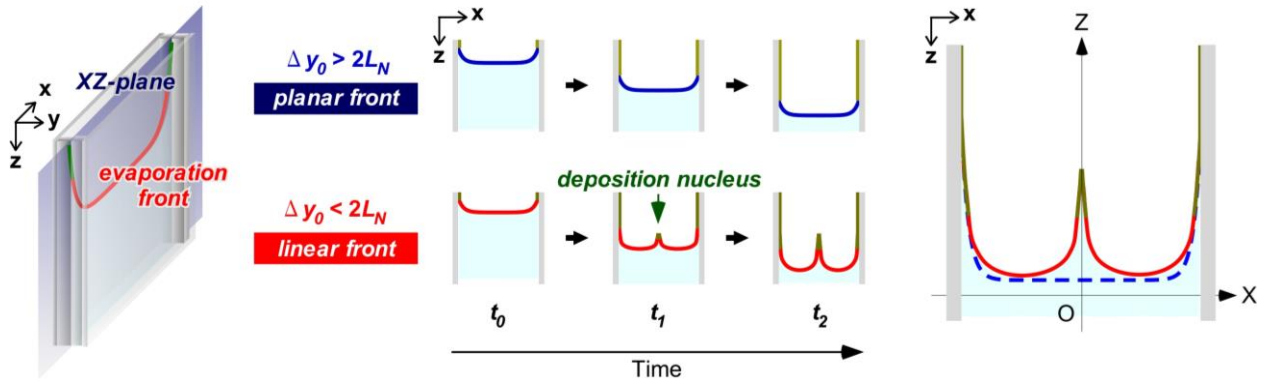

Figure 3.4. The interface in the *XZ*-plane of the linear front illustrated by the deposition of nucleus and splitting of meniscus.[29]

Simplifying equation (3.4),

$$Z = A[e^{\left(X-\frac{\Delta x_0}{2}\right)} + e^{\left(-X-\frac{\Delta x_0}{2}\right)}]$$

$$= Ae^{\left(-\frac{\Delta x_0}{2}\right)}[e^X + e^{-X}] \quad \textbf{or} \quad Ae^{\left(-\frac{\Delta x_0}{2}\right)}[2cosX] \qquad (\because\ e^X + e^{-X} = 2cosX)$$

<u>Case (i)</u> $Z = Ae^{\left(-\frac{\Delta x_0}{2}\right)}[e^X + e^{-X}]$

$$dZ = \{Ae^{\left(-\frac{\Delta x_0}{2}\right)}[e^X - e^{-X}]\}dX$$

Integrating the above equation will give us area under the curve. However, we want to derive the equation to calculate value of the meniscus length.

Now, length of the total curve (l) will be

$$dl = \sqrt{(dZ)^2 + (dX)^2} \qquad \ldots. (3.5)$$

Putting value of *dZ* in equation (3.5)

$$= \sqrt{\left\{Ae^{\left(-\frac{\Delta x_0}{2}\right)}[e^X - e^{-X}]\right\}^2 (dX)^2 + (dX)^2}$$

$$dl = [A^2 e^{(-\Delta x_0)}(e^X - e^{-X})^2 + 1]^{1/2} dX$$

Integrating *dl* will provide the equation for length of the meniscus with respect to value of *X*.

$$l = -iE(iX|4A^2 e^{-x_0}) + C$$

But, this is an imaginary solution and thus cannot be solved further.

Case (ii) $Z = Ae^{\frac{-\Delta x_0}{2}}(2cosX)$

$$dZ = -2Ae^{\frac{-\Delta x_0}{2}}(sinX)dX$$

Now, length of the total curve (*l*) will be as Eqn (3.5)

$$dl = [4A^2 e^{(-2\frac{\Delta x_0}{2})}(sin^2 X)(dX)^2 + (dX)^2]^{1/2}$$

$$= [A^2 e^{(-\Delta x_0)} 4sin^2 X + 1]^{1/2}\, dX$$

In order to calculate the length of the curve, the equation (3.4) was integrated as follows,

$$\int dl = \int [A^2 e^{(-\Delta x_0)} 4sin^2 X + 1]^{1/2}\, dX$$

$$l = E(X| - 4A^2 e^{-\Delta x_0}) + C \qquad \text{.....(3.6)}$$

Eqn. (3.6) is an Incomplete Elliptical Integral of the second kind. Solving this is beyond the scope of this research, so instead we have tried to simplify the equation further.

$$l = \int 2A[e^{(-\Delta x_0)} sin^2 X + \frac{1}{4A^2}]^{1/2}\, dX$$

Neglecting the second term, $1/4A^2$ as it is very small

$$\frac{1}{4A^2} \ll e^{(-\Delta x_0)} sin^2 X$$

Therefore,

$$l = 2A \int [e^{(-\Delta x_0)} sin^2 X]^{1/2}\, dX \quad \text{.....(3.7)}$$

$$= 2A \int e^{(-\frac{\Delta x_0}{2})} sinX \, dX$$

$$l = -2Ae^{-\frac{\Delta x_0}{2}} cosX + C$$

$$l = BcosX + C \qquad \ldots\ldots\ldots\ldots\ldots\ldots (3.8)$$

Where $B = -2Ae^{-\frac{\Delta x_0}{2}}$, constant

Considering the simplest condition of meniscus splitting at the exact center position and calculating the total length of curve for single and double menisci from Eqn (3.8),

I: Single meniscus, $X = 15$ mm (no nucleation)

Then, from Eqn (3.8) $l = 0.966B$

II: Double Menisci, $X = 7.5$ mm (nucleation at center)

$$l = l_1 + l_2$$

$$l_1 = l_2 = 0.991B$$

Therefore,

$$\frac{total\ length\ of\ curve\ for\ \boldsymbol{II}}{total\ length\ of\ curve\ for\ \boldsymbol{I}} = \frac{l_1 + l_2}{l} \frac{0.991B \times 2}{0.966B} = 2.05 .$$

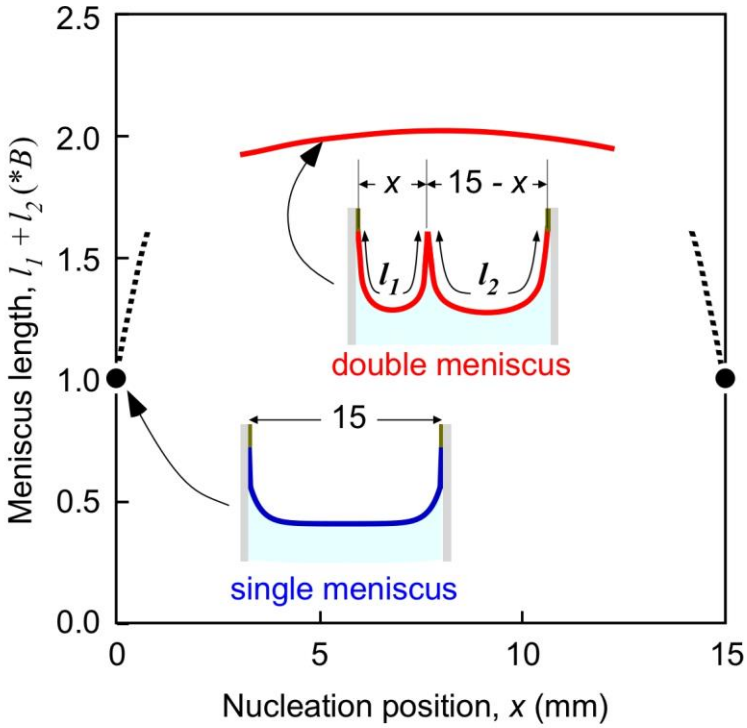

Figure 3.5 Estimated meniscus length with splitting as a function of the *x*-position for nucleation in a cell with *X*-width of 15 mm. $B = -2Ae^{-\frac{\Delta x_0}{2}}$, constant

3.4 Approximate analysis of a Triple menisci with two nucleation

When the width, x of the container with y = 1 mm was increased from 15 mm to 21 mm, simultaneous deposition of two nuclei was recorded. These two depositions splitted the original meniscus into three parts or three new menisci (**Fig. 3.6**). When estimating mathematically, we have two variables here along the x-axis, x_1 and x_2. And so, we need to define at least one to solve further.

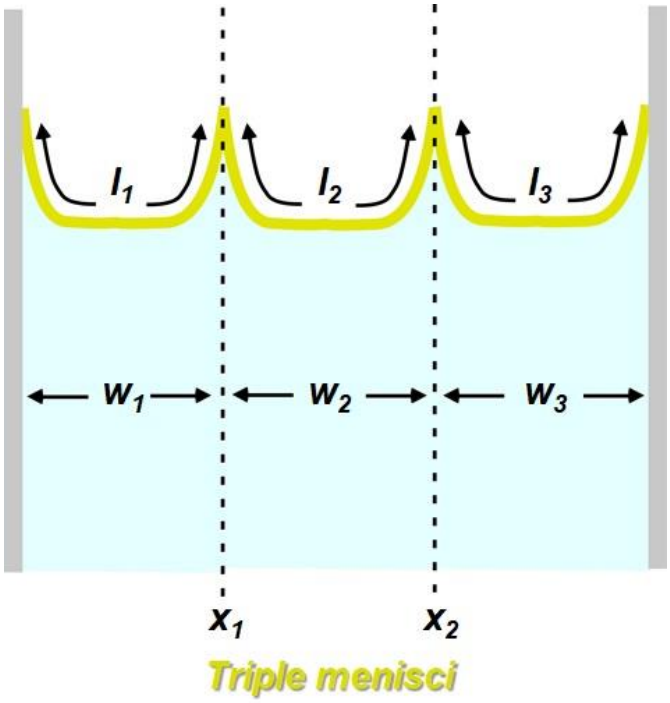

Figure 3.6 Schematic illustration for double nucleations with three menisci in a limited space of width 21 mm. Variables x_1 and x_2 denote the points of nucleations; w_1, w_2 and w_3 are the actual width lengths; l_1, l_2 and l_3 represent the individual meniscus lengths.

Specifying the conditions,

$$w_1 + w_2 + w_3 = 21 \text{ mm}$$

$$l_1 + l_2 + l_3 = l$$

taking $2 \leq x_1 \leq 10.5$;so $x_1 = w_1$

And, $w_2 = \left(\frac{21 - w_1}{2}\right)$ for the condition $w_2 = w_3$

Using Equation (3.8) to plot values of l as a function of x_1 we obtained the following **Fig. 3.7**, which demonstrates a maxima for meniscus length with nucleation around x ~ 7 mm.

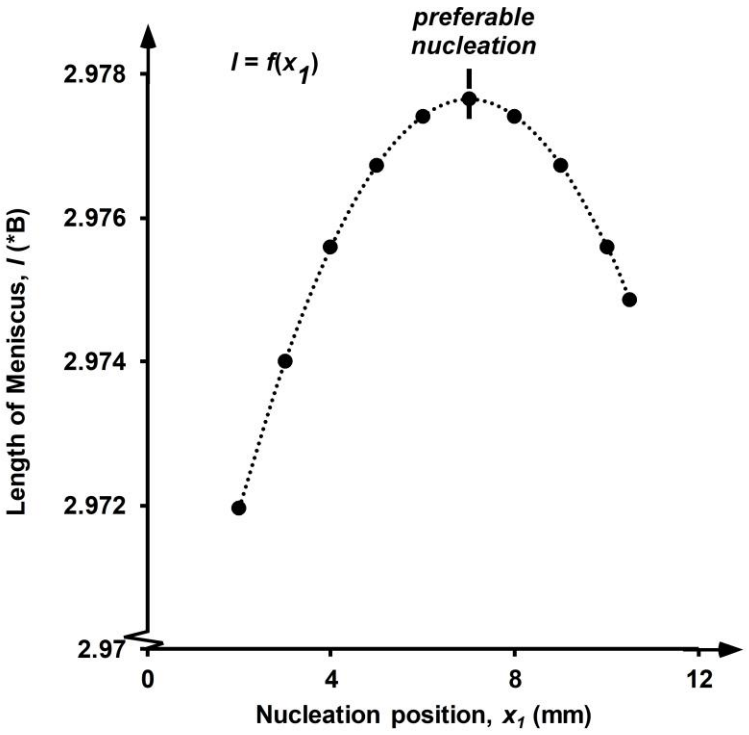

Figure 3.7 Plot for the length of the meniscus (l) as a function of position of first nucleation (x_1).

Thus, considering x = 21 mm as set of 10.5 mm, we can arrive at the following **Fig. 3.8**.

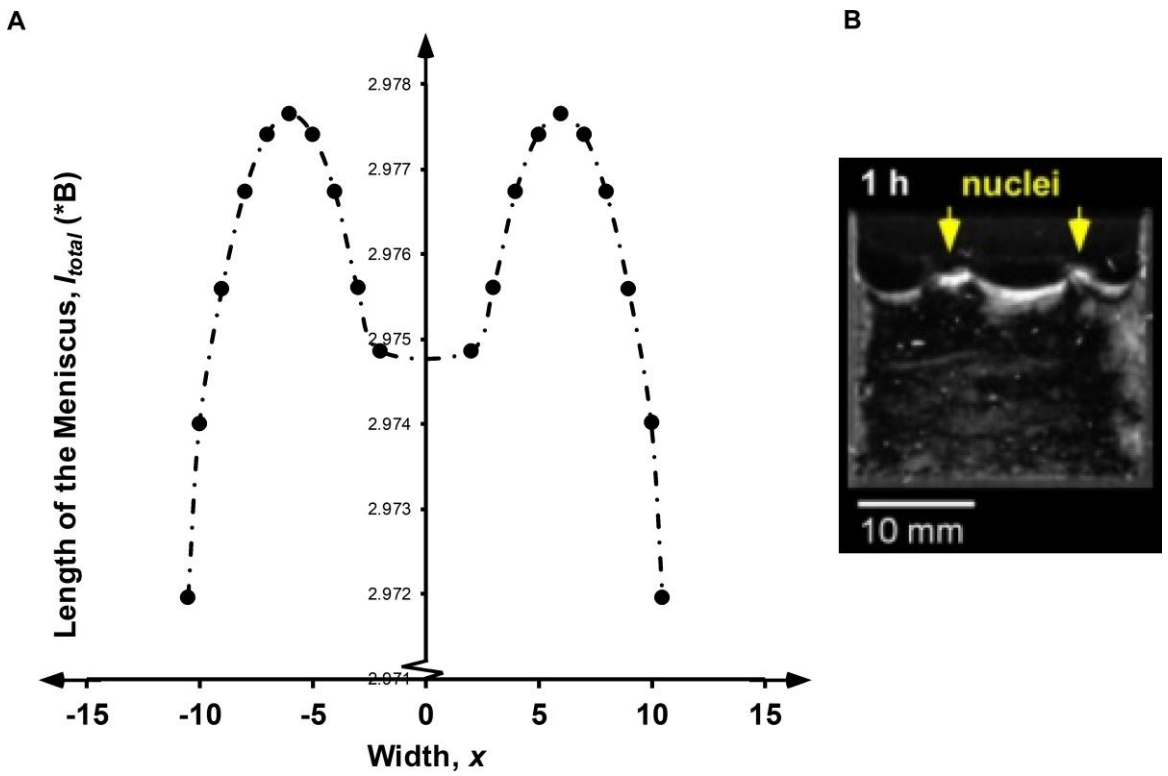

Figure 3.8 A. Estimation for the length of meniscus as a function of width, *x*. **B.** Polarized image of the experimental data (from Ref 23) with splitting of the drying interface/meniscus with two nucleations.

Therefore, two inflexion/maxima positions can be observed as favorable nucleating points for the polysaccharide to deposit and elevate the instability in the system. This is in agreement with the actual experimental result and thus strongly supports the partitioning phenomenon.

These estimations strongly mean that splitting the interfacial curve by deposition provides approximately two times larger area for evaporation front. Because of this favorable condition, the polymer deposits to partition the macrospace. The splitting of the evaporation front thus seems justified as it provides almost the double the area for water to escape in the limited space.

3.5 Generalization of the Phenomenon

In general, the length of the meniscus is given by the following equation,

$$l = \int 2A[e^{(-\Delta x_0)} sin^2 X + \frac{1}{4A^2}]^{1/2} dX$$

It is deduced from here that,

$$\Delta l \propto e^{-\Delta x_0} sin^2 x$$

The above dependency of increase in meniscus length is very straightforward.

- The exponential function signifies continuous increase in meniscus length as the width of the cell, *x* is increased. This is a very direct sensible observation.
- The dependence on sine function is indicative of inflexion points at regular intervals. These points can be thought of as the favorable spots for the polysaccharide to nucleate and deposit as a vertical membrane.

Basically, the plot of this proportionality between the values can give an insight about the increment in meniscus length over the width, *x* (**Fig. 3.9**).

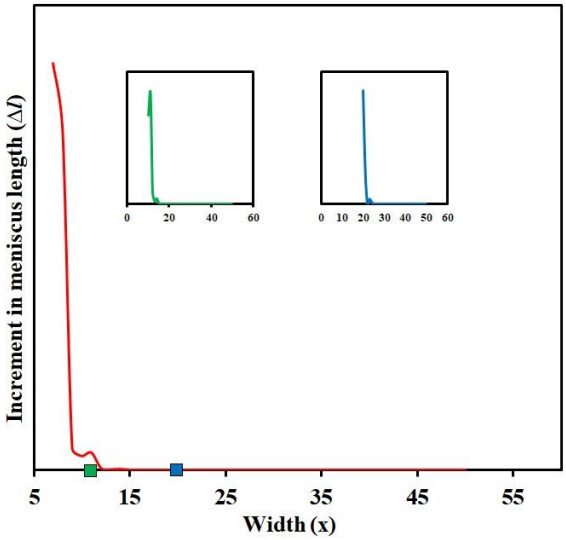

Figure 3.9 Estimation of length of increment in length (Δl) of meniscus over width, x.

As suggested, there is a maxima after every couple of distance, the apparent length remaining constant in that range around that value (inflexion point). It can be inferred from this plot that shorter meniscus comprises of more length over the surface. Thus, in a limited space with quasi-one-dimensional drying front, the evaporative interface splits into double/multiple menisci depending on the width, x of the container, for efficient evaporation process. From the mathematical analysis of the meniscus it is deduced that such a condition of meniscus splitting is advantageous by leading to an increased surface area availability for evaporation.

3.6 Conclusions

In this chapter, the correlation between the interfacial curve and the macro-space partitioning in limited space along the thickness, *y* and width, *x* of the evaporation front was clarified. I could derive an equation to quantify the meniscus splitting behavior.

1. By mathematical analysis of the gap available between parallel substrates, the evaporation front was ascribed to be either planar or linear. It was concluded that primarily a linear evaporation front instigates the nucleation and partitioning due to a majorly curved drying interface and less space for water evaporation.
2. During the drying from the linear front, splitting of the interfacial curve in the *X*-width provides much larger area for evaporation as compared to the originally single meniscus. Because of this favorable condition, the sacran microrods deposit to partition the macrospace during the drying process in limited space.

References

1. Chen, C. S., Mrksich, M., Huang, S., Whitesides, G. M. & Ingber, D. E. Geometric Control of Cell Life and Death Christopher S. Chen,. *Science.* **276**, 1425 (1997).

2. Von Erlach, T. C. *et al.* Cell-geometry-dependent changes in plasma membrane order direct stem cell signalling and fate. *Nat. Mater.* **17**, 237–242 (2018).

3. Hussain, S. *et al.* MreB filaments align along greatest principal membrane curvature to orient cell wall synthesis. *Elife* **7**, 1–45 (2018).

4. Flemming, H. C. *et al.* Biofilms: An emergent form of bacterial life. *Nat. Rev. Microbiol.* **14**, 563–575 (2016).

5. Mijailovich, S. M., Kojic, M. & Tsuda, a. Particle-induced indentation of the alveolar epithelium caused by surface tension forces. *J. Appl. Physiol.* **109**, 1179–1194 (2010).

6. Saffman, P. G., Sir Geoffrey Taylor, F. R. S. The penetration of a fluid into a porous medium or Hele-Shaw cell containing a more viscous liquid. *Proc. Royal Soc. Lond.* (1958).

7. Rondelez, J. B. B. and F. B.-W. and F. Exponential Growth of Fingering Instabilities of Spreading Films Under Horizontal Thermal Gradients. *Europhysics Lett.* **19**, 97 (1992).

8. de Gennes, P.-G., Brochard-Wyart, F. & Quéré, D. Capillarity: Deformable Interfaces BT - Capillarity and Wetting Phenomena: Drops, Bubbles, Pearls, Waves. 1–31 Springer New York (2004).

9. Yuan, Z., Burckel, D. B., Atanassov, P. & Fan, H. Convective self-assembly to deposit supported ultra-thin mesoporous silica films. *J. Mater. Chem.* **16**, 4637–4641 (2006).

10. Watanabe, S., Inukai, K., Mizuta, S. & Miyahara, M. T. Mechanism for stripe pattern formation on hydrophilic surfaces by using convective self-assembly. *Langmuir* **25**, 7287–7295 (2009).

11. Takeda, S. & Wiltzius, P. Growth of highly ordered colloidal crystals using self-assembly at liquid-liquid interfaces. *Chem. Mater.* **18**, 5643–5645 (2006).

12. van Dommelen, R., Fanzio, P. & Sasso, L. Surface self-assembly of colloidal crystals for micro- and nano-patterning. *Adv. Colloid Interface Sci.* **251**, 97–114 (2018).

13. Kaplan, C. N., Wu, N., Mandre, S., Aizenberg, J. & Mahadevan, L. Dynamics of evaporative colloidal patterning. *Phys. Fluids* **27**, 92105 (2015).

14. Zhang, J., Li, Y., Zhang, X. & Yang, B. Colloidal self-assembly meets nanofabrication: From two-dimensional colloidal crystals to nanostructure arrays. *Adv. Mater.* **22**, 4249–4269 (2010).

15. Han, W. & Lin, Z. Learning from 'coffee rings': Ordered structures enabled by controlled evaporative self-assembly. *Angew. Chemie - Int. Ed.* **51**, 1534–1546 (2012).

16. Nayak, S. & Andrew Lyon, L. Soft nanotechnology with soft nanoparticles. *Angew. Chemie - Int. Ed.* **44**, 7686–7708 (2005).

17. Ozin, G. A., Arsenault, A. & Cademartiri, L. *Nanochemistry*. (The Royal Society of Chemistry, 2008).

18. Jiang, P. *et al.* Single-Crystal Colloidal Multilayers of Controlled Thickness Single-Crystal Colloidal Multilayers of Controlled Thickness. **11**, 2132–2140 (1999).

19. Loudet, J. C., Yodh, A. G. & Pouligny, B. Wetting and contact lines of micrometer-sized ellipsoids. *Phys. Rev. Lett.* **97**, 1–4 (2006).

20. Madivala, B., Fransaer, J. & Vermant, J. Self-assembly and rheology of ellipsoidal particles at interfaces. *Langmuir* **25**, 2718–2728 (2009).

21. Alexander, C. Self-assembly of biopolymers – recent progress and future prospects. *Faraday Discuss.* **166**, 449-452 (2013).

22. Whitesides, G. M. Self-Assembly at All Scales. *Science.* **295**, 2418–2421 (2002).

23. Okeyoshi, K., Okajima, M. K. & Kaneko, T. Emergence of polysaccharide membrane walls through macro-space partitioning via interfacial instability. *Sci. Rep.* **7**, 5615 (2017).

24. Mitsumata, T. *et al.* Ionic state and chain conformation for aqueous solutions of supergiant cyanobacterial polysaccharide. *Phys. Rev. E* **87**, 42607 (2013).

25. Okajima-Kaneko, M., Ono, M., Kabata, K. & Kaneko, T. Extraction of novel sulfated polysaccharides from Aphanothece sacrum (Sur.) Okada, and its spectroscopic characterization. *Pure Appl. Chem.* **79**, 2039–2046 (2007).

26. Lajeunesse, E., Martin, J., Rakotomalala, N., Salin, D. & Yortsos, Y. C. The threshold of the instability in miscible displacements in a Hele–Shaw cell at high rates. *Phys. Fluids* **13**, 799–801 (2001).

27. Suzuki, A. Yoshikawa, S., Bai, G. Shrinking pattern and phase transition velocity of poly(N-isopropylacrylamide) gel. *J. Chem. Phys.* **111**, 360 - 367 (1999).

28. Suzuki, A. & Hara, T. Kinetics of one-dimensional swelling and shrinking of polymer gels under mechanical constraint. *J. Chem. Phys.* **114**, 5012–5015 (2001).

29. Okeyoshi, K., Joshi, G., Okajima, M. K. & Kaneko, T. Formation of Polysaccharide Membranes by Splitting of Evaporative Air–LC Interface. *Adv. Mater. Interfaces* **5**, 1–6 (2018).

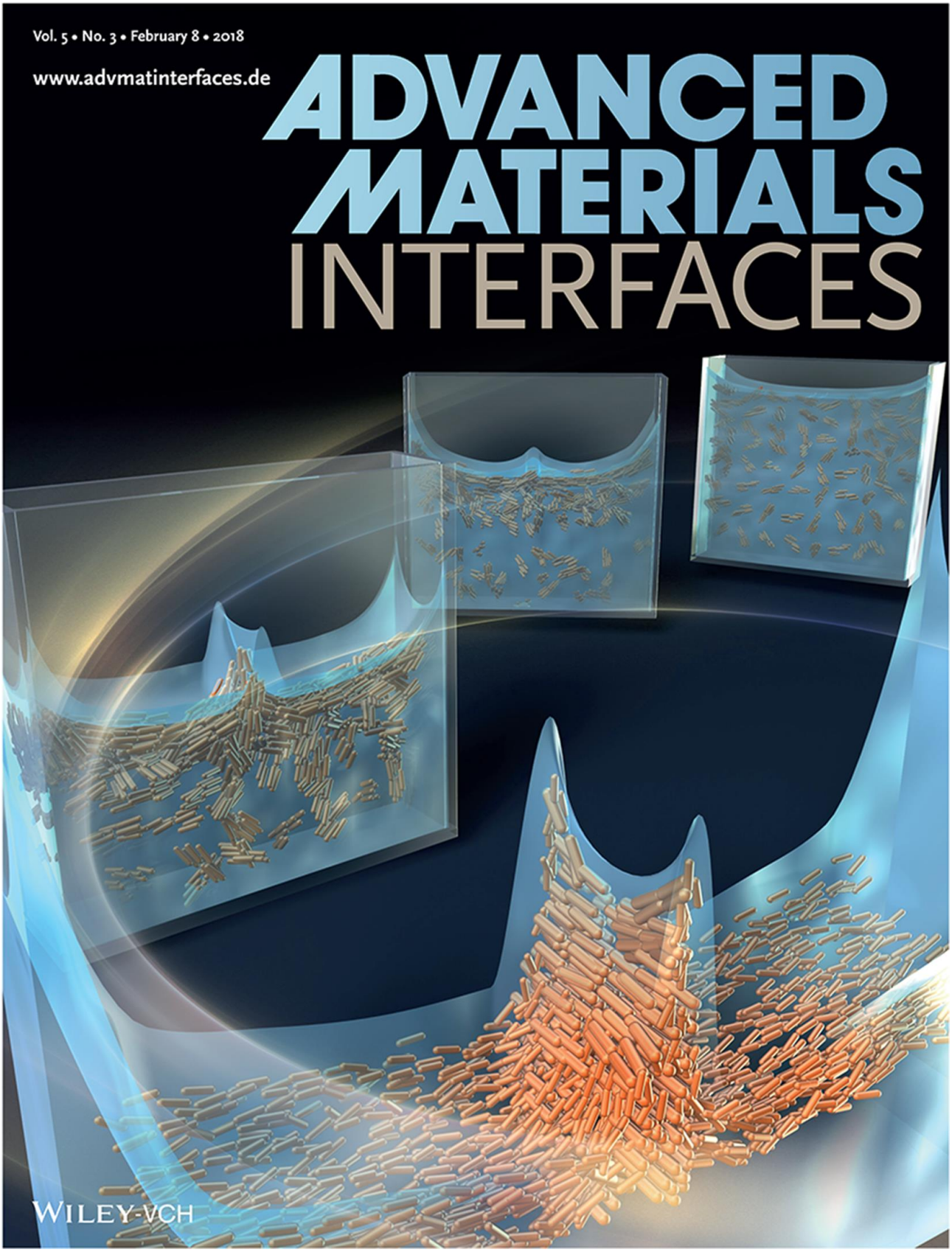
Vol. 5 • No. 3 • February 8 • 2018
www.advmatinterfaces.de
ADVANCED MATERIALS INTERFACES
WILEY-VCH

Chapter 4

Micro-Deposition Control of Xanthan on Evaporative Air-LC Interface

4.1 Introduction

Self-assembly of biopolymers like proteins and polysaccharides, through their liquid crystalline (LC) state, provides reconfigurable structures in nature [1–4]. These are effectively mimicked by researchers to develop highly ordered architectures [5–7] through various self-assembly processes [8–12]. Evaporation is often employed as a driving force to uniformly align the units beyond their individual LC domains [13–16]. By tuning the conditions of drying, we can gain control over their mobility and in turn control the orientation during deposition [17,18]. The experiments, however, involve challenging processes demanding high precision without achieving high orientation. Also, majority of the research works have been restricted to the use of synthetic materials and lately cellulose nanofiber/nanocrystal [19,20], in spite of the wide range of naturally available polymers. There has been a deficit of concrete references on the self-assembly behavior of biopolymers [21]. Specifically, their precise response to the drying environment as well as the corresponding structural deformation still remains elusive.

Recently, we reported the self-assembly of cyanobacterial exopolysaccharide, sacran [22,23] upon drying its aqueous LC solution from a limiting interface as an example of instability-driven pattern formation [24,25]. By controlling the cell width, the polysaccharide deposited to form multiple vertical membranes, bridging the millimeter-scale gap between the substrates. However, no variation in the deposited membranes or their orientation was obtained because sacran exhibited thermally-stable lyotropic state with its LC domains being non-responsive to the temperature in the range of 25 – 60 °C [26].

Here we aim to control the self-assembly of bacterial polysaccharide xanthan gum, from a limited space. It shows cholesteric [27] to isotropic phase transition with an increase in temperature [28] and thus the LC state can be manipulated (**Fig. 4.1**). The orientation of its LC domains could be guided by the evaporative interface upon changing the drying conditions. Furthermore, the deposited membranes will have oriented structures and hydrogels can be

prepared by annealing at a higher temperature. Such hydrogels with inherent biocompatibility and fast response rate have great demand for drug delivery, tissue engineering and biomimicking applications.

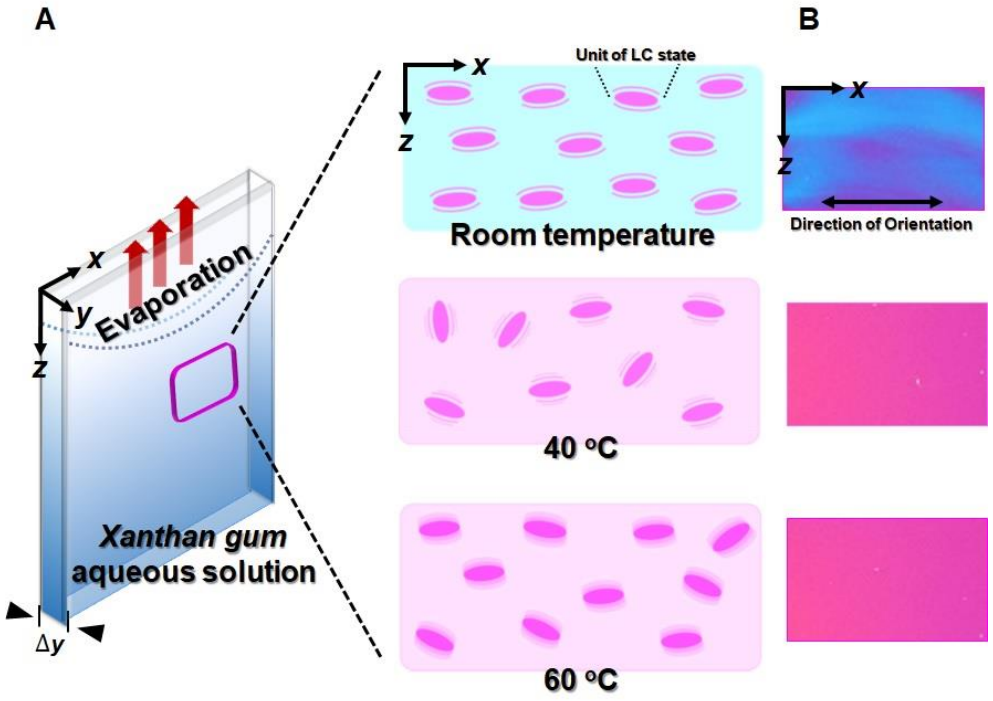

Figure 4.1 A. Schematic illustration of the increasing mobility of xanthan gum LC domains upon increasing the temperature in the drying experiment. **B.** Polarized images of the xanthan solution with a retardation pate of λ = 530 nm; corresponding to the respective temperatures showing the isotropization with temperature.

4.2 Materials and Methods

4.2.2 Materials: Xanthan gum extracted from *Xanthomonas campestris* was purchased from Taiyo Kagaku Co., Japan and used without further purification. Top-open cells were prepared with two glass slides and silicone spacer of desired thickness (0.2 or 0.5 mm). The glass slides were pre-cleaned by washing with acetone and spraying air using an air gun.

4.2.3 Preparation of xanthan solution: To an almost boiling deionized water, known amount of xanthan gum powder was added with continuous stirring, to get the desired concentration. The solution was covered with foil to prevent water evaporation. The solution was further stirred for 3 hours on minimum heat to eventually obtain a homogenous solution. Next, it was brought to room temperature and centrifuged using Qik spin QS7011 Microcentrifuge (6500 rpm; 5 min) to remove air bubbles, before using for the experiments. The solutions were used within two days of preparation.

4.2.3. Measurement of solution viscosity: Viscosity measurements were carried out by using a rheometer (MCR301, Anton Paar) with a stainless cone plate having a diameter of 50 mm (CP50, Anton Paar). The minimum torque which could be detected by the rheometer was 0.1 μNm. The temperature was controlled by using a Peltier plate during the measurement.

4.2.4 Drying experiments and observations under cross-polarized light: The solution was poured into the prepared top-open cell at room temperature and placed in an oven with an air circulator, preset at the desired temperature under atmospheric pressure. To monitor the orientation changes during the time course, samples were photographed through the cross-polarizers with a retardation plate of wavelength, λ = 530 nm placed between the sample

stage and the polarizer. Polarized microscopic observations were made using an optical microscope (BX51, Olympus) equipped with a CCD camera (DP80, Olympus). A first-order retardation plate with $\lambda = 530$ nm was placed in the light path.

4.2.5 Scanning electron microscopy analysis: The dried membranes were coated with Os using an osmium coater (Neoc-Pro, Meiwafosis Co., Ltd.) and observed using high resolution scanning electron microscope (Hitachi S-5200) with an acceleration voltage of 10 kV and a cold cathode field emission type electron gun.

4.3 Drying of xanthan solution in limited space

1 wt% aqueous xanthan solution was poured into a top-open cell with a 0.5 mm gap, at 25 °C ± 1. We could observe through cross-polarized light and a retardation plate (λ = 530 nm), that the solution displayed blue and yellow regions depending on the polymer chain orientation at 25 °C. However, the color changed to pink upon placing the solution in an oven set at 60 °C (**Fig. 4.2A**). This indicated that the liquid crystal (LC) state vanishes with an increase in temperature due to the thermotropic isotropization process. Just after initiating drying at 60 °C, it was observed that the interface remained highly oriented in stark contrast to the rest of the solution **(Fig. 4.2A**, **0.25 h**). From analysis of the solution intensity along the z-axis, the LC state was found just beneath the drying air-LC interface and not in the bulk solution (**Fig. 4.2B** and **C**).

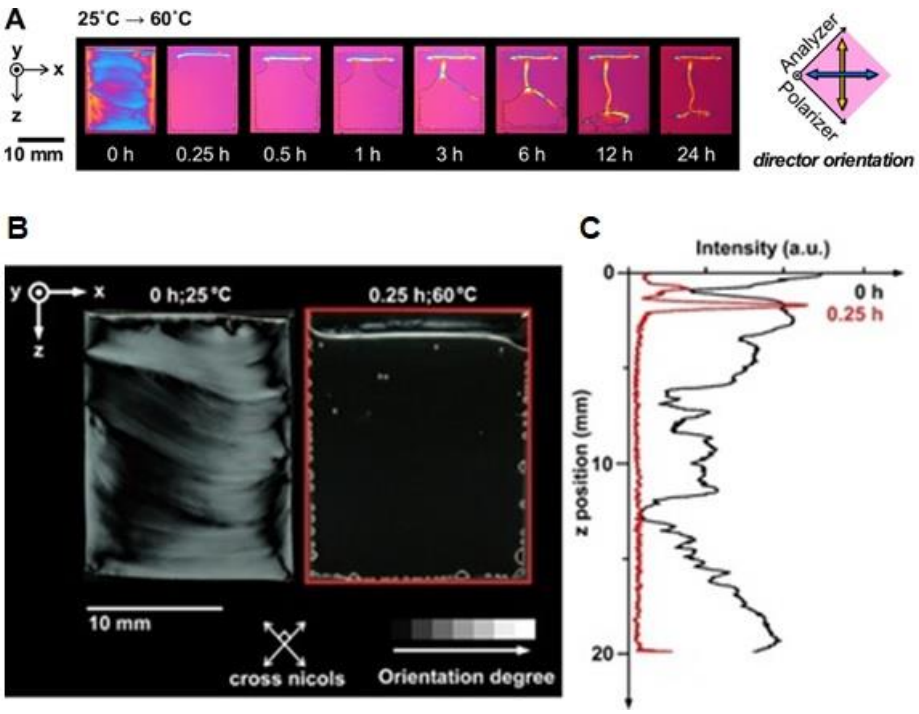

Figure 4.2 A. Side views of xanthan gum aqueous solution during drying from a top-open cell as observed under crossed-polarizers with a first-order retardation plate (λ = 530 nm). **B.** Polarized images of the 1 wt% xanthan solution before and after drying. **C.** Intensity variation along the *z*-position.

The air-liquid interface receded with evaporation and was consolidated of domains to form a lid-like structure lying along the *x*-axis. Subsequently, the air-liquid interface was redirected around the edges of this lid-like structure (**Fig. 4.2A**, **0.25-1 h**). The two interfaces moving from both sides of the lid, reunited at the center (**Fig. 4.2A**, **1-3 h**). It can be inferred that the restrained availability of space in the 0.5 mm wide cell which qualifies as a case of limiting evaporation front [25], caused this lid-like deposition. The deposited lid acted as a barrier to water evaporation and induced a state of non-equilibrium between deposition and hydration at the air-LC interface. This initiated the reunited part to nucleate as a vertical bridge and facilitate evaporation by providing more surface [25]. The bridging in the direction of the *z*-axis, became a vertical membrane (**Fig. 4.2A**, **3-24 h**). In the manner exemplified, lid-like transverse membrane and vertical membrane were generated from a limited space.

During the vertical membrane petrifaction (**Fig. 4.3Ai**), the polarized microscopic image showed birefringent repetitive hues. The depositing tip in **Fig. 4.3Ai-ii**, comprised of first-order white followed by the second-order repeating colors. This shift in colors hint towards the transformation in LC arrangement with respect to the exceedingly concentrated local environment [29]. The periodic structure in **Fig. 4.3A-iii** with ~500 μm interval should be the result of contortion in assembling of the LC units [30]. As represented in **Fig. 4.3B**, the display of second-order interference colors in the depositing structure indicates significant retardation of the light due to orientational changes. The interval was observed to decrease proportionally along the *z*-axis, as the polymer dried on the glass substrate in the form of a narrow vertical deposition. This structural distortion symbolizing the cholesteric LC character of xanthan also accompanied the lid formation (**Fig. 4.3C**).

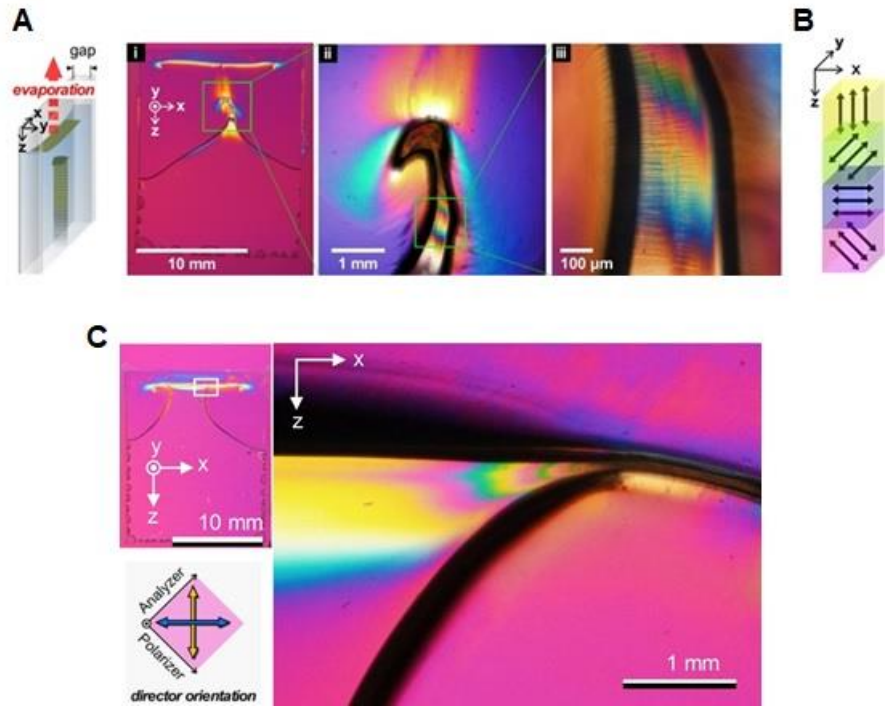

Figure 4.3 A. Microscopic images through first-order retardation plate just after the nucleation of the vertical membrane. **B.** Schematic illustration for the vertically strained liquid phase composed of cholesteric LC solution from a three-dimensional perspective. **C.** Polarized microscopic image of second-order interference colors as observed during the deposition of the horizontal lid.

4.4 Morphology of the deposited membranes

To clarify the microstructures of membranes, the lid and the vertical membrane retrieved after drying 1 wt% xanthan solution at 60 °C were scrutinized in three dimensions (**Fig. 4.4A**). From polarized light microscopic images of the lid in the *xy*-plane, a mosaic-like structure was observed with multiple domains 100 µm in diameter, accumulated in the central region (**Fig. 4.4B**). Because of such high concentration and high evaporation rate, there was not enough time to form a single macrodomain at millimeter-scale. Thus, the domains in 1 wt% xanthan solution were immediately arrested with their respective orientations at the air-LC interface, bridging the narrow gap. During the drying process in a limited space, the center position is preferred for nucleating as has been mathematically estimated in our previous work [25]. This initial lid with mosaic structure provided a contact line along the *y*-axis for the adjoining domains. As the evaporation progressed, the adjacent domains were stacked in the *y*-direction as a result of reorientation along the sides of this multi-domain bridge. Thus, the outer parts of the lid are unidirectionally aligned along the *y*-axis, signaled by the yellow color.

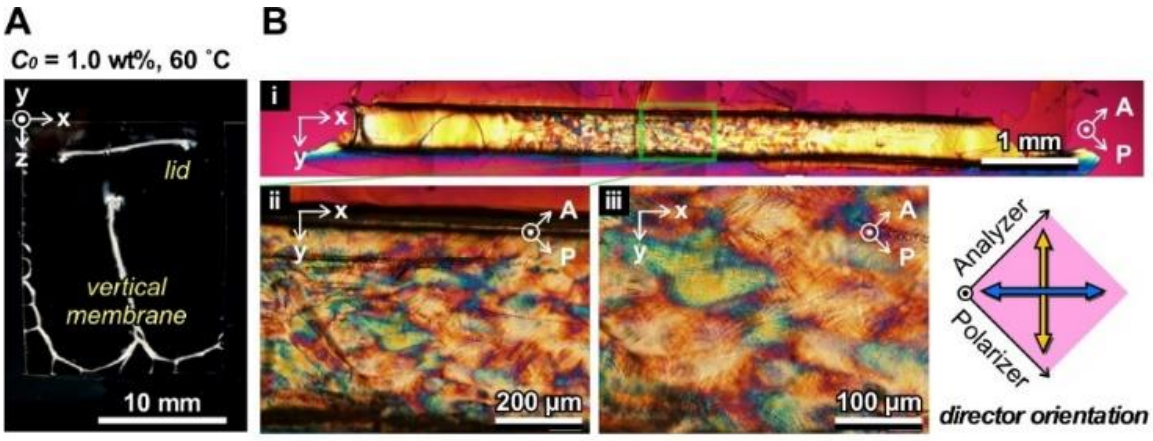

Figure 4.4 A. Image of the deposited structures obtained after complete drying under cross-polarized light. Cell dimensions = (15 mm, 0.5 mm, ~20 mm). Initial concentration of xanthan: 1.0 wt%. Drying at 60 °C under atmospheric pressure. **B.** Microscopic images of the horizontally deposited lid in *xy*-plane under cross-polarized light with a first-order retardation plate (λ = 530 nm).

Fig. 4.5A shows the polarized microscopic image of a vertical membrane with length > 10 mm. It displayed a yellow area below the nucleus and some discrete blue parts. To understand its structural features at the submicron scale, the dried membrane was observed by SEM (**Fig. 4.5B**). Both images showed that the membrane is composed of fibers ~50 nm diameter in orientation. The long axis of the fibers in the yellow part is parallel to the *z*-axis, and that of the blue part is parallel to the *y*-axis. Considering these drying records, macrodomains assemble in millimeter-scale along the *z*-axis to form the vertical membrane, observed as yellow (**Fig. 4.5C**).

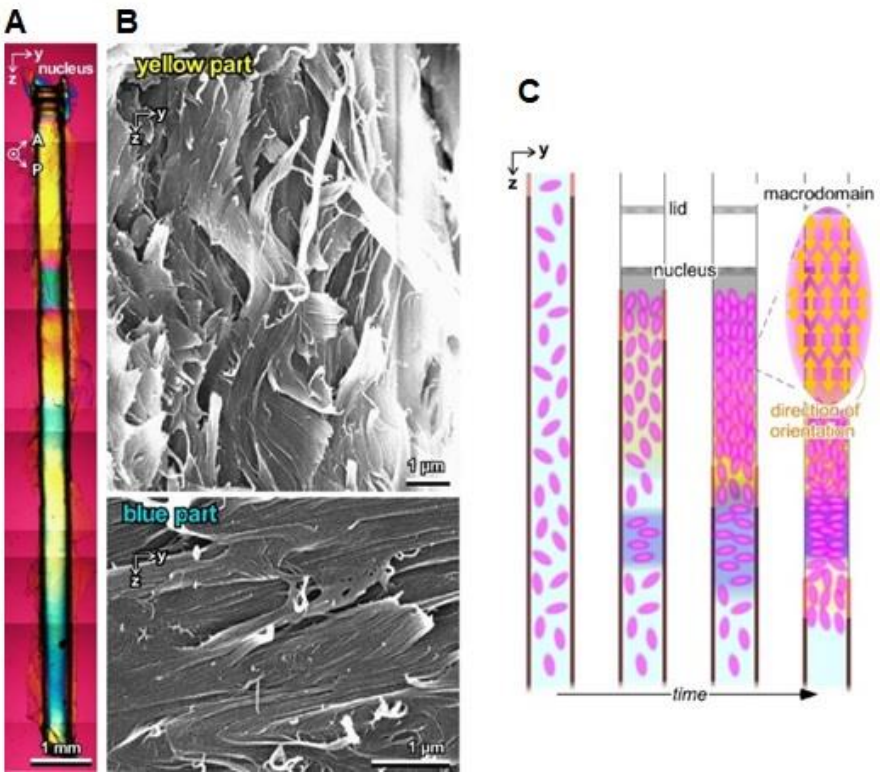

Figure 4.5 A. Microscopic images of the vertically deposited membrane in the *yz*-plane under cross-polarized light with a first-order retardation plate. **B.** SEM images of the vertical membrane. Yellow part and blue part represent the parts of polarized microscopic images of the vertical membrane in A. **C.** Schematic illustration of a vertical membrane formation along the *yz*-plane with the orientation of xanthan LC domains.

During condensation of the domains, some of them also settled along the *y*-axis, observed as blue. With the still rising concentration of the solution, these blue parts with the length of a millimeter are caught up between the larger yellow parts. Evidently, the drying air-liquid interface along the *yz*-plane promotes unidirectional alignment of LC domains majorly along the *z*-axis.

4.5 Lower concentration and drying temperature

To investigate effects of the initial concentration and temperature on the deposition, a similar experiment was performed with a lower concentration of xanthan solution, 0.5 wt%, at a lower drying temperature of 40 °C (**Fig. 4.6**). In this case, after lid deposition there was no further bridging deposition obtained and the solution took 45-48 h to dry completely at 40 °C, that is about three times longer than at 60 °C. Thus, the lid is also responsible for reducing the rate of water evaporation along with the lower drying temperature. **Fig. 4.6B** shows the dried lid membrane in the *xy*-plane under a polarized microscope, comprising of a distinct blue part in the center flanked by yellow parts. **Fig. 4.6B-iii** clearly shows the demarcated boundary of the initial bridge and the latter reoriented yellow part. It can be assumed that essentially, the gap was bridged by domains oriented with the air-liquid-solid contact lines along the substrates, i.e., the *x*-axis. Furthermore, during peeling it off from the substrates, the lid tore off with cracks in the *y*-direction (**Fig. 4.6B-ii**, arrows). This strongly suggests that the domains in the yellow part are oriented along the *y*-direction.

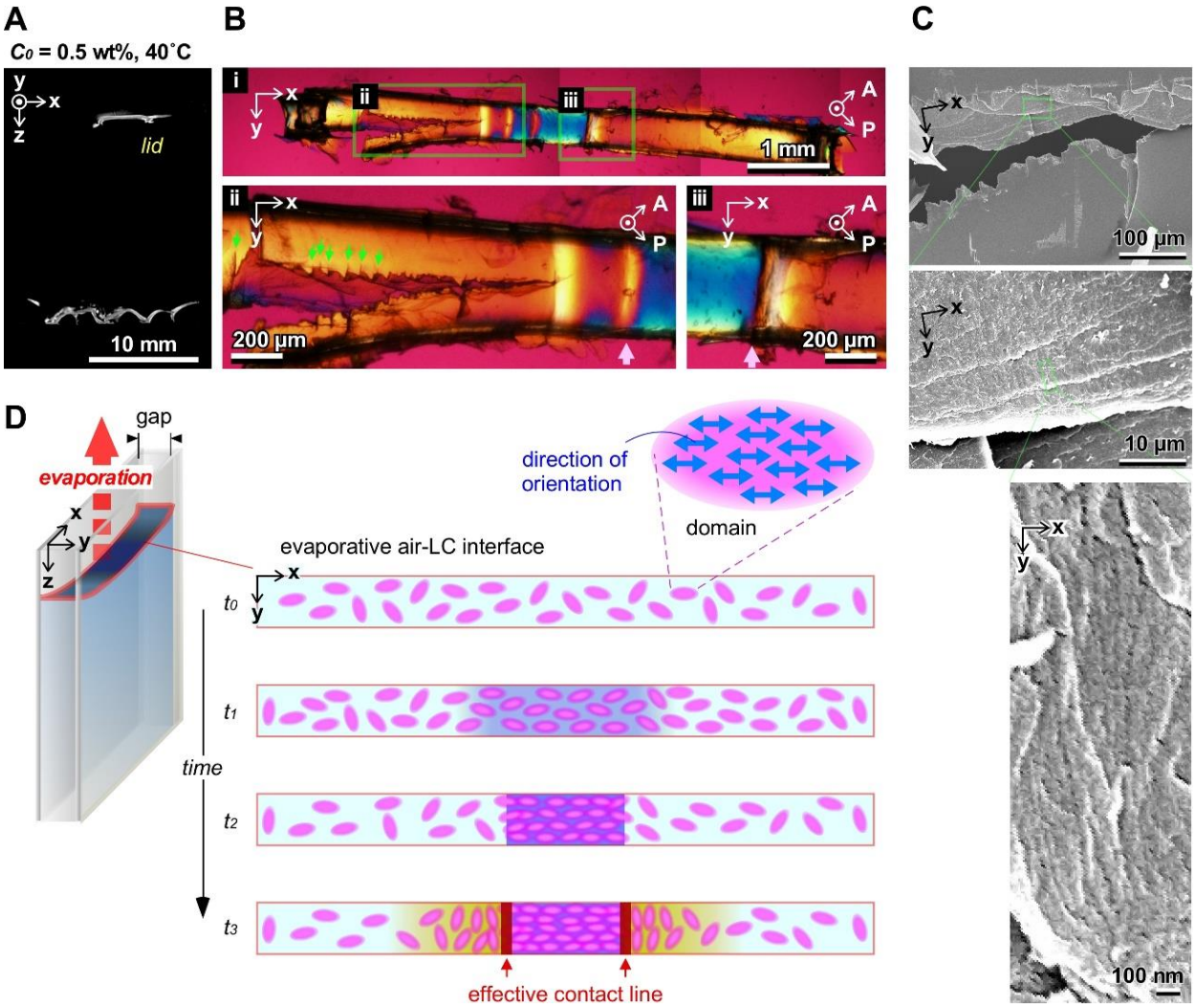

Figure 4.6 Microscopic images of the horizontally deposited lid of 0.5 wt% xanthan solution. A. Cross-polarized image of the horizontally deposited structure obtained after complete drying in the cell. Cell dimensions = (15 mm, 0.5 mm, ~20 mm). Initial concentration of xanthan: 0.5 wt%. Drying at 40 °C under atmospheric pressure. **B.** Microscopic images of the horizontally deposited lid as observed under cross-polarized light with a first-order retardation plate (λ = 530 nm). Arrows in image **ii**: cracks. Arrows in image **iii**: the boundary of reorientation. **C.** SEM images of the yellow area of the lid. **D.** Schematic illustration for the deposition of the bridge along *x*-axis parallel to the contact lines. This initial deposition provides effective contact lines and consequently leads to reorientation of adjoining domains along the *y*-axis.

To examine the microstructures in the lid, the torn part was analyzed by SEM (**Fig. 4.6C**). The yellow part of the lid was organized in layers along the *xy*-plane and fibers were stacked side by side along the *y*-axis within each layer. The magnified SEM image provides an explicit view of fibers within one of the layers. **Fig. 4.6D** is the schematic illustration of the process of lid deposition with well-ordered behavior of the domains in the *xy*-plane. Accordingly, the domains do not have any single preferred direction of orientation at the initial state ($t = t_0$). Evaporation forces the domains at the interface to align along the contact line of the substrate in the *x*-direction (t_1). A little while later (t_2), the oriented domains solidify in millimeter scale. These amalgamated LC domains act as a bridge, providing contact lines effectively along the *y*-axis (t_3). The newly acquired contact lines in *y*-direction trigger the switching of orientation of the adjacent domains, perpendicular to this blue bridge, constructing the outer parts of the horizontal lid membrane. In this manner, the LC domains reproducibly showcased a sophisticated level of arrangement by orienting step by step along two directions in a single deposited structure.

4.6 Temperature-concentration-morphology phase diagram

To discern the effect of the initial polymer concentration, C_0 and drying temperature on the bridging deposition, we prepared a phase diagram (**Fig. 4.7A**). At 25 °C, there were no bridging depositions obtained except sometimes in the case of 1.5 wt% solution. This implies, adequately concentrated solution can induce bridging deposition even at room temperature. At 40 °C, the horizontal lid structure could be observed for $C_0 \leq 1.0$ wt%. At higher concentration ($\geq$ 1.25 wt%), only the growth of vertical membranes could be observed without lid; at times a forked structure with the fusion of two vertical membranes. Furthermore, the trend at 40 °C could also be similarly observed at a temperature of 60 °C. Higher concentration favored early nucleation/s for growth of vertical membrane/s, in contrast to $C_0 \leq 1.0$ wt%. As schematically shown in **Fig. 4.7B**, for 1.0 wt% solution, the interface deposits transversely, bridging the substrate along the three-phase contact line. At this drying temperature of 60 °C, the lid partially blocks the evaporation flow which forces the nucleation for vertical membrane growth. Whereas at a higher concentration of 1.25 wt%, the LC domains are in close proximity and there is not enough space for reorientation. Therefore, the contact line promotes deposition of a nucleation point for the growth of a vertical membrane as the most favorable outcome

To explore the effect of viscosity on the bridging deposition, the viscosity of the solutions with various concentrations was measured as a function of temperature (**Fig. 4.7C**). At 25 °C, the viscosity showed a gradual increase with an increase in the C_0. Above a threshold concentration > 0.5 wt%, xanthan solution form gels, defined by oriented bundles of double helices acting as junction zones [31]. At 40 °C a jump in viscosity was visible from 0.2 wt% and 0.5 wt%, and again from 0.5 wt% to 1.0 wt%. Analyzing at 60 °C, viscosity value showed a leap from ~ 0.2 Pa•s for 0.5 wt% to ~ 0.7 Pa•s for 1.0 wt%. This is again because of sol-gel transition around this temperature region depending on the concentration. Thus, it

can be safely interpreted that for concentrated solutions, elevated temperatures favor comparatively higher viscosity values. Also, this is in agreement with the LC domains being densely packed in concentrated solution, possessing high viscosity and nucleating into vertical membranes. The viscosity values for $C_0 \geq 1.0$ wt %, seem to directly favor the partitioning phenomenon leading to vertical deposition. The optimum balance of initial concentration and temperature conditions is critical to obtain the desired deposited structures.

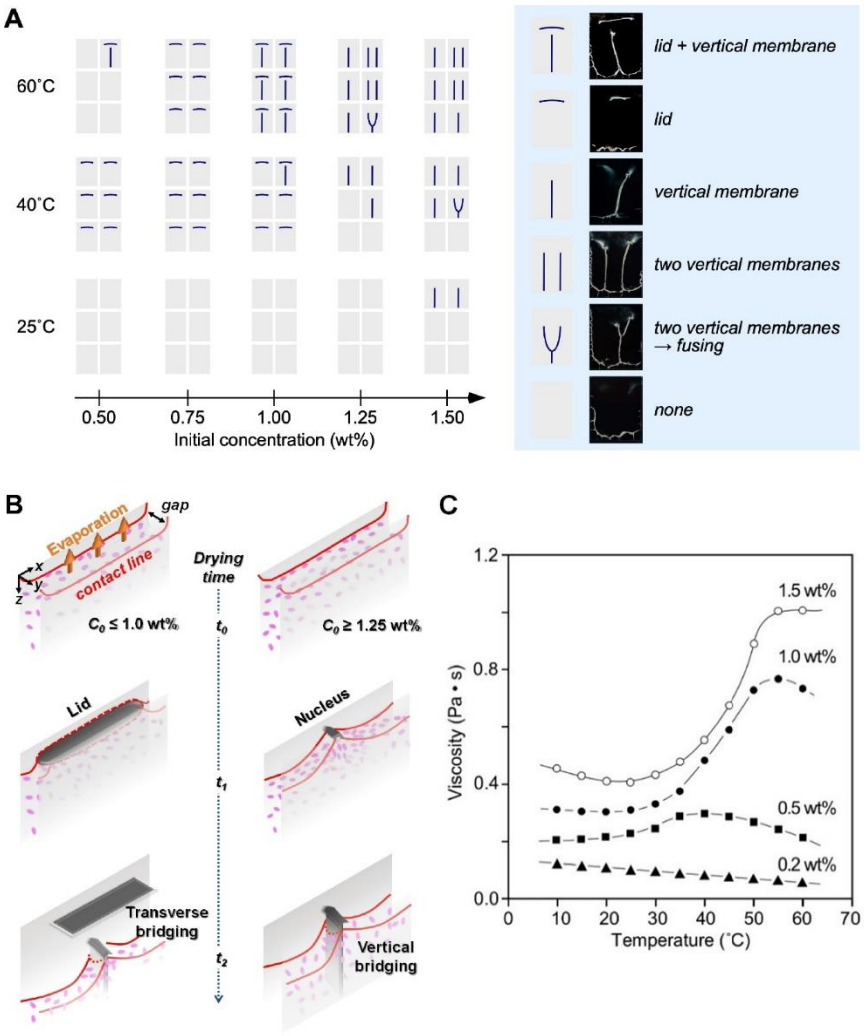

Figure 4.7. Deposition shapes obtained by concentrating xanthan solution from a limited space. A. Phase diagram of the depositions and their classification on the basis of initial concentration and temperature. Cell dimensions = (15 mm, 0.5 mm, ~20 mm); under atmospheric pressure. Number of the experiment for each condition, N = 6. **B.** Schematic illustration for the preferred deposition at the evaporative air-LC interface for solutions

having low and high concentration. **C.** Temperature dependence of viscosity of xanthan solutions at given concentration.

4.7 Physical crosslinking of membrane

By thermally annealing at 140 °C for 2 h, crosslinking points could be introduced in the deposited membranes [32]. As seen in **Fig. 4.8A**, the vertical membrane in water swelled anisotropically along its thickness, *x*-axis. The equilibrated swollen state was quickly achieved in less than 10 sec and the resulting hydrogels had seven times more thickness (*x*-axis) than that of the dried state with negligible swelling along *y*- or *z*-axis (**Fig. 4.8B**). Besides, closer inspection of the membrane revealed layered structure along the *yz*-plane (**Fig. 4.8C**).

The fibers were stacked densely within each layer with spacing between the layers. As a result, more amount of crosslinking points within each layer and lesser in the interlayer area should be introduced during the annealing. As a result, the crosslinked membrane swells in response to water uptake between the layers without swelling along the *y*-axis or *z*-axis. Moreover, the hydrogel showed reversible anisotropic swelling/deswelling behavior (**Fig. 4.8D**). As for the process from the wet to the dried state, the water was removed in an oven at 60 °C. After repeated cycles, the swelling state at dry/wet states showed similar values. This reversibility supports the idea that the crosslinking points between the layers are stable enough and the gel membrane is capable of water going in/out from in-between the layers.

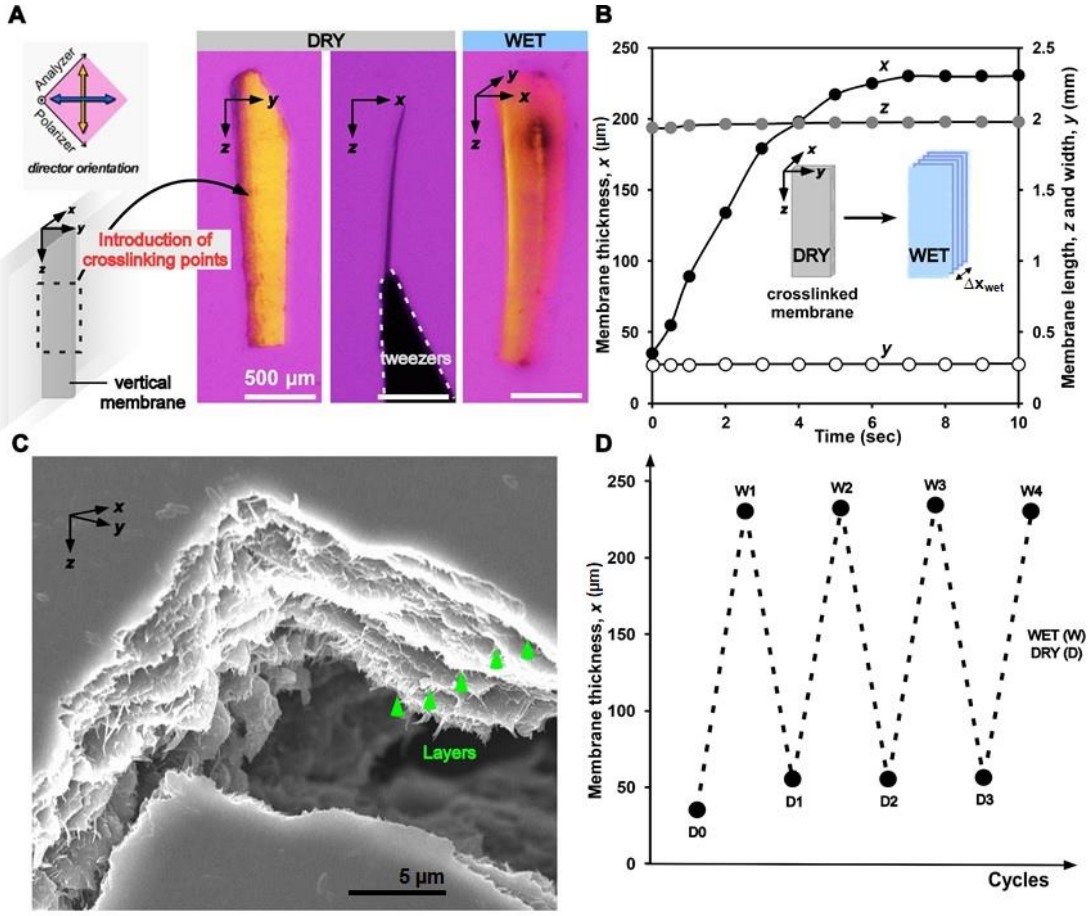

Figure 4.8. Anisotropic swelling of the xanthan membrane and its reversibility. A. Polarized images of the dry and wet states of vertical membrane. **B.** Swelling kinetics of xanthan hydrogel along the three axes. **C.** Cross-sectional SEM image of the dried membrane. **D.** The swelling-deswelling cycle of xanthan hydrogel with respect to *x*-axis.

4.8 Conclusions

Controlled orientation in deposited structures was achieved by regulating the drying temperature and initial concentration of the liquid crystal (LC) polysaccharide xanthan gum from a limited interface. Stepwise deposition of transverse lid-like membrane preceding the growth of a vertically deposited membrane bridging the two substrates was recorded. A temperature-concentration-morphology phase diagram could be formulated for the variety of deposited structures, as a significant development over the previous reports [24,25,33]. It indicated that higher concentration and higher temperature, induced the growth of vertical membrane/s more efficiently. Subsequent viscosity measurement showed that lower values of the solution viscosity witnessed only a lid membrane formation whereas higher values prompted vertically membranes to deposit. Furthermore, the crosslinked membrane showed reversibility of anisotropic swelling/deswelling, along its thickness. The results presented here provide an understanding of the behavior of polysaccharides under natural environment [21,34,35]. Differing from other works featuring orientation control of LC polymers [36–38], this interface-assisted condensation and deposition approach promises a versatile methodology of directional control to design novel biomimetic materials with highly-ordered structures.

References

1. Bouligand, Y. Liquid crystals and biological morphogenesis: Ancient and new questions. *Comptes Rendus Chim.* **11**, 281–296 (2008).

2. Mitov, M. Cholesteric liquid crystals in living matter. *Soft Matter* **13**, 4176–4209 (2017).

3. Saw, T. B., Xi, W., Ladoux, B. & Lim, C. T. Biological Tissues as Active Nematic Liquid Crystals. *Adv. Mater.* **1802579**, 1802579 (2018).

4. Alexander, C. Self-assembly of biopolymers – recent progress and future prospects. *Faraday Discuss.* **166**, 449 (2013).

5. Li, L. *et al.* A highly conspicuous mineralized composite photonic architecture in the translucent shell of the blue-rayed limpet. *Nat. Commun.* **6**, 1–11 (2015).

6. Soler-Illia, G. J. D. A. A., Sanchez, C., Lebeau, B. & Patarin, J. Chemical strategies to design textured materials: From microporous and mesoporous oxides to nanonetworks and hierarchical structures. *Chem. Rev.* **102**, 4093–4138 (2002).

7. Bhushan, B., Jung, Y. C., Niemietz, A. & Koch, K. Lotus-like biomimetic hierarchical structures developed by the self-assembly of tubular plant waxes. *Langmuir* **25**, 1659–1666 (2009).

8. Kato, T., Uchida, J., Ichikawa, T. & Sakamoto, T. Functional Liquid Crystals towards the Next Generation of Materials. *Angew. Chemie - Int. Ed.* **57**, 4355–4371 (2018).

9. Whitesides, G. M. Self-Assembly at All Scales. *Science.* **295**, 2418–2421 (2002).

10. Zhao, Y., Xie, Z., Gu, H., Zhu, C. & Gu, Z. Bio-inspired variable structural color

materials. *Chem. Soc. Rev.* **41**, 3297–3317 (2012).

11. Woltman, S. J., Jay, G. D. & Crawford, G. P. Liquid-crystal materials find a new order in biomedical applications. *Nat. Mater.* **6**, 929–938 (2007).

12. Joshi, G., Okeyoshi, K., Okajima, M. K. & Kaneko, T. Directional control of diffusion and swelling in megamolecular polysaccharide hydrogels. *Soft Matter* **12**, 5515–5518 (2016).

13. Grosso, D. *et al.* Fundamentals of mesostructuring through evaporation-induced self-assembly. *Adv. Funct. Mater.* **14**, 309–322 (2004).

14. Li, B., Puigmartí-Luis, J., Jonas, A. M., Amabilino, D. B. & De Feyter, S. Hierarchical growth of curved organic nanowires upon evaporation induced self-assembly. *Chem. Commun.* **50**, 13216–13219 (2014).

15. Roger, K., Liebi, M., Heimdal, J., Pham, Q. D. & Sparr, E. Controlling water evaporation through self-assembly. *Proc. Natl. Acad. Sci.* **113**, 10275–10280 (2016).

16. Zhang, L., Maheshwari, S., Chang, H. C. & Zhu, Y. Evaporative self-assembly from complex DNA-colloid suspensions. *Langmuir* **24**, 3911–3917 (2008).

17. Ozin, G. A., Arsenault, A. & Cademartiri, L. *Nanochemistry*. (The Royal Society of Chemistry, 2008).

18. Brinker, C. J., Lu, Y. F., Sellinger, A. & Fan, H. Y. Evaporation Induced Self-Assembly: Nanostructures Made Easy. *Adv. Mater.* **11**, 579–585 (1999).

19. Lagerwall, J. P. F. *et al.* Cellulose nanocrystal-based materials: From liquid crystal self-assembly and glass formation to multifunctional thin films. *NPG Asia Mater.* **6**, 1–12 (2014).

20. Giese, M., Blusch, L. K., Khan, M. K. & MacLachlan, M. J. Functional Materials from Cellulose-Derived Liquid-Crystal Templates. *Angew. Chemie Int. Ed.* **54**, 2888–2910 (2014).

21. Hamley, I. W. Liquid crystal phase formation by biopolymers. *Soft Matter* **6**, 1863–1871 (2010).

22. Okajima, M. K., Kaneko, D., Mitsumata, T., Kaneko, T. & Watanabe, J. Cyanobacteria that produce megamolecules with efficient self-orientations. *Macromolecules* **42**, 3057–3062 (2009).

23. Okajima, M. K., Sornkamnerd, S. & Kaneko, T. Development of Functional Bionanocomposites Using Cyanobacterial Polysaccharides. *Chem. Rec.* **18**, 1167–1177 (2018).

24. Okeyoshi, K., Okajima, M. K. & Kaneko, T. Emergence of polysaccharide membrane walls through macro-space partitioning via interfacial instability. *Sci. Rep.* **7**, 5615 (2017).

25. Okeyoshi, K., Joshi, G., Okajima, M. K. & Kaneko, T. Formation of Polysaccharide Membranes by Splitting of Evaporative Air–LC Interface. *Adv. Mater. Interfaces* **5**, 1–6 (2018).

26. Okeyoshi, K., Okajima, M. K. & Kaneko, T. Milliscale Self-Integration of Megamolecule Biopolymers on a Drying Gas–Aqueous Liquid Crystalline Interface. *Biomacromolecules* **17**, 2096–2103 (2016).

27. Livolant, F. & Bouligand, Y. Liquid crystalline phases given by helical biological polymers (DNA, PBLG and xanthan). Columnar textures. *J. Phys.* **47**, 1813–1827

(1986).

28. Figueiredo Neto, A. M. & Salinas, S. R. A. *The Physics of Lyotropic Liquid Crystals: Phase Transitions and Structural Properties*. *Monographs on the Physics and Chemistry of Materials* (Oxford University Press, 2005).

29. Gennes, P. G. de & Prost, J. *The Physics of Liquid Crystals*. (Clarendon Press, 1995).

30. Sengupta, A. Flow of Nematic Liquid Crystals in a Microfluidic Environment. in *Topological Microfluidics: Nematic Liquid Crystals and Nematic Colloids in Microfluidic Environment* 83–135 (Springer International Publishing, 2013).

31. Quinn, F. X., Hatakeyama, T., Takahashi, M. & Hatakeyama, H. The effect of annealing on the conformational properties of xanthan hydrogels. *Polymer (Guildf).* **35**, 1248–1252 (1994).

32. Okajima, M. K. *et al.* Anisotropic swelling in hydrogels formed by cooperatively aligned megamolecules. *RSC Adv.* **5**, 86723–86729 (2015).

33. Kaneko, T. Micelle-Mediated Self-Assembly of Microfibers Bridging Millimeter-Scale Gap To Form Three-Dimensional-Ordered Polysaccharide Membranes. *Langmuir* **34**, 13965–13970 (2018).

34. Pletikapić, G. *et al.* Self-assembly of polysaccharides gives rise to distinct mechanical signatures in marine gels. *Biophys. J.* **107**, 355–364 (2014).

35. Turner, R. D., Mesnage, S., Hobbs, J. K. & Foster, S. J. Molecular imaging of glycan chains couples cell-wall polysaccharide architecture to bacterial cell morphology. *Nat. Commun.* **9**, (2018).

36. Kato, T., Mizoshita, N. & Kishimoto, K. Functional liquid-crystalline assemblies: Self-

organized soft materials. *Angew. Chemie - Int. Ed.* **45**, 38–68 (2005).

37. Jeong, J. *et al.* Homeotropic alignment of lyotropic chromonic liquid crystals using noncovalent interactions. *Langmuir* **30**, 2914–2920 (2014).

38. Liu, Y. *et al.* Self-organized cholesteric liquid crystal polymer films with tunable photonic band gap as transparent and flexible back-reflectors for dye-sensitized solar cells. *Nano Energy* **26**, 648–656 (2016).

Chapter 5

Effect of the Size of the LC domain on Bridging Depositions

5.1 Introduction

The reasons for partitioning phenomenon held ground upon the reasons of high molecular weight of sacran along with a high viscosity. This can be easily understood as increase in the molecular weight also increases the rigidity or the persistence length of the polysaccharide which promotes liquid crystalline phase.[1–3] It was also experimentally demonstrated in case of another high molecular weight polysaccharide, xanthan gum as is shown in Chapter 3. However, form the concentration-morphology phase diagram of xanthan it was observed that 1.5 wt% xanthan solution, formed two nucleation and subsequent vertical membranes. From this result I inferred that possibly the concentration of the solution (or viscosity) can be another parameter behind partitioning the macrospace and the bridging of gaps. It would be interesting to compare molecular weights and concentration to uncover this hypothesis. Further, it has been calculated that a higher viscosity at the interface is generated as compared to the original bulk viscosity.[4] This possibly could be the force that facilitates the deposition of membranous structure. However, the extent of the role of viscosity in the whole process of deposition still remains unclear.

Another interesting aspect is the size of the LC structural unit (mesogen) of sacran. It has been reported to be 1 μm in diameter and < 20 μm in length, the aspect ratio being more than 20, when compared to other popular biopolymers like CNF, DNA.[5] The size and interactions between these mesogenic units has not been considered. The basic theory is that as the receding air-water evaporative interface reaches their location, the domains are formed like a crust/ skin-layer. In order to create a new surface, energy is needed which comes from the supplied temperature as thermal energy.[6] They experience capillary forces towards the substrate-wall as well as strong interparticle capillary interactions. In this competition of forces, the interparticle interaction is long-ranged and also stronger resulting in bridging depositions.[7,8] For instance, an anisotropic particle induces interfacial distortions all along its contour and

contributes to saddle-shaped interfacial deformations forcing particle attractions either tip-to-tip or side-to-side.[9,10] Furthermore, the orientation is primarily governed by the long-range order of the LC molecules when confined in a geometry.[11]

The biopolymers usually self-assemble to showcase a variety of hierarchical structures with different shapes and sizes. Depending upon the self-assembled structure, the physical property as well as functions varies. In particular, nature has devised ways to build materials with a unique combination of flaw tolerance along with high strength as seen in mollusk shells, mineralized tissues (bone, teeth).[12,13] The cell wall of plants is basically cellulose along with lignin and hemicellulose with a platelet form that induces assembly in the structure.[14] Taking inspiration from nature, platelet reinforced polymer matrices have been prepared as stronger and reliable contenders. These structures comprise of platelet-like building blocks in a layered polymeric matrix to render the original design of natural materials.[15–18]

In this chapter, I aim to clarify that by exploiting the shape and size of particle in a solution, highly oriented self-assembled structures could be generated. This conforms to be a highly synergistic approach in an accessibly convenient process of drying.

5.2 Molecular weight of the polysaccharide

The molecular weight of polysaccharides extracted from microorganisms tends to vary with the cultivation area, environment and even extraction techniques used. It has been related to the changes in certain properties as well, for example, as the molecular weight of sulfated fucans in certain polysaccharides increases their anticoagulant activity increases.[19,20] It is also related to the persistence length, or the measure of flexibility/rigidity of the polymer chain.[21]

For checking the bridging depositions as a function of molecular weight, I performed the drying experiments for three different polysaccharides with increasing order of molecular weight (**Fig. 5.1**).

Figure 5.1 Side views of cells with different polysaccharides after drying at 60 °C. Initial concentration of the polysaccharide solution, C_0 = 0.5 wt%. Dimensions of the drying cell: x = 15 mm; y = 0.5 mm; z = 20 mm.

It was observed that no deposition occurred for other polysaccharides, Na-alginate and xanthan gum with mol. weight as 10^5 and 10^6 g.mol^{-1} did not form any bridging structures whereas sacran with the highest mol. weight deposits as a vertically bridging structure.

Similarly, concentration of the solution used can also be assumed to be a factor in this phenomena as was seen with xanthan gum in Chapter 3. So next, I performed the experiment with increased concentration of only Na-alginate and xanthan gum (**Fig. 5.2**).

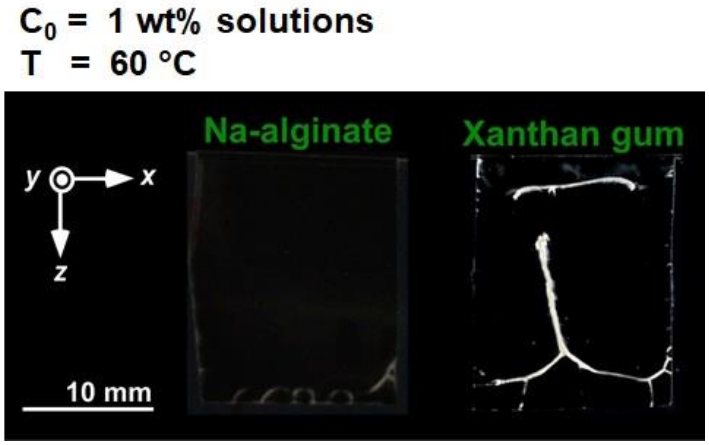

Figure 5.2 Side views of cells with 1 wt% Na-alginate and xanthan gum after drying at 60 °C. Dimensions of the drying cell: x = 15 mm; y = 0.5 mm; z = 20 mm.

1 wt% concentration for Na-alginate was still not enough to bridge the two substrates but for xanthan gum it was. Thus, concentration definitely helps in bridging depositions, but it is not the only factor.

This directs us to the fact that there is increased volume fraction of the drying solution which also acts as a major factor. This complementary experiment gives insight into concentration as an important factor responsible for bridging depositions. Increasing the concentration of polymer solution, in turn increases the number of LC units in the solution within close proximity. Hence, overall increases the particle-particle interactions (structural, intermolecular, hydrodynamic) and chances of bridging.

5.3 Viscosity of the solution

Viscosity of sacran solution has also been reported to be a major factor behind this phenomena in a limited space. To test this hypothesis, sacran solution with calcium ions as crosslinking agents was prepared. 20 mM calcium chloride ($CaCl_2$) was added to a 0.5 wt% sacran solution with continuous stirring for about an hour at 60 °C. Due to this crosslinking, the viscosity of the solution visibly increased as compared to pure 0.5 wt% sacran solution. The quantitative estimation was done by measuring the viscosity of the two solutions against an increasing shear rate. **Fig. 5.3a** shows the result of viscosity as a function of increasing shear rate of the solutions. Increasing the shear rate during measurement leads to decrease in the value of solution viscosity. This is a known trend for high molecular weight polysaccharide solutions like sacran and is referred to as 'shear thinning'.[22] However, when this solution of sacran with calcium ions was dried in a cell, bridging depositions were not found. On the other hand, I observed the famous patterns of the "stick-and-slip' motion of particles (**Fig 5.3b**).

Straight line stick and slip deposition patterns have been reported for spherical colloidal particles and was one of the first reported self-assembly methods. It has been extensively used for fabricating highly oriented and well-ordered nanoparticles, polymer, biomolecules *etc.* assemblies.[23–25] It is interesting to observe a concave curvature as oriented deposition instead of the normally observed line pining-depinning.

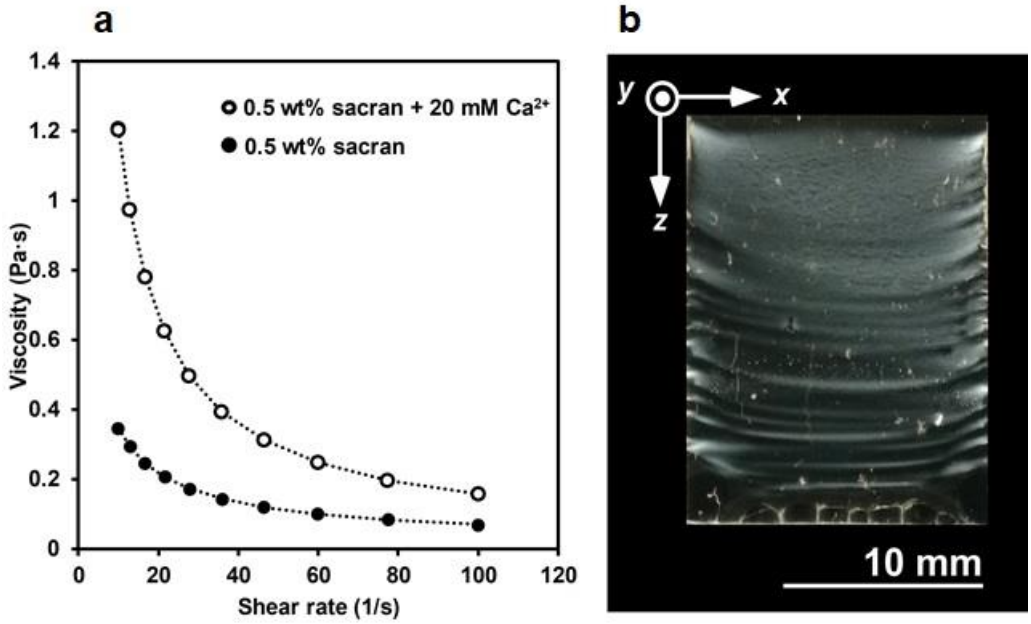

Figure 5.3 Effect of viscosity on deposition. **a.** Viscosity as a function of shear rate. **b.** Drying pattern for a solution of 0.5 wt% sacran with 20 mM Ca^{2+} ions. Cell dimensions; x = 15 mm, y = 1 mm, z = 20 mm; drying temperature = 60 °C.

The patterned deposition of sacran with calcium ion was unexpected and definitely needs further investigation as another route to prepare oriented structure with anisotropic particles. For the time being, I can safely conclude that viscosity provides the necessary deposition on the substrate to help initiate first of all pinning and later bridging of the gap. Thus, viscosity is not directly responsible for the partitioning but definitely paves the way for the same.

5.4 Size of the domain in LC solution (mesogen unit)

When the solution of sacran, obtained from Green Science Materials Inc. (GSM), was dried under regular conditions (x = 15mm; y = 1 mm; z = 20 mm; T = 60 °C) different patterns of depositions, arborescent in appearance, were observed. I judged from this observation that possibly the 1 mm space is too congested for this batch and therefore the polymer is depositing in such a manner. Thus, I repeated the experiment by just increasing the width of the cell as, y = 2 mm; 3 mm; 5 mm; keeping other conditions constant. As expected vertical bridging membranes as shown in **Fig. 5.4** deposited. However, it was astonishing to see bridging of up to 5 mm and even an 8 mm gap sometimes.

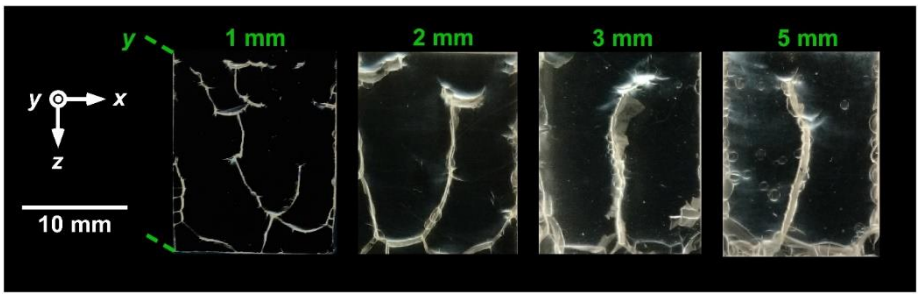

Figure 5.4 Bridging of the glass substrates with a wider gap, y.

It was not a one-time deposition as the sacran GSM batch bridged the wider gap each time upon repeated drying experiments. Speculating the reason for this behavior was difficult as the material was same, with the same properties. Next, I checked the upper limit of maximum gap it can possibly bridge. Cells with a silicone spacer of 8 mm and 10 mm were prepared, sandwiched between the non-modifies glass slides and the experiment was performed at 60 °C.

Increasing the width further to y = 10 mm, the solution was dried to test the bridging ability of the sacran GSM solution. However, only side wall adsorptions were obtained in this case (**Fig. 5.5**). This signaled the maximum limit to the width bridging ability of sacran GSM solution which turns out to be ~ 5-8 mm.

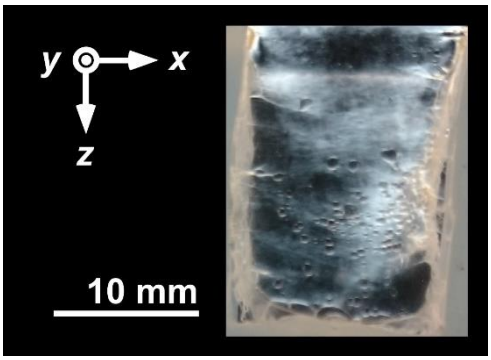

Figure 5.5 Side wall adsorption of sacran GSM batch in a gap of 10 mm.

5.4.1 Bridging of a wider gap

It was baffling to observe a batch of sacran with a width bridging maxima at y = 1 mm whereas another batch of the same material with a five times limit of y = 5 mm. To explore the reason behind this phenomenon, I analyzed the dried film obtained from a 0.5 wt% solution in a 5 mm wide cell check its structural units.

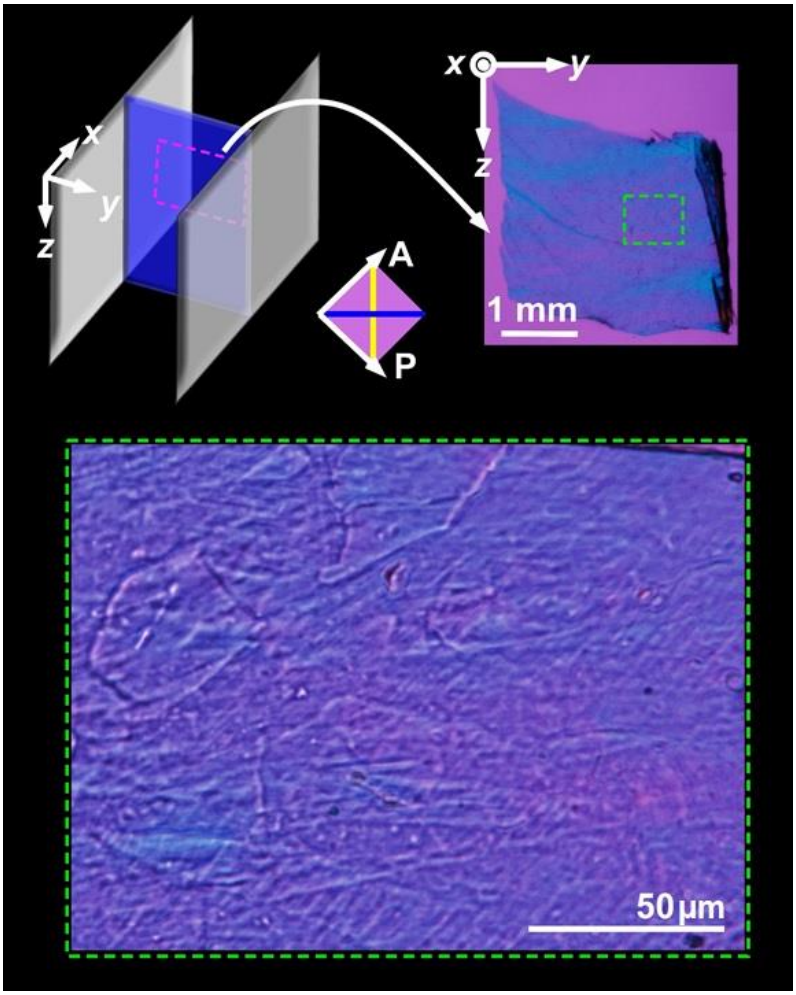

Figure 5.6 Microscopic images of the membrane obtained in a 5 mm gap.

From **Fig. 5.6** I observed that even in such a wide gap the film was still highly oriented as could be clearly seen by the blue color under the polarized microscope. I could also identify huge platelet-like units alongside the reported rod-like units of sacran under higher magnification. These platelets were found to have variations in size from 50 – 100 μm. These platelets were also visible on the glass substrate. This implies these micron-sized units are part of the sacran solution (**Fig. 5.7**).

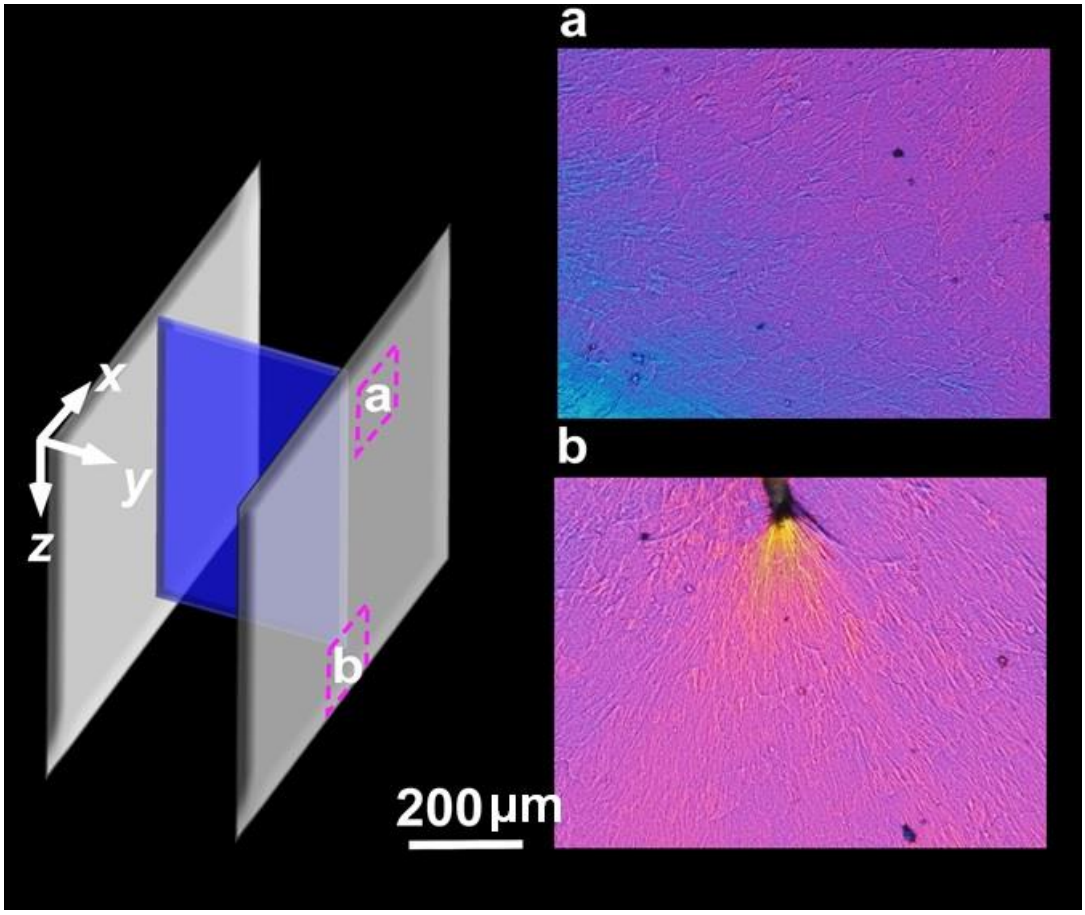

Figure 5.7 Microscopic images of the substrate around the deposited membrane showing platelet-like structures.

Such a structure, probably a result of large scale self-assembly, provides direct indication towards the role of structural units and their size in different geometries occurring in nature.

Firstly, it is obvious that the non-modified glass give access to high surface anchoring strength[26,27] for the polysaccharide solutions used in our experiment along with the actual interface-assisted ordering. The most influential interparticle interaction arises at an interface because of lateral capillary forces with the overlap of individual deformations at interface.[28,29] It can be inferred that the order is partially propagated to adjacent liquid crystal units via additional anisotropic interactions.[30]

I tried centrifugation of a dilute sacran GSM solution to see if the platelets can be possibly separated. 0.1 wt% solution was centrifuged for 1 hour at ~ 48,000 RCF (20,000 RPM)[31] but no visible change in the solution was observed and there was no sedimentation (**Fig. 5.8**). Thus, these 2D platelets are a result of self-assembly of sacran LC units and are an integral part as higher order aggregates.

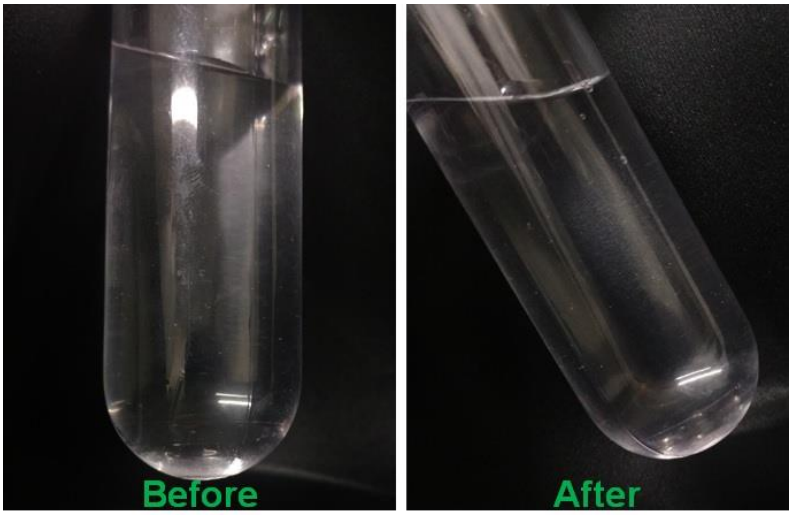

Figure 5.8 Images of the 0.1 wt% sacran GSM solution before and after centrifugation.

5.4.2 Hypothesis for bridging of a wider gap

Making sure that the platelets and rod-shaped LC units co-exist in sacran GSM solution, the process of formation of the bridge membrane was to be investigated. Is it similar to the case of bridging in a limited gap of 1 mm? To answer this question, I started with a closer examination of the nucleating part of the membrane to analyze the process from where it all started. As seen under the microscope in **Fig. 5.9a** the initial nucleus was found to be a thin bridge with a concave structure. Upon inspecting from the top, it was found to be oriented along the *x*-direction (**Fig 5.9b**).

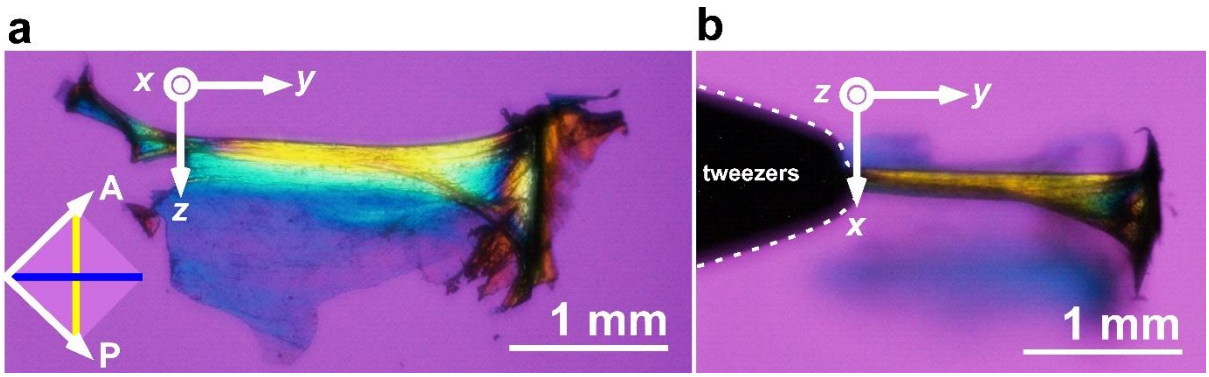

Figure 5.9 Microscopic images of the nucleus of a 5 mm wide membrane. **a.** side view **b.** top-side view.

Self-assembly via evaporation is considered as a versatile process to arrange large-scale and long-range particles in high order. The initiation step that is pinning on the substrate is dependent on the size of the particle. Bigger the size of the particle/unit, longer it stays pinned onto the substrate.[32] The most probable reason behind such a wide bridging deposition is due to the strong lateral capillary interactions in the sacran solution amongst the platelet-like units supported by the rod-shaped units (**Fig. 5.10**).

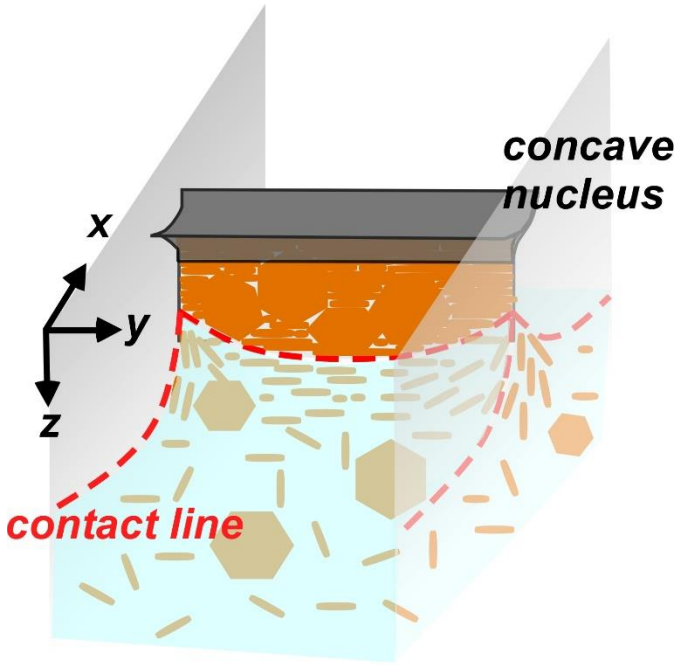

Figure 5.10 Schematic illustration of the deposition of solution with rod- and platelet-shaped LC domains during the evaporation process in a wider gap, *y*.

Instead of the usual competition between the pinning force and the capillary force during the course of evaporation which result in the stick and slip pattern, here the capillary forces are strengthened along the *y*-direction. In this way, with several pinned deposits threading throughout vertically down the *z*-axis as the evaporative interface recedes, a thin membrane grows.

5.5 Conclusion

In this chapter, I could achieve a deeper insight into the factors governing the deposition of the LC polysaccharide units. The bridging depositions were previously thought to be only as a result of the limited space that the polysaccharide LC solution was confined within.

- I tested the generally accepted conditions of molecular weight of the polysaccharide and the viscosity of its prepared solution. The preliminary results demonstrated that higher molecular weight and concentration of the solution were directly favoring depositions with bridging of the gap between the substrates.

- Unexpectedly, viscosity of the solution was found to be not directly responsible for bridging the gap. It was however, observed to be responsible for pinning of the polymer on the substrate and probably as an initiating point for further deposition.

- The main result concluded in this chapter was regarding the size of the self-assembled LC units wherein they could bridge a wider gap. With the bigger sized units in the solution, strong lateral capillary forces acted upon the pinned deposit on the substrate with ultimate bridging of the wider gap.

References

1. Nishinari, K. & Takahashi, R. Interaction in polysaccharide solutions and gels. *Curr. Opin. Colloid Interface Sci.* **8**, 396–400 (2003).

2. Marguerite, R. Relation between the molecular structure of some polysaccharides and original properties in sol and gel states. *Food Hydrocoll.* **15**, 433–440 (2001).

3. Hamley, I. W. Liquid crystal phase formation by biopolymers. *Soft Matter* **6**, 1863–1871 (2010).

4. Madivala, B., Fransaer, J. & Vermant, J. Self-assembly and rheology of ellipsoidal particles at interfaces. *Langmuir* **25**, 2718–2728 (2009).

5. Okeyoshi, K., Okajima, M. K. & Kaneko, T. Milliscale Self-Integration of Megamolecule Biopolymers on a Drying Gas–Aqueous Liquid Crystalline Interface. *Biomacromolecules* **17**, 2096–2103 (2016).

6. de Gennes, P.-G., Brochard-Wyart, F. & Quéré, D. Capillarity: Deformable Interfaces BT - Capillarity and Wetting Phenomena: Drops, Bubbles, Pearls, Waves. in (eds. de Gennes, P.-G., Brochard-Wyart, F. & Quéré, D.) 1–31 (Springer New York, 2004).

7. Yunker, P. J., Still, T., Lohr, M. A. & Yodh, A. G. Suppression of the coffee-ring effect by shape-dependent capillary interactions. *Nature* **476**, 308–311 (2011).

8. Dufresne, E. R. *et al.* Flow and fracture in drying nanoparticle suspensions. *Phys. Rev. Lett.* **91**, 1–4 (2003).

9. Loudet, J. C., Yodh, A. G. & Pouligny, B. Wetting and contact lines of micrometer-sized ellipsoids. *Phys. Rev. Lett.* **97**, 1–4 (2006).

10. Loudet, J. C., Alsayed, A. M., Zhang, J. & Yodh, A. G. Capillary interactions between

anisotropic colloidal particles. *Phys. Rev. Lett.* **94**, 2–5 (2005).

11. Ryu, S. H. & Yoon, D. K. Molecular Orientation of Liquid Crystals on Topographic Nanopatterns. *ACS Appl. Mater. Interfaces* **8**, 17707–17712 (2016).

12. Lowenstam Heinz A. & Weiner Stephen. On Biomineralization. *Paleobiology* **16**, 521–526 (1990).

13. Pletikapić, G. *et al.* Self-assembly of polysaccharides gives rise to distinct mechanical signatures in marine gels. *Biophys. J.* **107**, 355–364 (2014).

14. Newman, R. H., Hill, S. J. & Harris, P. J. Wide-Angle X-Ray Scattering and Solid-State Nuclear Magnetic Resonance Data Combined to Test Models for Cellulose Microfibrils in Mung Bean Cell Walls. *Plant Physiol.* **163**, 1558–1567 (2013).

15. Das, P., Thomas, H., Moeller, M. & Walther, A. Large-scale, thick, self-assembled, nacre-mimetic brick-walls as fire barrier coatings on textiles. *Sci. Rep.* **7**, 1–13 (2017).

16. Bonderer, L. J., Studart, A. R. & Gauckler, L. J. of Platelet Reinforced Polymer Films. *Science.* **319**, 1069–1073 (2007).

17. Cataldi, P. *et al.* Effect of graphene nano-platelet morphology on the elastic modulus of soft and hard biopolymers. *Carbon N. Y.* **109**, 331–339 (2016).

18. Britain, G. on the Actual Contribution of Platelet-Reinforced Brittle-Matrix Composites. **41**, 1825–1839 (1993).

19. Chevolot, L. *et al.* Further data on the structure of brown seaweed fucans: Relationships with anticoagulant activity. *Carbohydr. Res.* **319**, 154–165 (1999).

20. Holdt, S. L. & Kraan, S. Bioactive compounds in seaweed: Functional food applications and legislation. *J. Appl. Phycol.* **23**, 543–597 (2011).

21. Lei, S. & Feng Edmund, T. Polysaccharides, Microbial ☆. *Ref. Modul. Life Sci.* 482–494 (2017). doi:10.1016/B978-0-12-809633-8.13102-4

22. Mitsumata, T. *et al.* Ionic state and chain conformation for aqueous solutions of supergiant cyanobacterial polysaccharide. *Phys. Rev. E* **87**, 42607 (2013).

23. Aksay, I. a *et al.* Microscopic patterning of orientated mesoscopic silica through guided growth. *Nature* **390**, 674–676 (1997).

24. Watanabe, S., Inukai, K., Mizuta, S. & Miyahara, M. T. Mechanism for stripe pattern formation on hydrophilic surfaces by using convective self-assembly. *Langmuir* **25**, 7287–7295 (2009).

25. Mino, Y., Watanabe, S. & Miyahara, M. T. In Situ observation of meniscus shape deformation with colloidal stripe pattern formation in convective self-assembly. *Langmuir* **31**, 4121–4128 (2015).

26. Jerome, B. Surface effects and anchoring in liquid crystals. *Reports Prog. Phys.* **54**, 391 (1991).

27. Leonard, S. W., Mondia, J. P., van Driel, H. M., Toader, O. & John, S. Condensed Matter and Materials Physics. *Phys. Rev. B* **61**, 2389–2392 (2000).

28. Kralchevsky, P., Denkov, N. D. Capillary forces and structuring in layers of colloid particles. *Curr. Opin. Colloid Interf Sci.* **6**, 383-401, 2001.

29. Kralchevsky, Peter A. & Nagayama, Kuniaki. Capillary interactions between particles bound to interfaces, liquid films and biomembranes. *Adv. Colloid Interface Sci.* **85**, 145–192 (2000).

30. Brown, A. B. D., Smith, C. G. & Rennie, A. R. Fabricating colloidal particles with photolithography and their interactions. *Phy. Rev. E.* **62**, 951–960 (2000).

31. Okeyoshi, K., Osada, K., Okajima, M. K. & Kaneko, T. Methods for the self-integration of megamolecular biopolymers on the drying air-LC interface. *J. Vis. Exp.* **2017**, 1–7 (2017).

32. Shmuylovich, L., Shen, A. Q. & Stone, H. A. Surface morphology of drying latex films: Multiple ring formation. *Langmuir* **18**, 3441–3445 (2002).

Chapter 6

General Conclusions and Future Prospects

The self-assembled structures in natural environment have inspired researchers since a long time. Learning from the nature and employing natural products as well as similar techniques in material designing, has covered a wide field since its inception. Regulating evaporation to control the self-assembly of particles from a solution has emerged as a radical technique considering the variety of applications generated. Liquid crystalline materials, both synthetic as well as from natural sources, have been utilized in preparation of functional materials due to their inherent nature of order and mobility. Orientation control in these materials require the use of complicated techniques/setup and synthetic reagents with long difficult procedures. The routinely used self-assembling techniques suffer from major challenges of fast solvent evaporation rates, instabilities in the fluid flow, non-uniform deposition *etc*.

The simple process of drying-induced self-assembly, using sacran as an LC polymer, gave the impetus to consider evaporative deposition behaviors in a restricted space. Although there are limitations with respect to observing the bulk drying process, we were able to obtain direct evidence from the crossed-polarized setup (**Fig. 6.1**). Observation of the drying through the cross-polarizers, led to monitoring of the process and understanding the critical role of LC state.

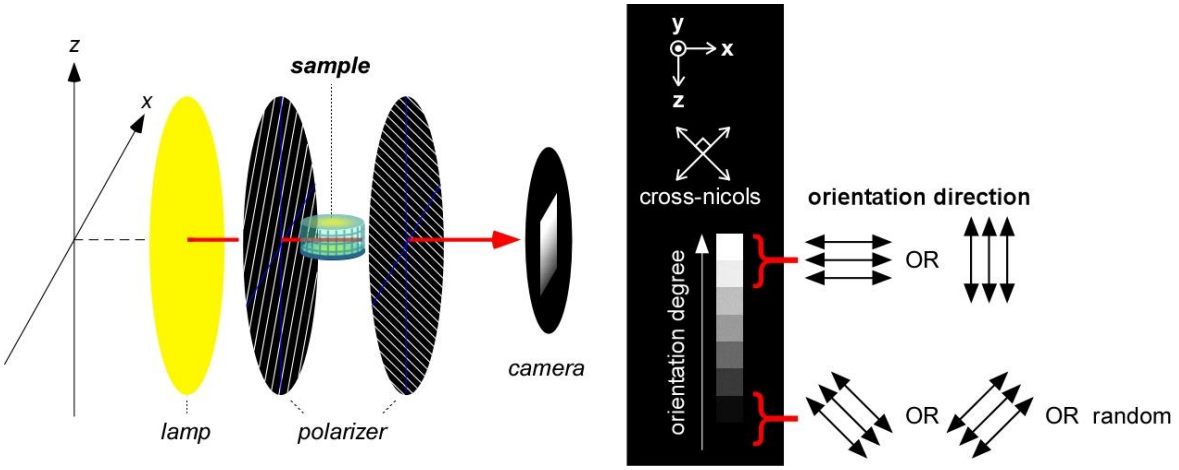

Figure 6.1 Schematic illustration of the experimental setup used for observation under cross-polarized light. The polarizers were normally adjusted to 45° and 135°.

A first-order retardation plate of 530 nm wavelength, placed between the sample and the polarizer, was used to clarify the orientation directions in the solution and the deposited structures.

In **Chapter 2**, by drying sacran solution from the planar geometry of the container, a dried film was obtained. This dried polymer film was crosslinked by thermally annealing at a higher temperature and thus gel film was prepared which swelled in water uniaxially along its height. The diffusion kinetics was analyzed for this physically crosslinked hydrogel, swelling anisotropically by using the standard equations employed for polymer matrices. It was shown that the majority of water uptake occurred along the edges with swelling along the vertical direction. The SEM images of the dried film revealed a well-organized layered structure along the *xy*-plane that helped in explaining the swelling process (**Fig. 6.2**).

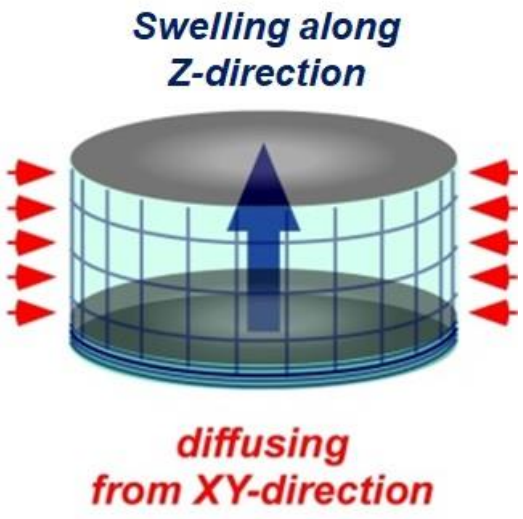

Figure 6.2 Schematic illustration for the swelling and diffusion direction in the sacran hydrogel.

By evaluating the interfacial curves of a limited geometry in **Chapter 3**, it was shown that a thickness of 1 mm was mostly a curved interface and thus posed as s linear evaporation front, with confined geometry. Moreover, the standard equation of a meniscus was extended to incorporate the cases of both, a descending as well as an ascending meniscus.

$$\frac{\partial^2 z}{\partial^2 x} = \kappa^2 z$$

I derived the equation for the length of the meniscus as,

$$\int dl = \int [A^2 e^{(-\Delta x_0)} 4sin^2 X + 1]^{1/2} \; dX$$

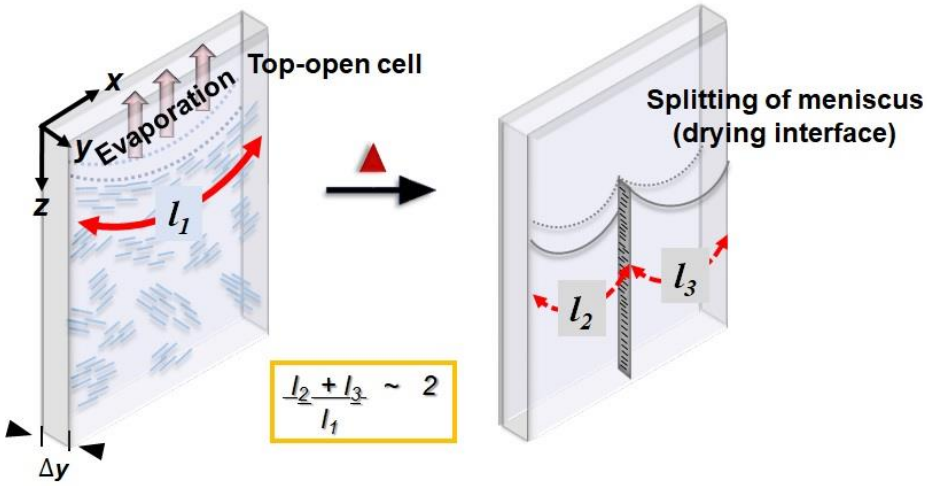

Figure 6.3 Schematic illustration of the drying process of a LC solution in a limited space resulting in splitting of the interface and formation of two menisci.

Simplifying the above equation, I approximated the values for a single meniscus as compared to the case of a split meniscus as shown in **Fig. 6.3**. The double menisci were found to be twice as efficient as the original single meniscus in providing surface for evaporation. It was concluded from the mathematical analysis that the vertical membrane formation in the top-

side-open cell with a narrow gap is a result of splitting of the initially single curve into multiple interfacial curves in order to facilitate water evaporation in the confined environment.

The theoretical estimations are just small steps towards understanding this unique phenomenon and its full implication is still unknown. Further analysis and possible computational modelling can be greatly helpful in exploring the basic nature and periodicity in the partitioning phenomenon..

In the previous reports, we had only observed splitting of the meniscus and deposition of a vertical membrane, bridging the glass substrates. In **Chapter 4** the focus was to control the process of deposition and consequently observe the changes in orientation of structures. By orientation control it was aimed to basically manipulate the mobility of the LC domains to guide them to a desired deposition. This was achieved by using another high molecular weight polysaccharide, xanthan gum. Whereas, the LC domains of sacran have been shown to be highly stable even up to a temperature of 60 °C; the LC state of xanthan gum, in complete contrast to sacran, has been reported to be sensitive to temperature in the range of 25 – 60 °C. This meant that the liquid crystallinity of the solution decreases with increase in temperature due to this supplied thermal energy that boosts the mobility of the LC domains. Therefore, by changing the drying temperature it was possible to control the mobility of the LC domains and also the orientation.

By monitoring the experimental conditions, a concentration-temperature-morphology phase diagram was successfully formulated for drying of xanthan gum in a limited space (**Fig. 6.4**).

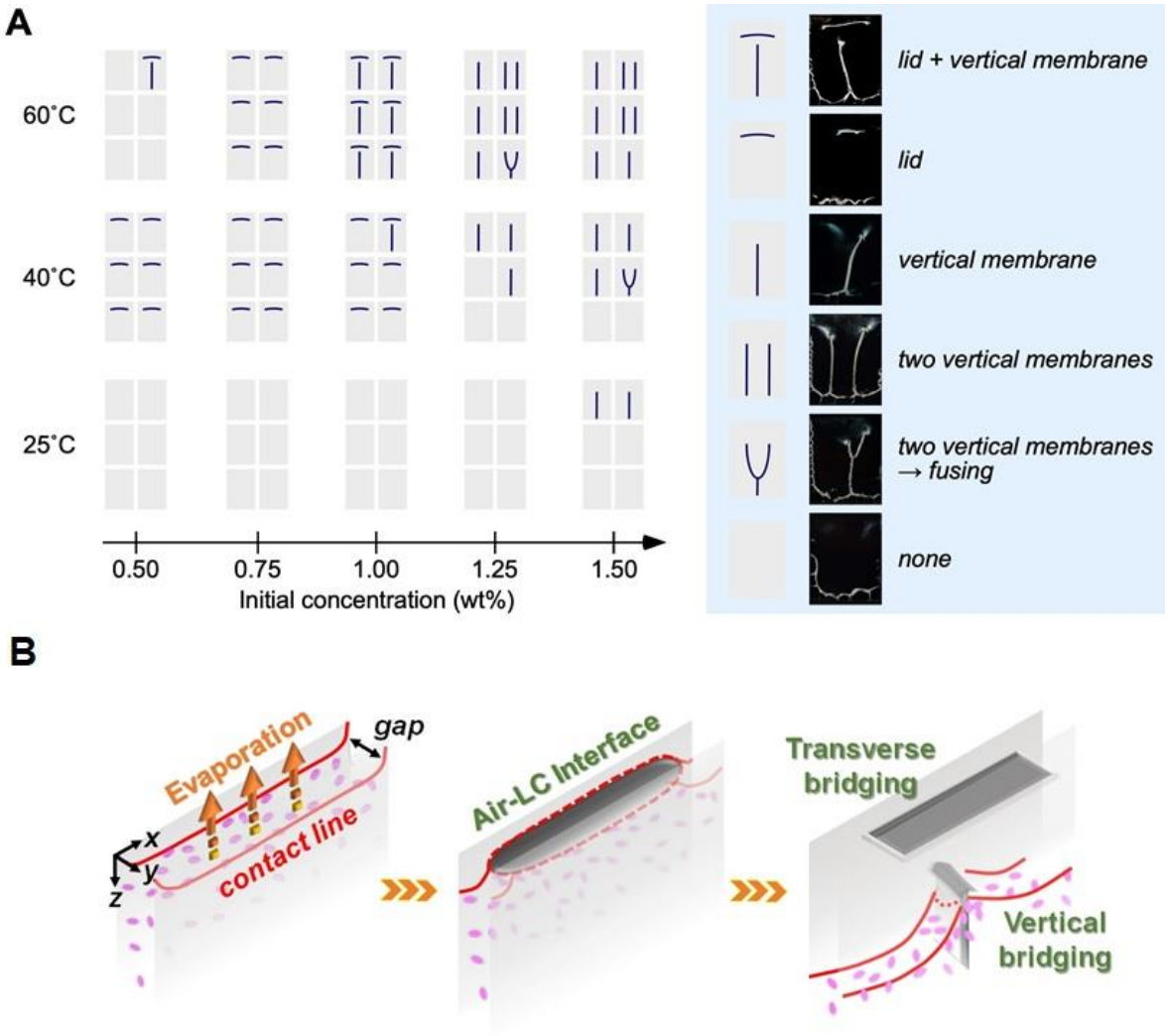

Figure 6.4 Drying of xanthan gum LC solution from a linear evaporation front. A. Phase diagram the depositions and their classification on the basis of initial concentration and temperature. Cell dimensions = (15 mm, 0.5 mm, ~ 20 mm); drying under atmospheric pressure. Number of experiments for each condition, $N = 6$. **B.** Schematic illustration of the bridging depositions obtained for xanthan solution.

The drying of xanthan gum solution and its evaporation-induced deposition under a confined rectangular geometry gave some unexpected results and demonstrated that the orientation of LC domains could be controlled. It also stands as the first example of another polysaccharide reproducing the partitioning behavior, initially shown with sacran. Still, the results obtained with xanthan gum have led to springing of new questions and curiosities. 0.5 wt% sacran splits

a 15 mm interface into two menisci whereas a 1.5 wt% xanthan gum solution splits the same interface into three menisci. Thus, there are not just two or three factors governing the splitting of meniscus, but several of them.

Understanding the factors affecting the bridging deposition became more interesting , when the size of the domains was also found to be responsible, as presented in **Chapter 5**, 0.5 wt% sacran solution was able to bridge up to 8 mm of a gap, where the 1 mm gap was previously reported to be the upper limit. The self-assembled platelet-like structure in sacran solution was hypothesized to be a major force behind this wide bridging deposition. By staying pinned for a longer time as compared to their smaller-sized counterparts, the platelet structures held on to the evaporative interface through strong lateral capillary interaction (**Fig. 6.5**).

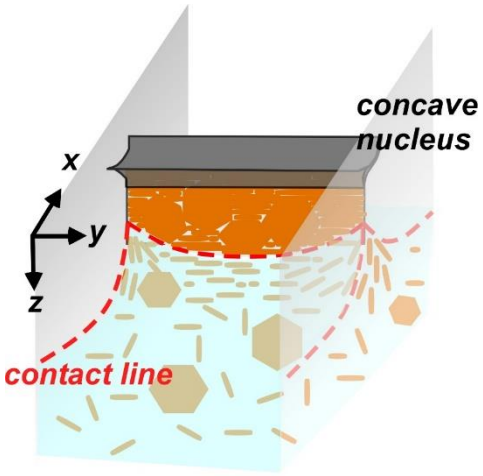

Figure 6.5 Schematic illustration of the deposition of solution with rod- and platelet-shaped LC domains during the evaporation process in a wider gap, *y*.

Topics for further research

- Firstly, all the drying experiments reported in this thesis were performed using non-modified glass slides. It is anticipated that surface chemistry is essential in the movement and cumulative deposition of the structure. Investigating the effect of hydrophobicity of the substrate on the mobility and deposition patterns of the anisotropic particles would make an interesting topic for further study.

- Secondly, the polysaccharide solutions were prepared in deionized water. Addition of some external agent like surfactant or salt can be assumed to affect the solution properties of these polysaccharides and thus can affect the deposition process. The results of Chapter 5 (topic 5.2) demonstrating oriented deposition in the form of catenary curves provides multiple ideas and can be further pursued.

- Most importantly, it was observed that the number of splitting were dependent on factors like the geometry, polysaccharide used, molecular weight, concentration and also temperature of the drying experiment. Consideration of all the parameters into a single theoretical model can give some definite results in future.

List of Accomplishments

A) Publications in peer-reviewed Scientific journals

1. **Gargi Joshi**, Kosuke Okeyoshi, Tetsu Mitsumata and Tatsuo Kaneko

   "Micro-Deposition Control of Polysaccharides on Evaporative Air-LC Interface to Design Quickly Swelling Hydrogels"

   Journal of Colloid and Interface Science, 2019, 546, 184-191.

2. **Gargi Joshi**, Kosuke Okeyoshi, Maiko K. Okajima and Tatsuo Kaneko

   "Directional control of diffusion and swelling in megamolecular polysaccharide hydrogels"

   Soft Matter, 2016, 12, 5515-5518. *Selected as Back Cover*

3. Kosuke Okeyoshi, **Gargi Joshi**, Maiko K. Okajima and Tatsuo Kaneko

   "Formation of Polysaccharide Membranes by Splitting of Evaporative Air-LC Interface"

   Advanced Materials Interfaces, 2018, 5, 1701219. *Selected as Back Cover*

4. Kosuke Okeyoshi, **Gargi Joshi**, Sakshi Rawat, Saranyoo Sornkamnerd, Kittima Amornwachirabodee, Maiko K. Okajima, Mayumi Ito, Shoko Kobayashi, Koichi Higashimine, Yoshifumi Oshima and Tatsuo Kaneko

   "Drying-induced self-similar assembly of megamolecular polysaccharides through nano and sub-micron layering"

   Langmuir, 2017, 33, 4954-4959. *Selected as Front Cover*

5. Kosuke Okeyoshi, Takeshi Shinhama, Kulisara Budpud, **Gargi Joshi**, Maiko K. Okajima and Tatsuo Kaneko

   "Micelle-mediated Self-assembly of Microfibers Bridging Millimetre-scale Gap to form 3D-ordered Polysaccharide Membranes"

   Langmuir, 2018, 34, 13965-13970. *Selected as Back Cover*

B) <u>Manuscripts in preparation</u>

6. Kosuke Okeyoshi, Miki Yamashita, Tadashi Sakaguchi, Kulisara Budpud, **<u>Gargi Joshi</u>** and Tatsuo Kaneko

   "Effect of Evaporation Rate on Meniscus Splitting with Formation of Vertical Polysaccharide Membranes"

   submitted

7. **<u>Gargi Joshi</u>**, Kosuke Okeyoshi, Maiko K. Okajima and Tatsuo Kaneko

   "Platelet-shaped LC Domains assist Deposition of Polysaccharide Bridging Centimeter Gap upon Evaporation"

   In preparation

8. **<u>Gargi Joshi</u>**, Kittima Amornwachirabodee, Maiko K. Okajima and Tatsuo Kaneko

   "Preparation of Chemically-crosslinked Heterogenous Hydrogels"

   In preparation

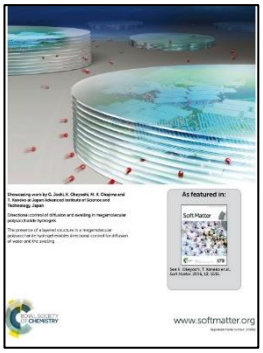

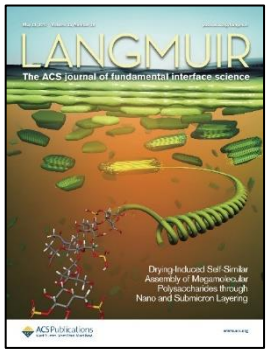

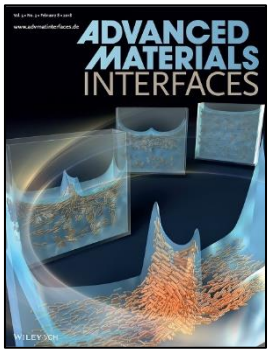

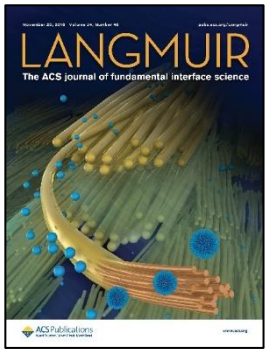

C) <u>Peer-reviewed Proceedings</u>

<u>Gargi Joshi</u>, Kosuke Okeyoshi, Maiko K. Okajima and Tatsuo Kaneko

"Splitting of Meniscus at Air-LC Interface of Megamolecular Polysaccharide and its Theoretical Evaluation"

Abstracts of Papers, ***255th ACS National Meetings & Expositions***, 2018, pages POLY-758

D) International Conferences (Peer-reviewed)

1. Gargi Joshi, Kosuke Okeyoshi and Tatsuo Kaneko

   "Controlling the oriented deposition of LC polysaccharide at evaporative interface in a confined geometry"

   Chemistry, Physics and Biology of Colloids and Interfaces, Eger, Hungary, May 2019 [Oral]

2. Gargi Joshi, Kosuke Okeyoshi, Tetsu Mitsumata and Tatsuo Kaneko

   "Deposition control of LC polysaccharide at evaporative interface to design quickly swelling hydrogels"

   MRS Spring Meeting, Phoenix, Arizona, USA, April 2019 [Oral]

3. Gargi Joshi, Kosuke Okeyoshi, Maiko K. Okajima and Tatsuo Kaneko

   "Evaporation induced self-assembly of megamolecular polysaccharides through planar and linear air-LC interfaces"

   1st International Meeting on 4D Materials and Systems, Yonezawa, Japan, August 2018

   Best Poster Presentation Award

4. Gargi Joshi, Kosuke Okeyoshi, Maiko K. Okajima and Tatsuo Kaneko

   "Planar versus linear evaporative air-LC interfaces for drying induced self-assembly of megamolecular polysaccharides"

   The 10th International Conference of Modification, Degradation and Stabilization of Polymers, Tokyo, Japan, September 2018 [Poster]

5. Gargi Joshi, Kosuke Okeyoshi, Maiko K. Okajima and Tatsuo Kaneko

   "Splitting of meniscus at air-LC interface of megamolecular polysaccharide and its theoretical evaluation"

   255th ACS National Meeting, New Orleans, Louisiana, USA, March 2018 [Oral]

6. Gargi Joshi, Kosuke Okeyoshi, Maiko K. Okajima and Tatsuo Kaneko

   "Directional control of diffusion and swelling in LC polysaccharide hydrogels with laminated structure for developing anisotropic soft materials"

   11th SPSJ International Polymer Conference. Fukuoka, Japan, December 2016

   Young Scientist Poster Award

7. Gargi Joshi, Kosuke Okeyoshi, Maiko K. Okajima and Tatsuo Kaneko

   "Directional control of diffusion and swelling in hydrogels prepared from cyanobacterial exopolysaccharide"

   11th International Gel Symposium. Chiba, Japan, March 2017

   RSC Soft Matter Poster Award

8. Gargi Joshi, Kosuke Okeyoshi, Maiko K. Okajima and Tatsuo Kaneko

   "Control of uniaxially-swelling hydrogels prepared from megamolecular polysaccharide towards developing anisotropic soft materials"

   DU-JAIST Indo-Japan Symposium on Chemistry of Functional Molecules/Materials. Delhi, India, February 2016

   Best Oral Presentation Award

E) <u>Domestic Conferences (Peer-reviewed)</u>

1. <u>Gargi Joshi</u>, Kosuke Okeyoshi and Tatsuo Kaneko

   "Self-assembled deposits of LC polysaccharide obtained in confined space by manipulating temperature and concentration"

   67th Symposium on Macromolecules, SPSJ, Hokkaido, September 2018 [Oral]

2. <u>Gargi Joshi</u>, Kosuke Okeyoshi, Maiko K. Okajima and Tatsuo Kaneko

   "Meniscus splitting at air-LC interface in drying process of megamolecular polysaccharides"

   66th Symposium on Macromolecules, SPSJ, Ehime, September 2017. [Oral]

3. <u>Gargi Joshi</u>, Kosuke Okeyoshi, Maiko K. Okajima and Tatsuo Kaneko

   "Directional control of diffusion and swelling in renewable water-absorbers derived from megamolecular cyanobacterial exopolysaccharides"

   EcoDePS, Tokyo, December 2016 [Oral and Poster]

4. <u>Gargi Joshi</u>, Kosuke Okeyoshi, Maiko K. Okajima and Tatsuo Kaneko

   "Control of uniaxially swelling hydrogels prepared from megamolecular polysaccharide towards developing anisotropic soft materials"

   SPSJ-Hokuriku, Ishikawa, November 2015 [Oral]

5. <u>Gargi Joshi</u>, Kosuke Okeyoshi, Maiko K. Okajima and Tatsuo Kaneko

   "Kinetic studies of uniaxially-swelling polysaccharide hydrogels toward novel anisotropic soft materials"

64th Symposium on Macromolecules, SPSJ, Sendai, September 2015

Best Poster Award

F) Awards and Grants

1. Awarded 2018 **JAIST Off-campus Grant** for conducting research at University of Helsinki, Finland for (May-July 2018).

2. Received **JSPS KAKEHNI** Research Grant (Grant-in-Aid for JSPS Fellows #JP18J11881) for the financial year 2018-2020.

3. Awarded **JSPS Fellowship** for Doctoral Course (Financial support for Research and Life from April 2018- March 2020).

4. Awarded 2018 **JAIST Foundation Research Grant** for students to present in academic conference in 255th ACS National Meeting (New Orleans, USA).

5. Selected for 2017 fully-funded **Overseas Training Programme** JAIST-SIIT Workshop on "Advanced Science and Technology Workshop" in Bangkok, Thailand.

6. Awarded the 2017 **JAIST President Award** for social and extra co-curricular activities.

7. Received 2016 **Doctoral Research Fellowship** (special type) awarded by JAIST to 1 student per country per year.

8. Presentation Awards

- **2018:** 1st International Conference on 4D Materials and Systems

  Best Student Poster Award

- **2017:** 11th International Gel Symposium

  RSC Soft Matter Best Student Poster Award

- **2016:** 11th SPSJ International Polymer Conference, IPC

  Young Scientist Poster Award

- **2016:** Indo-Japan Symposium on Chemistry of Functional Molecules/Materials

  Best Oral Presentation Award

- **2015:** Symposium on Macromolecules, SPSJ

  Best Student Poster Award


高分子学会優秀ポスター賞
Gargi Joshi 殿
Kinetic studies of uniaxially-swelling polysaccharide hydrogels toward novel anisotropic soft materials


Certificate of Recognition
Best Paper Award


THE SOCIETY OF POLYMER SCIENCE, JAPAN
IPC 2016
YOUNG SCIENTIST
POSTER AWARD
Ms. Gargi Joshi

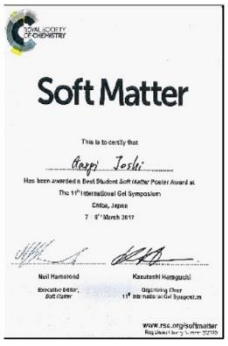
Soft Matter
This is to certify that
Gargi Joshi
Has been awarded a Best Student Soft Matter Poster Award at
The 11th International Gel Symposium
Chitai, Japan
7 - 8th March 2017
Neil Hammond
Executive Editor, Soft Matter
Kazutoshi Haraguchi
Organising Chair
11th International Gel Symposium
www.rsc.org/softmatter


First International Conference on 4D Materials and Systems
Aug. 26-29, 2018
Best Poster Presentation Award
This award is presented to
Gargi Joshi
Japan Advanced Institute of Science and Technology
for the topic
"Evaporation Induced Self-Assembly of Megamolecular Polysaccharide through Planar and Linear Air-LC Interfaces"